Alma Mater Studiorum – Università di Bologna

DOTTORATO DI RICERCA IN

CHIMICA

Ciclo XXX

Settore Concorsuale: 03/A2

Settore Scientifico Disciplinare: CHIM/02

COARSE-GRAINED MODEL FOR THE SIMULATION OF "ACTIVE DROPS"

Presentata da: Dr. Marco Macis

Coordinatore Dottorato   Supervisore

Prof. Aldo Roda   Prof. Francesco Zerbetto

Esame finale anno 2018

Table of contents

1. Introduction

"The scientific theorist is not to be envied. For Nature, or more precisely experiment, is an inexorable and not very friendly judge of his work. It never says "Yes" to a theory. In the most favorable cases it says "Maybe," and in the great majority of cases simply "No." If an experiment agrees with a theory it means for the latter "Maybe," and if it does not agree it means "No." Probably every theory will someday experience its "No"; most theories, soon after conception." (A. Einstein; note dated November 11, 1922.)

The computational chemistry is one of the most modern chemistry branch, born and developed in concomitance with the extreme improvement of the calculation power.

With the help of calculators, theoreticians are able to solve chemical problems and propose models able to predict or prove experimental evidences.

The classical interpretation of the scientific method is based on hypothesis formulations derived from experimental deductions. The subsequent protocol of hypothesis validation and formulations of explanatory theories represent an important step in the process of phenomena comprehension.

Nowadays, a well-founded hypothesis is not only the one that derived from empirical deduction but also the one based on solid theoretical models. The experimental deduction can be considered as an essential point for a theoretical study, triggering the possibility to understand characteristics and properties of phenomena and to derivate relative explanatory models. Theoretical/computational works can be considered indispensable, with a deep interpenetration with experiments. The experimental part can no longer leave aside from theoretical model and explanations, the progress of the science depends in fact on the comprehension of the phenomena and cannot be only dependent on series of deduction. The possibility to understand the nature allows to obtain another central capacity: the ability to predict its behavior. From this point of view, human beings are the only animal species having developed this aptitude in a conscious way. The other species on earth follows the nature behavior in a pure instinctive way, without a deep comprehension of the cause-effect relationship. Understand the behavior and the properties of a material means have some possibility to control them and formulate more reliable hypothesis based on the prediction of their characteristic.

From a chemical point of view, the development of theoretical models based on the comprehension of chemical phenomenon experimentally observed, is the goal of the theoretical chemistry. The possibility to formulate relations between the chemical structure

of a material and its properties (electrical, mechanical, photochemical etc.), the ability to classify chemical functional groups in relation to their reactivity or the capacity to purpose mechanistic explanation of chemical reactions are some examples.

With the development of theoretical chemistry, experimentalists are able to perform experiments based on stronger hypothesis an so with an higher probability to have success. In case of a chemical reaction, a theoretical model formulated to explain molecular reactivity can restrict the window of the possible reactions, reducing the number of laboratory test that have to be done. This have a lot of implications also in terms of environmental safety (solvent and reagent waste reduction, decreasing of animal tests etc.).

As in the most strict interpretation of the Galilean method, the right mathematical explanation gives the right phenomena explanation. For this reason, because all the theoretical models, including the chemical ones, are normally supported by a strong mathematical background, the use of calculators is deserved and the computational cost represent one of the most limitation factor in this field.

The number of equations to be resolved depends both on the model details and system dimension and the improvement of the computational power will allow to expand the horizon of this branch of chemistry.

The mathematical bases under a model, follows the characteristics of the problem that is facing and not secondary, its dimension. Quantum-mechanics is used for example to obtain detailed value of the energy of small molecular systems, both in ground and exited state. A theoretical study of photochemical and photophysical problems can be a good way to understand how the nature use the energy of the sun to perform activities, with the possibility to mimic their behavior or implement them on human-made devices.

An example can be the study of the photosystems inside chloroplast and the analysis of the photophysical process that govern the eyesight in animals.[1-3]

The discovery of the existence of conical intersections between energy potential curves is one of the recent example of how QM theoretical model can provide explanation to unpredictable experimental results of non-radiative decay of excited species.[4,5]

Another intriguing application of QM model is the capacity to determine with an high level of accuracy the geometry of a chemical species based on the approximate resolution of the Schrödinger equation. This can have a lot of implications, especially in the determination of the transition state geometry for a particular chemical reaction, understanding the reactive behavior of chemical species and the possibility to give an explanation to data obtained from kinetic studies.

In relation to the computational cost, the configurational study of many-body systems cannot be performed in a QM way and for this reason the implementation of classical models, lighter compared to the QM ones, were deserved.

In classical models, the interaction between atoms and molecules are govern by classical physics and the position of the atoms, in space and time, depend from the integration of the Newton equation of motion.

The Molecular Dynamic technique allows for example to perform studies on big molecular systems without losing the atomistic detail. The coarse-grained dynamic techniques is instead based on the discretization of the space by the use of soft-sphere with interpenetration capacity, these particles are fundamental units of the dynamics. With a clever implementations of the equations able to govern the thermal energy and the inter-particle interactions, coarse-grained dynamic allows to extremely simplify the system under study, eliminating most of the details that cannot be neglected in a full-atomistic representation.

During the three years of my PhD activity I worked on the development of a mechanical coarse-graining model with the aim to study the dynamics of fluid droplets with peculiar "active" behaviors.

After a broad introduction of some computational methods, including the ones implemented to perform the studies in object, the dissertation explore in three chapters the applications, the properties, the characteristics and the results obtained during my research activity.

Each one of the three chapter is arranged in a quite independent way from each other, having its own introduction, description and conclusion.

In chapter 3 will be presented the implementation of a model able to describe the general adhesion properties and morphological characteristics of a living cell onto a proper chemical functionalized surface.

Although the absence of molecular details in the cell structure, the model reproduce peculiar properties of living cells with a good agreement with some experimental results.

In chapter 4 another biological application will be shown through an implementation of the model presented in chapter 3. The growth of a neuritis guided by the presence of a chemical asymmetrical gradient onto a surface will be faced.

The favorable interactions with the particles that constitute the surface gradient encourage the neuritis to growth influencing the growth direction.

At the end, chapter 5 will describe a wide systematic scheme of simulations with the aim to understand the behavior of a fluid droplet deposed onto a surface and influenced by the presence of a mobile perturbation.

In this last case, three fundamental parameters, essential to describe the dynamic activity of the droplet, were independently changed in order to observe their effect as single entities or in cooperative mode. A total of 150 simulation were performed and a general explanation of the trends observed will be shown. The ability to control the motion of fluid micro-drops can open a wide range of possibilities in the design of new devices such as micro-pumps, micro-engines or micro-reactors.

This thesis work describe in a wide and exhaustive way the possible use of particle-based models to simulate mesoscopic phenomena with different origin.

My activity was focused on the study of active droplets, with the development of a mechanical model with peculiar characteristics able to induce fluid droplets to behave like entities able to smart react under external stimuli of perform active processes from their inside.

The introduction and the implementation of elements in the model able to close the gap between a passive/inanimate droplet to a biological organism was one of the main achievements obtained during my PhD.

2. Computational methods

In this chapter a general description of the computational methods used during my PhD thesis will be presented.

In particular, an overview of Molecular Dynamics (MD), Dissipative Particle Dynamics (DPD) and other computational tools and their features will be provided.

2.1. Molecular Dynamics

The Molecular Dynamics technique is one of the most powerful computational tools for solving, numerically, a many body problem or, from a chemistry point of view, a many atoms system.

MD allows to understand the behavior of big molecules in different environments and in different conditions and is able to consider, simultaneously, many kinds of intra-molecular and inter-molecular interactions. It can also be coupled with quantum-mechanics (QM) calculation techniques.

The importance of the connection between MD and QM is due to the fact that MD is based on a classical engine or, in other words, all the equations that govern MD, derives from classical physics and not from quantum-mechanics. For this reason, the possibility to use QM and MD together allows to expand the range of use of the technique and to find solutions for different chemistry problems.

In molecular dynamics, the use of classical physics instead of a QM description is mostly due to computational cost related to the size of the system. The description of a polymer or a protein of thousands of Dalton, solvated by a solvent, with a QM approach, is still impossible in terms of complexity and computational costs.

If QM is widely used for the electronic description (orbitals, energy, charges etc.) of relatively small molecules, the use of MD is in any case necessary and still accurate to obtain some properties or to understand the behavior of huge molecular systems.

In MD, the Newton equations of motion govern the dynamics of the atoms present in the system through the forces that acts on each of them. The acceleration and the direction of the motion of each individual atom is determined by the interaction, in a classical view, between itself and the other atoms present in the simulation or, in other cases, by an applied external force (e.g. an external electric field).

Every atom, at each step of the simulation, is characterized from its position and its momentum. At each time-step (t_0) of the simulation, each atom is in a position expressed

by the three spatial coordinates (x, y, z). The position at time t_0 is determined by the previous position and momentum and is due to the force generated by the influence of the other atoms in the position at the previous time-step (t_0-1).

For a system of N atoms, the force can be expressed by:

$$F_i = m_i \cdot a_i = m_i \cdot \frac{d^2 r_i}{dt^2} , \qquad i = 1, 2, 3, ..., N \qquad (2.1)$$

where r_i represent the position of the i-th atom at time t and F_i is the total force acting on it. The calculation of the force at every time step is the most time consuming part of an MD simulation.

2.2. Molecular Mechanics

Molecular mechanics (MM) is a branch of the computational chemistry that describes the behavior of atoms and molecules, in terms of classical potential energy functions.

The goal of MM, an integral part of MD, is to give an accurate description of the system in terms of potential energy (V), that is the fundamental quantity required in order to have a complete view of the system.

Understanding the potential energy of a molecule in a particular environment, and at a particular time step, means to have the possibility to understand how the system will evolve in time. As the potential energy at each time step depends on the position of every atom (e.g. all the atoms of a protein and all the atoms of the solvent in which is immersed), it is possible to use it for deriving forces, accelerations and, at the end, new positions of the atoms in the next time step, and repeat the procedure in a theoretically infinite loop. In a conservative system, the force and the gradient of the potential energy are related

$$F = -\frac{dV}{dr_i} \qquad (2.2)$$

The potential energy of a molecular system is the summation of the potential energy terms derived from bonded and non-bonded interaction, of every single atom, with its neighbors (normally within a certain cut-off radius).

$$V_{TOT} = V_{BOND} + V_{NONBOND} = (V_{STRETCH} + V_{BEND} + V_{TORS}) + (V_{VDW} + V_{EL}) \qquad (2.3)$$

Where $V_{STRETCH}$, V_{BEND}, V_{TORS} are the stretching, bending and torsional potential originating from the relative movement of the atoms conditioned by the presence of a chemical bond, while V_{VDW}, V_{EL} are the potentials derived from Van Der Walls and electrostatic (non-covalent) interactions.

The ensemble of the different formulations used to describe all the different interactions that an atom can share with its neighbors is commonly called Force Filed (FF). A FF is a set of equations used to describe interatomic, covalent and non-covalent relations. equation (2.4) shows the functions that describe the GAFF force field (Generalized Amber Force Field), commonly used for the simulations of organic molecules:[6]

$$V_{TOT} = \sum_{bonds} K_b \left(r - r_{eq} \right)^2 + \sum_{angles} K_a \left(\theta - \theta_{eq} \right)^2 + \sum_{dihedrals} \frac{V_d}{2} [1 + cos(n\varphi - \gamma)] +$$

$$\sum_{i<j} [\left(\frac{A_{ij}}{R_{ij}^{12}} - \frac{B_{ij}}{R_{ij}^{6}} \right) + \frac{q_i q_j}{\varepsilon R_{ij}}] \qquad (2.4)$$

V_{TOT} is the potential energy of the system, K_b, K_a and V_d are force constants that defines the strength of a bond, the rigidity of an angle and a torsional interaction. The last summation in equation (2.4) represents non bonded interactions, for each pair of atoms, in the form of a Lennard–Jones potential for V_{VDW} and Coulombic interaction for electrostatic attraction or repulsion.

It is important to emphasize that equation (2.4) only represent a possible set of interactions, which in this case constitute the GAFF.

In other FF the equations used to describe some of these interactions can be different. For example, in two distinct force fields, the same chemical bond can be represented in two different ways, for instance in one case with a Morse potential and in another case with a simple hookean harmonic potential (see Figure 2.1).

Additional terms can be also added for the description of particular phenomena such as π - π interactions, polarization, and some strong non-bonded interaction.
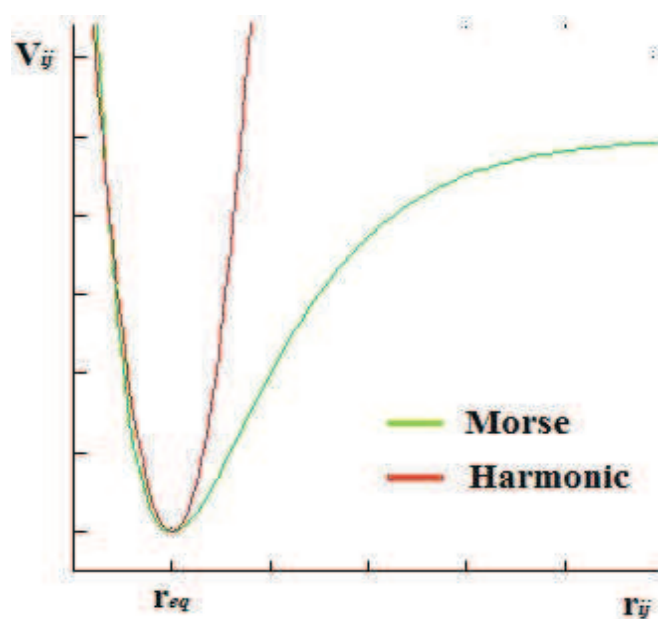
Figure 2.1. Comparison between a Morse potential (green) and a hookean harmonic potential (red). r_{ij} is the inter-atomic distance, V_{ij} is the potential energy. The equilibrium distance (r_{eq}) corresponds to the minimum of both potential curves.

The parameterization of a FF is crucial for the accuracy of the calculation and for the solution of a wide variety of chemical problems of different molecular systems.

Parameterize a FF means to associate parameters and constants to a particular atom type. Each force field, in fact, contains its own list of atom types (see Table 2.1 for the list of the basic atom types in GAFF) which are a special classification of chemical elements, based on the different characteristics they can express inside a molecule and in a particular environment.

Table 2.1: Basic atom types in GAFF (from ambermd.org).

Atom type	Description	Atom type	Description
c	sp2 C in C=O, C=S	o	sp2 O in C=O, COO-
c1	sp1 C	oh	sp3 O in hydroxyl group
c2	sp2 C, aliphatic	os	sp3 O in ether and ester
c3	sp3 C		
ca	sp2 C, aromatic		
n	sp2 N in amide	s2	sp2 S (p=S, C=S etc)
n1	sp1 N	sh	sp3 S in thiol group
n2	sp2 N with 2 subst. readl double bond	ss	sp3 S in -SR and SS
		s4	hypervalent S, 3 subst.
n3	sp3 N with 3 subst.	s6	hypervalent S, 4 subst.
n4	sp3 N with 4 subst.	hc	H on aliphatic C
na	sp2 N with 3 subst	ha	H on aromatic C
nh	amine N connected to the aromatic rings	hn	H on N
		ho	H on O
no	N in nitro group	hs	H on S
		hp	H on P
f	any F	p2	sp2 P (C=P etc)
cl	any Cl	p3	sp3 P, 3 subst.
br	any Br	p4	hypervalent P, 3 subst.
i	any I	p5	hypervalent P, 4 subst.

Understanding the role and the origin of the forces and potentials is crucial for understanding how MD, and other kind of coarse grained simulations, works.

Force Fields designed for MD are commonly called empirical FF, because their parameterization directly on experimental observations of atoms and molecules. This is one of the most differences between MD and QM. In QM some atoms and molecules properties can be calculated from first principles without primitive information on the system under study. This is the case of ab-initio methods, where the Schrödinger equation may be calculated without the use of any experimentally-derived parameter.

In the framework of the integration algorithms, acceleration calculated from the forces is used for the calculation of the new atom position in the next time step, after the correction derived from the application of the thermostat and barostat (in a canonical or in an isothermal-isobaric ensemble).

There are a variety of algorithms used for integrating the Newton equations of motion; the Verlet algorithm is one of the more common.[7]

Verlet algorithm allows to obtain the position of the particles at the next step from the position at the previous two time step, as follows:

$$\vec{x}(t + \Delta t) = \vec{x}(t) + \vec{v}(t)\Delta t + \frac{\vec{a}(t)\Delta t^2}{2} + \frac{\vec{b}(t)\Delta t^3}{6} + \cdots \qquad (2.5)$$

$$\vec{x}(t - \Delta t) = \vec{x}(t) - \vec{v}(t)\Delta t + \frac{\vec{a}(t)\Delta t^2}{2} - \frac{\vec{b}(t)\Delta t^3}{6} + \cdots \qquad (2.6)$$

equation (2.5) and (2.6) represent the Taylor expansion of the position vector at time t. The accuracy of the method depends on the degree to which the expansion is truncated.

The sum of equations (2.5) and (2.6) allows to erase the first and the third-order terms and obtain the final equation where the velocity vector is not explicitly present.

The position vector at timestep ($t+\Delta t$) can be so expressed as follows:

$$\vec{x}(t + \Delta t) = 2\vec{x}(t) - \vec{x}(t - \Delta t) + \vec{a}(t)\Delta t^2 + \cdots \qquad (2.7)$$

Although the velocity is not present in the algorithm, it is possible to derive it from the trajectories and so from the position vector at different time step:

$$\vec{v} = \frac{\vec{r}(t + \Delta t) - \vec{r}(t - \Delta t)}{2\Delta t} \qquad (2.8)$$

2.3. Coarse Grained Dynamics

The brief description of Molecular Dynamics methods was a necessary step to introduce in a more detailed description another type of dynamics, the coarse grained (CG) dynamics.

Simulations based on a CG approach differ from MD in some fundamentals but they use the same MD engine in terms of integration of the Newton's equations.

Since a large part of my PhD work was focused on CG, a description of how it works is necessary.

One of the problem of a computer simulation is the computational cost, that is the time required to solve all the equations needed to obtain the new particle coordinates starting from the previous positions.

Given a system consisting of N particles, considering all the number of pair interactions, it is proportional to N^2. This means that the total computational cost increases quadratically when the system becomes bigger and the number of particles increase.

For this reason, some tricks are always used in order to reduce the number of degrees of freedom or, in other words, the number of equations to solve at every time-step. Some of these tricks are based on the reduction of the number of interactions, for instance, with the

creation of particles lists (e.g. Verlet list or Cell list, see Appendix 1) and the introduction of cut-off radius (r_c) for the exclusion of all the interactions between the couples of particles with distance above r_c.

Despite the improvements in the efficiency of the algorithms and the enormous increase in performance of the computers, the impossibility to simulate, in a reasonable amount of time, big chemical systems considering all the atoms details (in a QM way an also with a classical approach), is still a matter of fact.

In a coarse grained simulation, atoms and molecules are grouped inside bigger particles which can be considered new fundamental elements of the simulation. A big molecule, for example a polymer, can be represented by an ensemble of particles where each one ideally contains a group of atoms or the entire repetitive unit (Figure 2.2 b). Water can be represented by an ensemble of particles where each particles contains a certain number of H_2O molecules, (Figure 2.2 a).
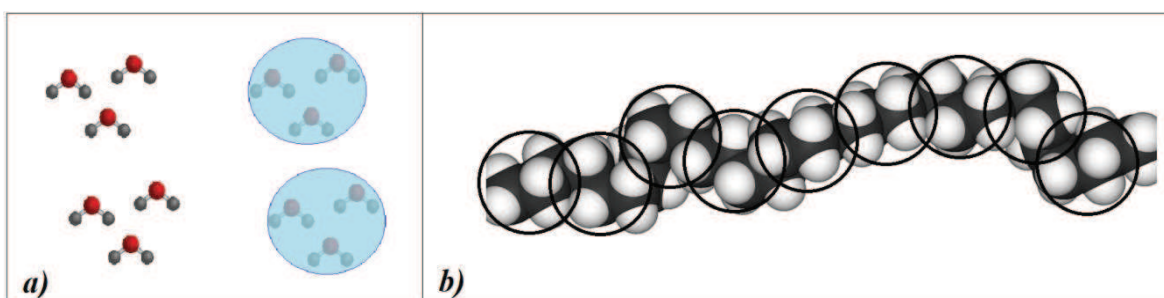

Figure 2.2. a) Three water molecules can be grouped inside a single beads. b) A polymer can be simplified as a chain of beads, in case of polyethylene every single CH_2 can be represented as a bead and between two beads one can establish an interaction to mimic the CH_2-CH_2 bond.

In a CG simulation the number of particles of a certain system can be drastically reduced. It is clear that with this approach it is possible to simulate bigger systems than in a fully atomistic approach, with a direct consequence for the computational cost.

An important aspect in CG methods is the choice of the interactions between the particles. The set of interactions have the aim to reproduce the physical and chemical properties of the system under study. For example, an ensemble of beads (a synonym of particles widely used in CG models) that represents a water environment have to mimic the behavior of a real water system and reproduce its properties.

In any case, the simplification of the system in terms of number of equations that have to be solved is remarkable, as shown in Figure 2.3.

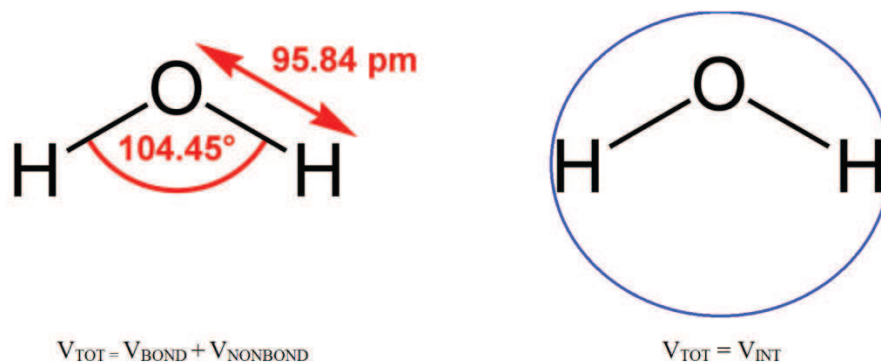$V_{TOT} = V_{BOND} + V_{NONBOND}$ 　　　　　　$V_{TOT} = V_{INT}$

Figure 2.3. An atomistic representation of a water molecule is shown on the left. The potential is due to the summation of all the intra-molecular interactions, V_{BOND}, and also the inter-molecular interactions, $V_{NONBOND}$, formed by all the pair interaction between every single atom of one molecule with every single atom of every other molecules in the system. A coarse grained approach, to the right, consists in the representation of the water molecule as a spherical particle. The potential is due only to inter-particle interactions, V_{INT}, between couple of beads.

2.4. Dissipative Particle Dynamics

Dissipative particle Dynamics (DPD) is a computational method based on a coarse grained approach, where an efficient combination of equations allows to reproduce, in a simple way, equilibrium processes of interacting particles. Time and length scale of this computational method belong to the mesoscale regime (Figure 2.4).
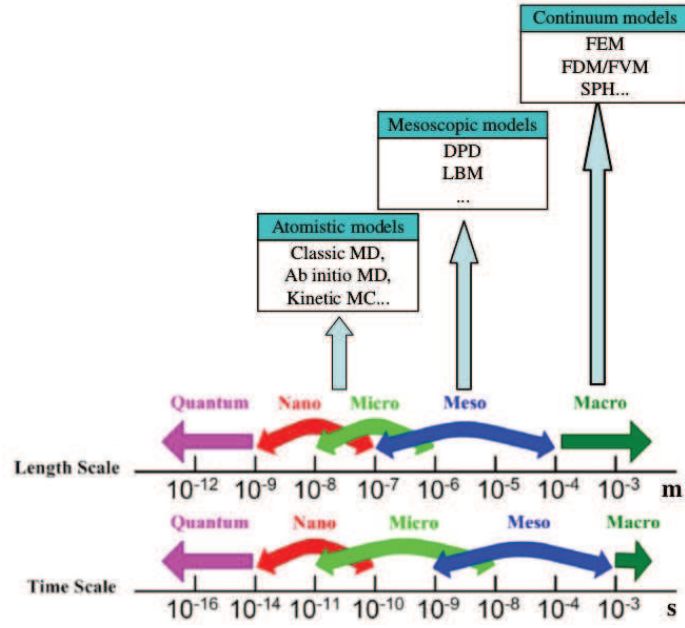
Figure 2.4. Comparison between different computational methods in terms of size and time scale for the integration of Newton's equations. Dissipative Particle Dynamics works in the range of the mesoscale allowing to simulate bigger systems and to observe phenomena that occur at bigger timescales than in Molecular Dynamics. Image from ref. 8.

As stated by Moeendarbary et al. DPD is "arguably one of the best mesoscale simulation techniques, and in the near future, has the potential to emerge as an even more widely used modeling and simulation technique for many complex fluid systems".[9]

DPD may be considered as a thermostat, similar in some aspect to the Langevin thermostat: the particles, which obey to the fluctuation dissipation theorem, are constrained to maintain a certain kinetic equilibrium dependent on the assigned temperature.

The initial development of DPD is due to the works of Hoogerbrugge and Koleman[10,11] and the subsequent reformulation of P. Español, R. D. Groot and P. B.Warren[12,13] which explained the proper relationship for the maintenance of the thermodynamic equilibrium in the full respect of the fluctuation-dissipation theorem.

In dissipative particle dynamics, particles, that represent cluster of molecular moieties (or in some case a single molecule), interact via conservative, dissipative and fluctuating (random) forces.

The total force, F_{DPD}, that acts on every single particles, is given by

$$F_{DPD} = \sum_{i \neq j}(F_{ij}^D + F_{ij}^R + F_{ij}^C) \qquad (2.9)$$

where F^D, F^R and F^C, are the dissipative, the random and the conservative force respectively. F_{DPD} is the result of a pairwise sum of the three force components cited above and it is used as input force for the integration of the Newton's second law.

The core of the system, the thermostat, that allows the particles to be stable around a chosen kinetic energy, is made by the random force and the dissipative force.

The dissipative force, that ideally represents the cooling part of the thermostat, can be expressed as follow:

$$F_{ij}^D = -\gamma\omega^D(r_{ij})(\hat{r}_{ij}v_{ij})\hat{r}_{ij} \qquad (2.10)$$

where v_{ij} is the relative velocity between two beads, $\hat{r}_{ij}$ is the unit vector, γ is the friction constant and ω^D is the weight function for the dissipative force.

In practice, γ is a parameter that determines the magnitude of the friction and is weighted by a function proportional to the relative position of the two particles examined. The dissipative force is also directly proportional to the relative velocity and for this reason becomes bigger as the relative velocity of the particles increases.

The random force, that is the heater of the particles, has the following form

$$F_{ij}^R = -\sigma\omega^R(r_{ij})\hat{r}_{ij}\varepsilon_{ij} \qquad (2.11)$$

where σ is the statistical noise amplitude, ω^R is the weight function for the random force and ε_{ij} is a random variable that describes the so-called white noise.

Like the dissipative force, the random one has a parameter for the amplitude of the noise and a weight function, dependent on the relative position, that weighs the same amplitude.

The noise amplitude is related to the thermal energy k_bT as

$$\sigma^2 = 2\gamma k_b T \qquad (2.12)$$

while the weight functions, dependent on the relative distance between the particles, are not independent but coupled together

$$\omega^D = (\omega^R)^2 \qquad (2.13)$$

The relation shown in (2.13), allows dissipative and random forces to be linked and makes the thermostat satisfy fluctuation-dissipation theorem.

A simple way to explain fluctuation-dissipation theorem is to consider a system made by a particle moving inside a fluid at thermal equilibrium. During its movement the particles encounter the resistance of the fluid and brakes, the kinetic energy of the particle is transformed into heat and transferred to the fluid molecules that, occasionally, pushes the particles provoking a change in its direction (Brownian motion) and an increase of its velocity. The result of this process is a continuous fluctuation of the kinetic energy of the particle around the value determined by the temperature of the bath and so the thermal energy of the system.

The variable ε in equation (2.11), that describe the white noise, assumes only values between 0 and 1, has zero mean and unit variance. White noise, that is implemented in the thermostat, does not provide any bias to the particle direction, ensuring a perfect random walk and, consequently, a pure Brownian motion.

Random and dissipative forces, together, brake the particles that are moving too fast and speed up the particles that are too slow, allowing, on average, the maintenance of the equilibrium in terms of kinetic energy, strictly related to the reference temperature.

From a theoretical point of view the DPD thermostat could be used stand-alone, completely decoupled from the conservative term.

The conservative term, in fact, describes the chemical interaction between the particles and its mathematical form depends on the type of particles and the type of system that have to be simulated.

DPD thermostat could be used to simulate a large variety of particle-based systems with different properties and different characteristics. The most common conservative interactions used in DPD simulations is a pair-wise soft potential interacting between beads. Being soft, the potential allows the partial interpenetration of the beads, forbidding the presence of empty space inside the system.

2.4.1. The Conservative Force

Hoogerbrugge and Koleman, the fathers of DPD, originally thought this technique as an engine for a system made by soft sphere, with the idea to simulate fluid systems thus reducing the computational costs.

Other developers of the method, such as D. Groot and P. B. Warren, made improvements trying to close the gap between atomistic and mesoscopic simulations, developing new features such as the introduction of an electrostatic interaction between soft particles and establishing a direct contact between the Flory-Huggins theory of polymers and the parameters of the conservative soft force.[12,14,15]

The description of the particle interaction inside our model it is implemented in its most common and simple form, namely as a linear function.

Because of its simple mathematical expression, the use of a proper linear force is a clever solution for our purpose and for the representation of a system made by soft spheres, where a moderate penetration between beads is allowed to preserve the system continuity. The most common and widely used DPD conservative force is, in fact, a linear repulsive force, where the interaction between beads is only governed by the slope of the linear function. An important addition introduced in our model is the use, in addition to the repulsive force, of an attractive force that allows us to reproduce attractive phenomena inside the model. This idea comes from the purpose to use the model for the simulation of "active" phenomena and so as to reproduce behaviors far from equilibrium. It is important to cite that in order to improve the computational method and extent its field of use, P. Warren and other workers in the field, also proposed different formulations for conservative force, introducing attractive components or, for example, equations able to change in relation to the local density of beads inside the simulation box.[16-18]

As described for the thermostat, also the conservative force acts between pair of beads. Inside a simulation box, different types of beads can coexist in order to represent different chemical entities. One of the simplest cases that could be described is the phase separation between two fluids, simulated as two different types of beads, e.g beads of type A and beads of type B (Figure 2.5). The system interactions will be described by three terms of the conservative force: the first governs the interaction between beads of type A and beads of the same type (A-A self-interaction), the second between beads of type B (B-B self-interaction) and the third term describes the interaction between beads of type A and beads of type B (A-B cross-interaction).
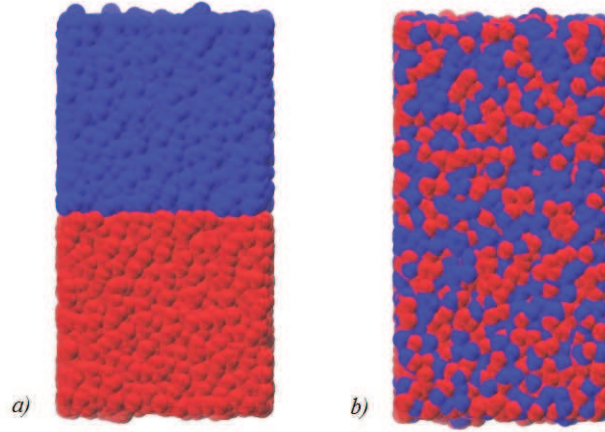
Figure 2.5. Final snapshots of two DPD simple simulations where only two types of beads are present in the simulation box, type A in red and type B in blue. For the simulation at least three parameters of the conservative force are necessary: the self-interaction A-A, the self-interaction B-B and the cross interaction A-B. a) A and B have a strong cross repulsive interaction and two phases are formed (e.g. water and oil). b) A and B have a low repulsive interaction and they can easily mix (e.g. water and ethanol).

The conservative force, in both soft repulsive and attractive forms can be expressed as follows:

$$F_{ij}^C = f_{ij}^C(r_{ij})\, \hat{r}_{ij} \qquad (2.14)$$

$$f_{ij}^C \begin{cases} a_{ij}\left(1 - \dfrac{r_{ij}}{r_c}\right)\cdot \hat{r}_{ij}; & r_{ij} \leq r_c \\ 0; & ;\quad r_{ij} \leq r_c \end{cases} \qquad (2.15\ a)$$

$$f_{ij}^C \begin{cases} a_{ij}\left(1 - \dfrac{r_{ij}}{r_{c1}}\right)\cdot \hat{r}_{ij}; & r_{ij} \leq r_{c1} \\ b_{ij}\left(1 - \dfrac{r_{ij} - r_{c1}}{r_{c2} - r_{c1}}\right)\cdot \hat{r}_{ij}; & r_{c1} \leq r_{ij} \leq r_{c2} \\ 0\,; & r_{ij} \geq r_{c2} \end{cases} \qquad (2.15\ b)$$

where r_{ij} is the distance between two beads, r_c, r_{c1}, r_{c2} are three different cut-off radii that determine if the force is switched on or off depending on the distance between the two beads; a_{ij} and b_{ij} are parameters applied for every couple of beads type and represent the maximum force that can be expressed between two beads of the specified type. In our model, b_{ij} is always negative, meaning an attractive force, while a_{ij} is always positive, preventing the particle fusion.

If only the repulsive component is activated in the model, only equation (2.15a) is used; if an additional attractive force is switched on with the introduction of a negative parameter b, then equation (2.15b) is implemented (Figure 2.6).
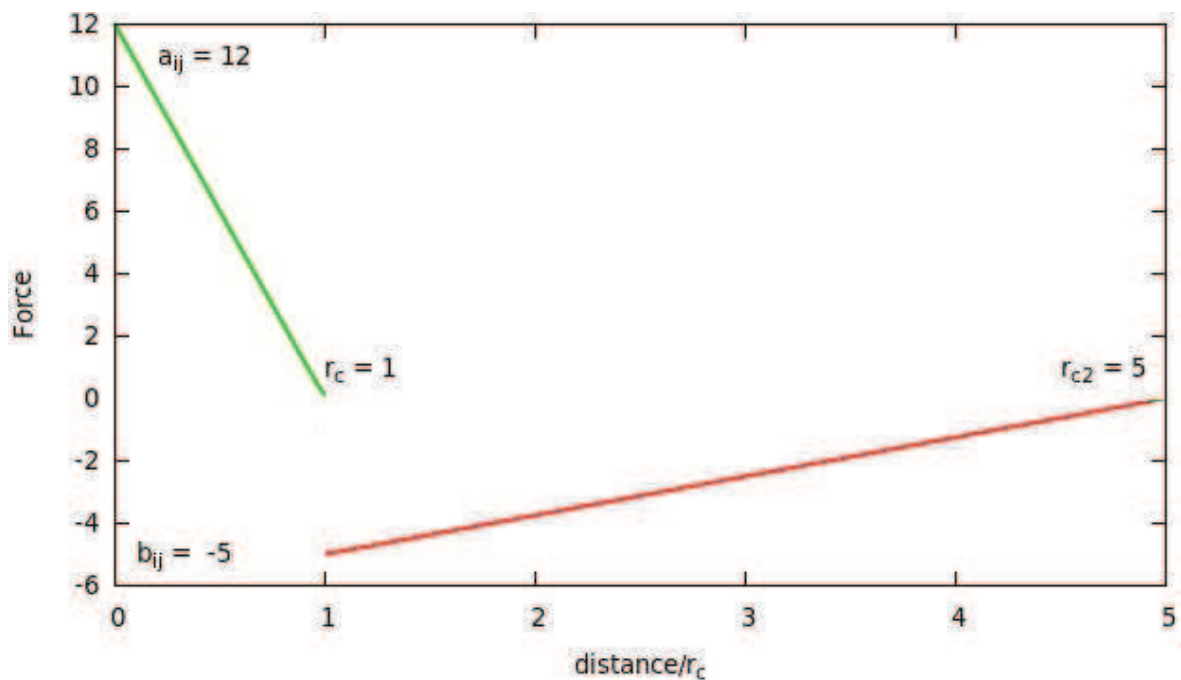

Figure 2.6. Graphical representation of (2.15b) implemented in the model. The repulsive part of the force is showed in green and the attractive part in red. The parameters a_{ij} and b_{ij} are the maximum repulsive force and the maximum attractive force, respectively. The two cut-off radii are also showed; above r_{c2} the force is 0.

Concluding this theoretical chapter, it is possible to observe how Dissipative Particle Dynamics is a simulation technique with many similarities with Molecular Dynamics in terms of computational procedures. The treatment of boundary conditions, the application of pairwise forces for the evaluation of neighbor interactions, the way to integrate the equation of motion are some example of this strict relationship. The main difference between the two techniques is undoubtedly the different range of application in terms of

length and time scales, that allows DPD to be an innovative and important tool for the evaluation of properties that do not appear at atomistic level but that are close to those of the continuum. The conservative force in DPD, although it could be arbitrarily complicated, is made by soft forces, considerably simpler than a Force Field implemented in MD, allowing to reduce computational costs.

At the end, as in MD, the use of neighbor lists, the parallelization of the processes and the implementation of software able to run on Graphic Processing Units, will allow to solve more and more complex problems and simulate bigger systems, increasing the degree of details of every single model under study.

2.5. Computational methods Appendices

In the following Appendices, a short introduction to some computational useful tools will be presented. In all the simulations related to this thesis work, the tools in Appendix 1 and 2 are in some of their form implemented, in order to reduce the computational cost and obtain better system properties representation.

2.5.1. Computational methods Appendix 1

Verlet list and cell list

Each particle in a simulation box is able to establish an interaction with all the other particles present. For this reason, the calculation scales as N^2 and the computational cost increases quadratically with the system size in terms of particles number.

Because the value of pair interactions depends to the interparticle distance, some tricks can be applied to the computational procedure in order to reduce the number of interactions and increase the scalability. This is the case of Verlet list and cell list algorithms, both based on the assumption that beyond a certain distance between two particles, their interaction can be considered too small to be important.[19-21]

The basic concept under the Verlet list procedure, consists in the creation of a neighboring list of atoms for each atom in the simulation box. This list of atoms is updated periodically in a fixed interval of timesteps, allowing the calculation of all the pair distances only fewer times during the simulation. In this way the system scales as "m x N", where m is the average number of atoms that constitute the lists.

The list of neighboring atoms contains only the atoms below a certain distance from the reference one, this distance has to be chosen as a compromise between a small value, that

reduces the number of atoms in the list, and a high value, that produces a more accurate model but increases the number of pair interactions. To create the list, all the atoms inside a sphere (3D view) of a fixed radius, also called cut-off radius, is built around the reference one.

In order to increase the accuracy and avoid a too frequent update of the list, a so called "skin" is added to the cut-off radius to increase the number of atoms under consideration (Figure 2.7). A fundamental assumption of this procedure is the list invariance between two subsequent updates, the update frequency depends on the value of the cut-off radius and the skin, as well as on how fast the atoms moves.
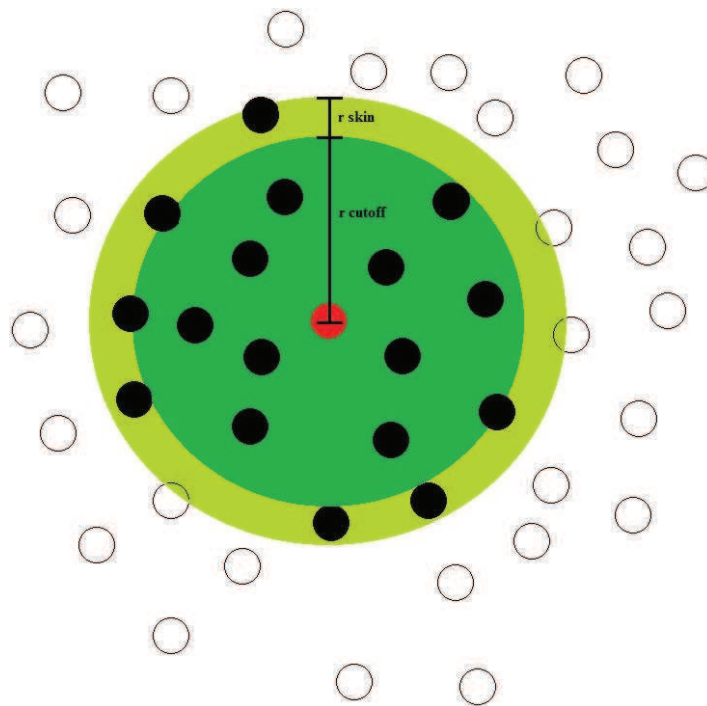
Figure 2.7. Verlet list conventional scheme: only the pair interactions between the red atom and its neighbors are calculated every timestep. Each atom in the simulation has an imaginary circle (2D representation) containing its neighbors, here represented by black filled spots. The core, here in dark-green, delimited by the cutoff radius, the outer layer, light-green, depends on the skin value.

The cell list is in some aspect similar to the Verlet list and has the aim to reduce the number of pair interactions and, as consequence, the computational cost.

At the beginning of the simulation, the box it is partitioned in cells with the edge equal or greater than the cut-off radius. After this process, a list of cell neighbors is created and remains fixed for all the simulation time. All the atoms inside a cell are labeled with an

index and compared with the atoms inside the neighbor cells. The assignment process of each atom to the appropriate cell scales as N and the number of pair interactions are restricted for the atoms belonging to the same cell or the neighbor ones.

Sincein the standard application of cell list, the cell size cannot be smaller than the cutoff radius, the probability of jumping in the calculation between atoms having a distance smaller than the cutoff radius it is 0.

Verlet and cell list are some methodological examples of how it is possible reduce the computational cost without affecting the simulation results. They are widely used in computational chemistry both in MD and CG dynamics. In the case of CG, the list is not based on atom comparison but on their fundamental entity, the beads.

2.5.2. Computational methods appendix 2

Periodic Boundary conditions

Periodic boundary conditions (PBC) are special boundary conditions used when the system under study can be well defined through an infinite set of repetitive units.

This is the typical case of a molecule immersed in a medium where the interactions with the box boundaries could create artifacts and does not represent the bulk properties of the system. The application of (PBC) avoids the excessive increase of the computational costs (the use of bigger boxes), suppressing border effects and the relative confinement problems, allowing to obtain better results using a smaller number of particles.

The application of PBC implies the creation of an infinite set of imaginary cells that are the exact replication of the simulation box, also called unit cell, in all three space dimensions (Figure 2.8). A particle that approaches the box border does not bounce on it, but it is able to pass through and to be projected exactly in the opposite side of the box with the same motion properties in terms of velocity and direction, without any border perturbation.

Another way to see this useful artifact is considering that every particle which experiences the simulation box from one side is replaced with another one, with exactly the same properties, on the other side of the box.
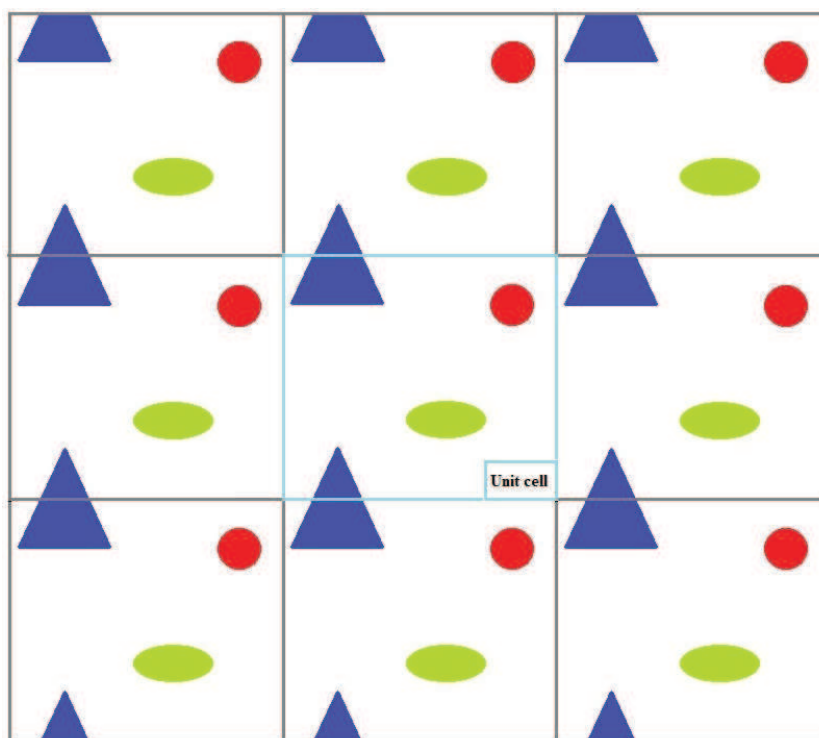
Figure 2.8. Schematic view of 2D PBC. The unit cell, delimited by the light-blue square, is replicated in all directions to form the imaginary cells. The blue triangle, that is passing the upper border, appears in the lower side of the box without any perturbation of the system.

In order to avoid self-interactions between a particle and its images, the cut-off cannot exceed the half of the shortest side of the simulation box, this caution defines the minimum image convention. Also the dimension of the unit cell has to be chosen carefully in relation to the system under investigation. Head-tail interaction of a big molecule inserted in a box too small is a typical artifact that has to be avoided in order to obtain reliable results.

Since the properties of the unit cell defines all the system, the application of Periodic Boundary Conditions, allows to reduce the computational costs and represents one of the most used tools in computational chemistry.

As in crystals, the shape of the unit cell has to be replicated in the three dimensions and for this reason spherical or elliptical shape of the unit cell are not allowed.

Obviously the PBC tool has to be applied when a bulk behavior is under study, in case of the investigation of a confined system, as in the simulation of particles behavior inside a vessel, the reflective boundary conditions, where each box wall allows elastic collision, represents a better solution.

24

3. Cell spreading, adhesion and morphology

3.1. Introduction

With the increase of the computer power and the improvement of the simulation techniques and algorithms, computational science has the opportunity to investigate more complicated and larger systems.

This fact opens new possibilities, especially in the field of bio-systems, which have intrinsically a complicated nature and are made by large molecular complexes.

Computational chemistry can assist in the development of the theoretical understanding of the biological processes that occur inside a living cell. For example the conformation of proteins, their functions and the catalytic effects of enzymes can be investigated with computational chemistry methods.

Molecular Dynamics studies of β-Amyloid peptides and fibrils are an example of how it is possible to look inside a protein structure in order to understand its behavior in terms of conformational changes and find structure-properties relations. Especially in the brain, the continuous cascade of ions, keep proteins and other molecular structures in permanent contact with electric fields. As an example, Toschi, Lugli and coworkers investigated β-Amyloid single peptides and studied the effects of electric fields on its structure and the possible implication on the formation of aggregates.[22,23] Andujar also investigated the effect of C_{60}, on the structure of β-Amyloid fibril, that is an actual target in the fight against the Alzheimer disease[24].

Until now, the study of single molecules, their reactivity and their general properties, has been the most important contribution in this field by theoretical chemistry but the possibility to expand the horizon, including the investigation of ensemble of molecules, or the study of the general behavior of entire cells, or even clusters of them, is now the frontier.

Some mechanical properties of living cells, such as their spreading, their deformation, and the interaction with the external environment, are not due to a single metabolic process but arise from the general activity of the entire cell. For this reason some different and more general approaches, distinct from classical molecular dynamics and quantum chemistry, can be developed with the aim of showing general properties of large systems.

Different computational techniques, ranging from continuum models such as Finite element methods (FEM), to coarse grained models, or combinations of them, can be used to show and predict cells activity.

Pivkin and Karniadakis developed a Coarse Grained model able to represent the shape and the properties of the red blood cells (RBC) membrane, as showed in Figure 3.1. They modeled the cell membrane using a "collection of points which are the vertices of the RBC surface triangulation", as the meshing procedure of Finite Element Method. The dynamics of the meshed membrane is governed by a set of equations, like in a ball and stick modeling.[25]
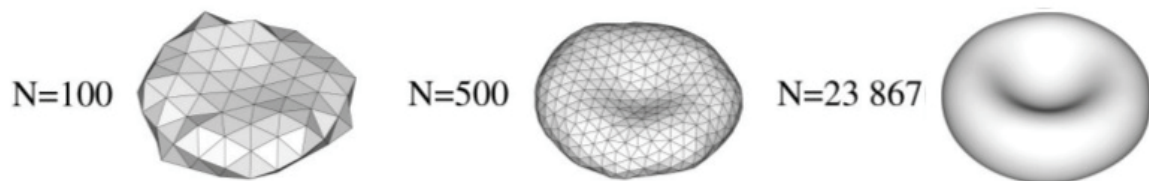
Figure 3.1. Membrane model for RBCs. Increasing the number of vertices means increasing the accuracy of the model (and also the number of degrees of freedom of the problem to solve) and closing the gap with a continuum model. Image adapted from ref. 25.

Inspired by previous simulations of cell motion in a tube flow by Pozrikidis,[26] the DPD technique and the associated coarse-grained discretization of the medium was used to simulate the flow of the blood in the body vessels.

Improvements of this remarkable study has been presented in others papers by Karniadakis, Fedosov and coworkers. The authors demonstrated the accuracy of the membrane model and the fluid flow in comparison with experimental results.[27-28] As an example of how powerful the development of computational tools for biological simulation in the mesoscale range can be, Fedosov and Gompper were also able to simulate, the phenomenon of white blood cells margination in body vessels with a similar improved coarse grained technique.[29]

During my PhD research activity, I worked on the development of a coarse grained computational model able to investigate some particular properties that living cells express in the processes of adhesion to a surface, such as shape deformation. In the following pages, I will present a brief review of what are the biological aspects that govern cells morphology and some mechanical and numerical models created with the aim to predict or rationalize their behavior.

A focus on the morphology can help to understand cells mechanical properties that may have consequences in the cell fate. An impressive example of this can be the work of

Kilian et al. where they show that stem cells attached onto a chemical patterned surface deform their original spherical shape, thus provoking a cascade of metabolic signaling that are even able to modify their differentiation.[30-31] The authors demonstrated that by patterning and functionalizing, with a microcontact printing technique, the surface where the cells are growing, it is possible to regulate the fate of mesenchymal stem cells. A cell round shape, for instance, promotes adipogenesis. On the other hand, a high cell spreading causes cells to become osteoblasts. The distribution of adhesive cues and consequently the spreading area distribution can also drive the cell to proliferation or to death, therefore regulating apoptosis.[32]

The works of Kilian, Chen and others demonstrated how the cellular shape can be used as a macroscopic observable to understand, induce and modify the cell fate. An important consequence of this can be the possibility to focus the attention on the representation of the macroscopic nature of cells. The properties of a cell, its biological activity and its mechanical properties are a combination of molecular interactions and chemical reactions. The study of the "building-blocks" that make the living cell can be carried out with experimental and computational tools focused on the nano- and sub-nanometric scale of length. Although their knowledge gives information about the cell behavior, the investigation of phenomena at molecular level has to be avoided if phenomena that occur at a higher scale of length are to be observed.

In mechanical terms, a cell can be considered as soft matter endowed with viscoelastic properties. This approach reduces greatly the number of degrees of freedom that have to be addressed and allows to simulate a larger systems, in the range of micrometers. The viscoelastic nature of a living cells has been tested repeatedly, for example recording the time required to recover their original shape after expulsion from a micropipette.[33]

Using a continuum mechanical model, based on a Newtonian fluid drop core encapsulated by a cortical shell, Evans and Yeung were able to describe numerically the entry process of a cell inside a micropipette.[34]

Can et al. proposed a similar but more complete model for the study of the dynamics of liquid drops under an extensional force. The model consisted in three regions characterized by differences in their surface tension: the outer membrane, the shell region and the soft core. The model "can explain several characteristics of leukocytes" and can be used as an example for a smart representation of living cells behavior without the use any inner cellular detail.[35]

Another way to investigate how cells govern their shape could be the introduction of an explicit representation of the cytoskeleton. Cellular cytoskeleton plays a fundamental role in cells, it largely governs their mechanical properties, the rigidity and integrity. It rules the movement, the migration under external stimuli and also, as previously showed, can induce the expression of particular metabolic cascade as a consequence of cell shape modification. The cytoskeleton acts like a scaffold inside a cell. It is able to separate and protect each organelle that, as consequence, is not free to fluctuate like in a simple water-like environment.

In a eukaryotic cell, the cytoskeleton is formed by a network of proteins such as actin, tubulin, myosin, spectrin, that are arranged in microtubules and filaments.

Spectrin forms pentagonal and hexagonal arrangements in the inner side of the plasma membrane, forming a scaffold structure fundamental for the maintenance of the membrane and cell integrity. It is connected to the cytoskeleton filaments in the cytoplasm and plays a key role also in the elasticity and rigidity of the entire structure (Figure 3.2).
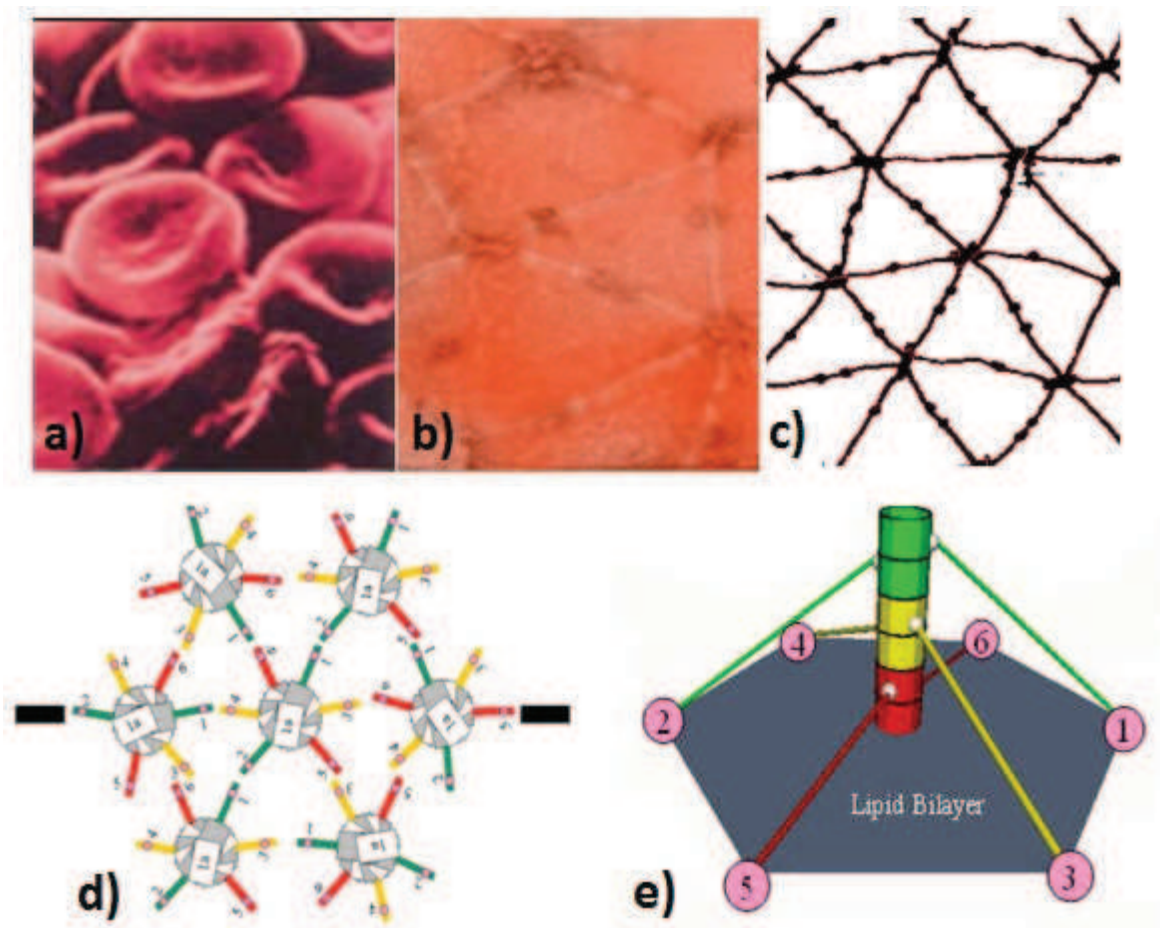
Figure 3.2. Schematic representation of spectrin in red blood cells: a) External view of a red blood cell; b) The spectrin network under the membrane in red blood cells; c) Model of the hexagonal network; d) The hexagonal network in detail, at the center of each hexagon a protofilament of actin acts as ligand between the membrane skeleton, made by spectrin, and the rest of the cytoskeleton; e) Side view of a spectrin network hexagon, where it is shown how spectrin attaches to a precise position the protofilament via actin-binding protein spectrin. These images are taken from the works of C. Vera, R. Skelton, F. Bossens and L. A. Sung of UC San Diego, for more details consult ref. 36.

In muscles, actin and myosin act together allowing the movement or providing force for the functioning of an organism. In other eukaryotic cells, myosin can literally walk on actin filaments to help in the regulation of the rigidity of the structure, in relation to the situation that the cell is facing. The cytoskeleton, in fact, is not a static structure, but due to the continuous process of polymerization and depolymerisation of actin filaments, can govern the cellular movement with the formation of protrusions, or stretch the cell when adhesion complexes are formed (Figure 3.3). When, for example via the extracellular matrix (ECM),

a cell probes the external environment and senses good affinity with some portion of the surface where the cell is laying, a process of adhesion is activated and the polymerization of the actin can guide the cell to reach the more favorable substrate. By consuming ATP, myosin can walk on the actin filaments transporting organelles and covering large distances inside a cell. Other specific proteins can also help in the transport of endocytotic and fagocytotic vesicles travelling for long distances in the cytosol.
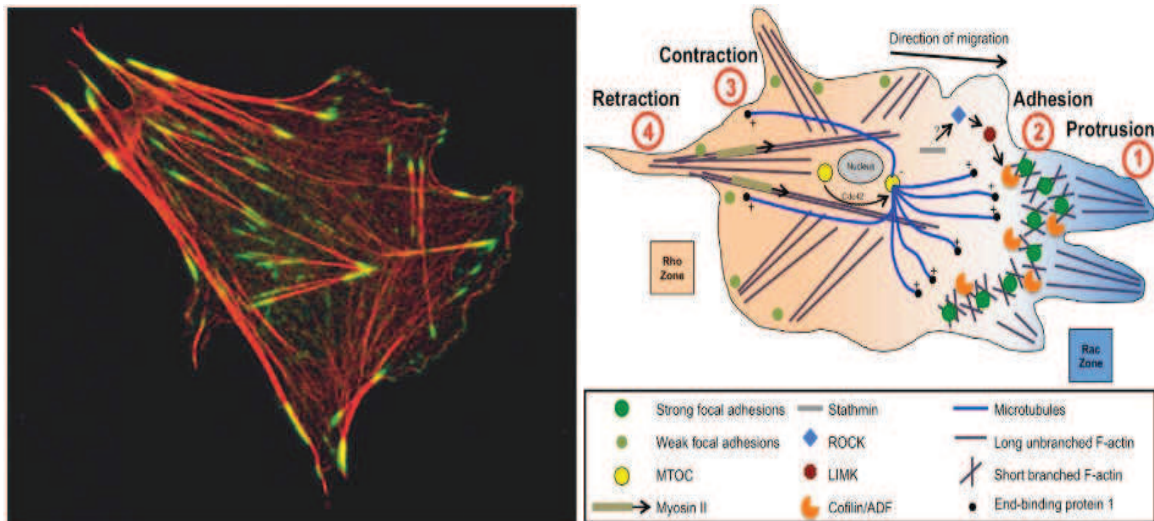

Figure 3.3. To the left, the picture of a living cell with many protrusions on its edges. The actin fibers, in red, push the membrane and induce cell deformation, another protein, paxilin in green, has the aim to attach the actin to the extracellular matrix giving a direct and strong contact for the cell to the surface. The adhesion points are non-static allowing the cell to change its shape and move. Image adapted from ref. 37. To the right a schematic model of the cell migration process. Image from ref. 38

Although an explicitly treatment of the cytoskeleton is a non trivial argument, tense-cable models[39] and spectrin-actin networks[40] are some examples of how it is possible to govern and control dynamics and forces that play roles in the processes related to cells deformation, movement and spreading.

From a computational point of view, designing a model with a full explicit representation of the cytoskeleton means a dramatic increase of the degrees of freedom and the number of equations to solve. In order to represent the cell mechanical properties accurately approximations have to be applied. This can be done by decreasing the spatial resolution of the cytoskeleton with a simplification of its molecular arrangement (e.g. using a polymer coarse grained representation of the actin filaments), or by the implementation of a set of

equations able to reproduce the cell mechanical properties without introducing an explicit cytoskeleton structure.

In the case of the model developed in this thesis, the second option was pursued and one of the major achievements of my PhD work was the accurate modeling of a cell mechanical and morphological properties, without the need of an explicit cytoskeletal representation.

3.2. Introduction to the Coarse-Grained model

In the computational methods chapter, I had the possibility to explain the mathematical background of the model that I am going to describe here in simpler terms. The idea of modeling a living cell using a coarse grained approach comes from previous work where the DPD technique was used to model a water droplet able to sense the changes in the surface hydrophilicity.[41]

When I write "modeling a living cell", I do not use a proper terminology for the description of the model. In practice, the reduction of the number of degrees of freedom that enables us to describe a cell makes our soft-sphere aggregate similar to an "active drop". An important review of Lach, Yoon and Grzybowski gives a really deep description of the state of the art in this field, taking into consideration how an "active" droplets can be close to a living cell, and a "dead" cell can be close to an "inactive" droplet.[42]

The major difference between an inactive piece of matter and a living one is the way to use the energy in order to overcome thermodynamically unfavorable pathways.

A molecule or an aggregate of molecules can explore only regions of potential energy surface that are allowed by the exploitation of the environmental thermal energy. A cell can instead use its reserve of energy (metabolic pathways) to overcome thermodynamically unfavorable energy barriers, performing activities that are a clear representation of non-equilibrium processes.

One of the main important points to clarify is that living matter is able to produce the required energy from inside, when it is needed, while inactive objects need an external energy supply to brake equilibrium.

From an experimental point of view, making a drop "active" means triggering a non-equilibrium process by acting on the ambient condition and observe its behavior in comparison with the one expressed by a living cell.

Bacteria are able to sense the different concentration of oxygen in water and orientate their movement; other flagellated photosynthetic bacteria are able to move, in a certain environment, in the direction of the major quantity of light.

Chemotaxis and phototaxis are relatively easy to reproduce in droplets.[43-48]

A living cell responds to changes in the external chemical environment or light with a cascade of metabolic reactions, while one or more simple chemical or photochemical reactions are used to drive droplets movement.

Other experimental work was focused on the creation of droplet-reactors, also called "protocells", where chemical reactions are performed inside a confined droplet structure such as a liposome.[49-51]

All the papers cited above are examples that go in the direction of understanding how living cells work, how they behave and how they use their properties.

Also in computational terms I showed some important achievements in the field of simulations of cell properties or part of them.

After this long introduction, I would like to come back to the aim of this dissertation. The main objective of my PhD work was the development of a coarse grained model able to mimic some mechanical properties of living cells, especially those connected to their morphology.

Dallavalle et al. introduced a smart use of Dissipative Particle Dynamics, describing the adhesion dynamics of "active drops" on surfaces with different chemical affinity and the motion of single drops and cluster of them in order to mimic and reproduce some peculiar properties of cells.[52]

In their coarse-grained description only a soft repulsive linear force was used to simulate all the different interactions between beads. The model described in a proper way the dynamical and static interactions of the drop with the surface with respect to biological cell. The recruitment of group of cells on a patterned surface, an interesting aspect for biomedical devices, is well described by the model, as showed in Figure 3.4.

This coarse-grained model represented the starting point of my research work.
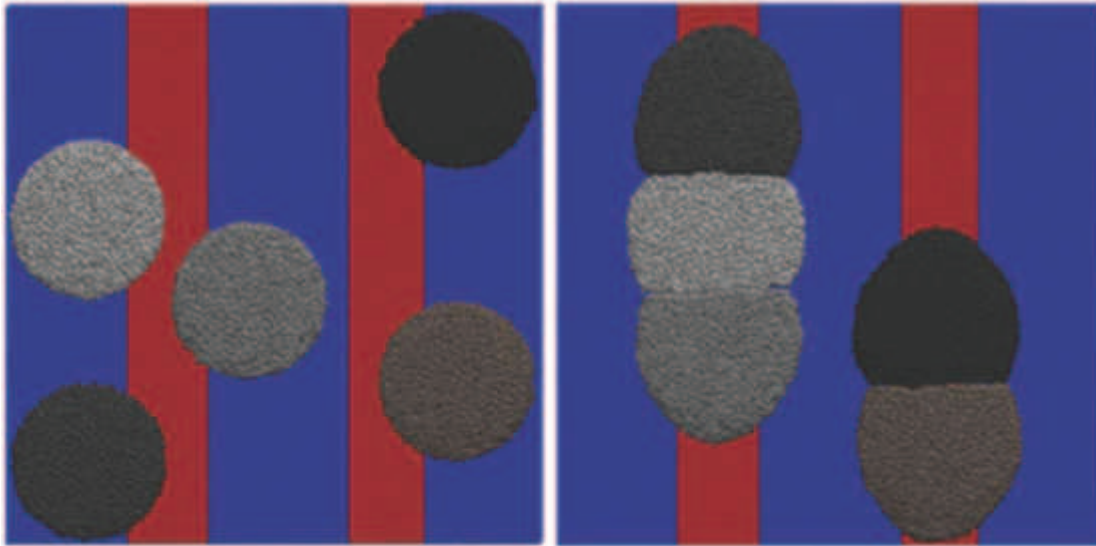
Figure 3.4. Top view of simulated "active droplets" (different grays colors) on a functionalized surface (active part in red). Left, the system at the beginning of the simulation; right, the system at the end, where the drops, that behave like cells, are recruited on the functionalized part of the surface. Image adapted from Figure 5 of ref. 52.

3.3. Description of the model

It is important to clarify that all the parameters are in dimensionless units. Later on a chapter will explain the conversion between the DPD parameters and physical units. The dimensions for distances and forces were defined a priori. They were chosen starting from experimental data of living cell sizes and from the magnitude of the adhesion forces they can express. In particular the length scale assumption for distance unit, 1 r_c, is 1.5 µm, while 1 unit of force has the value of $1x10^{-11}$ N. Although Dallavalle et al. introduced in the model different elements of complexity, such as the functionalization of the surface in order to investigate the recruitment process or the induction of a directed and biased migration, one of the main limitations of their representation was the inability to reproduce cells deformation in the presence of a patterned surface. My work started with the aim to improve the cell coarse-grained model, in order to made it more general and able to mimic a wider range of cells properties, first of all their morphology on patterned surfaces (see Figure 3.5).
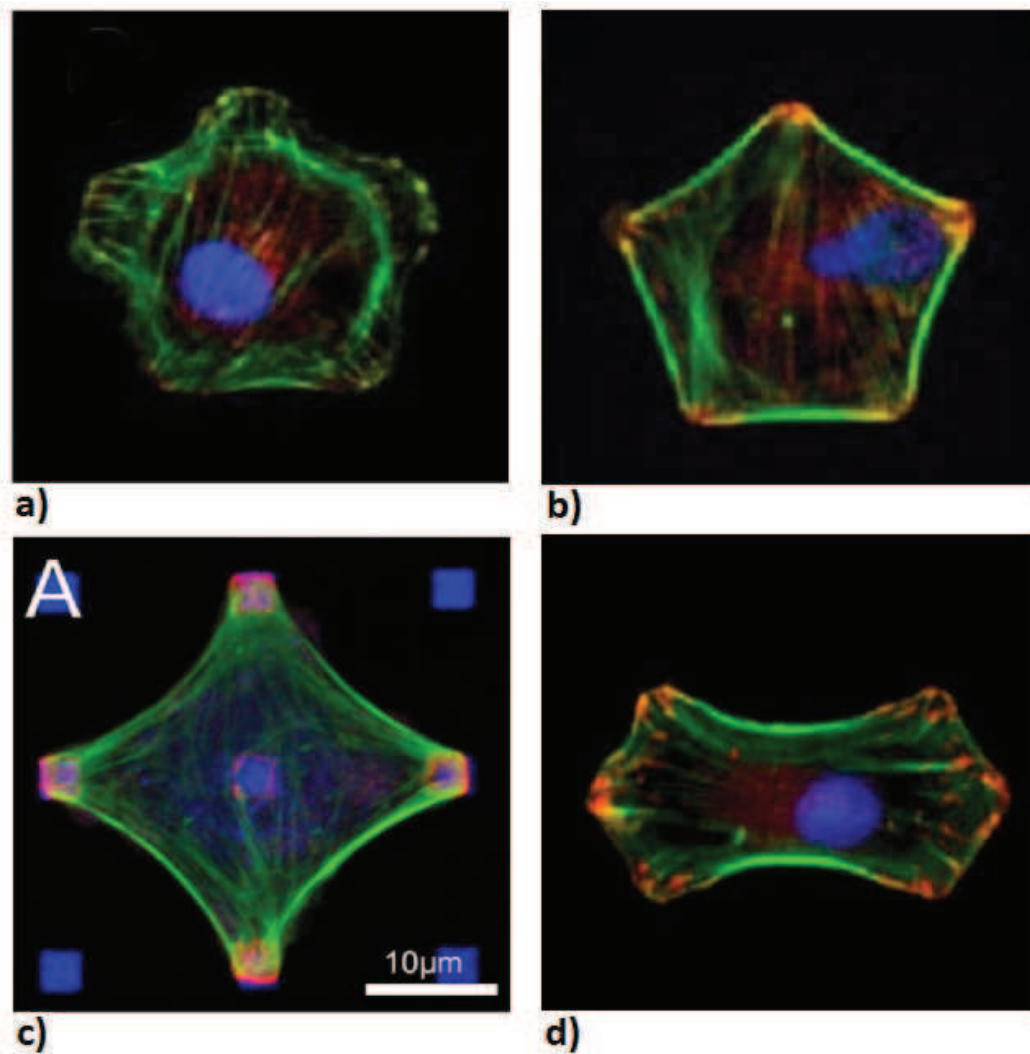
Figure 3.5. Experimental cell shapes used as reference for the simulations: a) flower-like; b) pentagon-like; c) square-like; and d) stretched-hexagon. [ref. 30 a, b ,d and ref. 53 c]

One of the limitations of the original model comes from its simplicity in the definition of the conservative force describing the inter-particle interactions. As I described in the computational methods section, a simple DPD simulation can be run using only a set of linear repulsive forces (see equation 2.15a). The affinity between different kinds of particles can be described by changing the value of the parameter a_{ij}: the greater the parameter, the greater the repulsive interaction. A simple system can be made by only three types of beads, one describing the drop, one describing the surface and one the medium (see Figure 3.6). For the droplet to retain integrity during the simulation, the repulsive parameter (a_{DD}) between droplet beads "D" has to be lower than the parameter a_{DM} between droplet beads and medium beads "M". Similarly, in order to avoid phenomena of

total surface wetting, the droplet-droplet parameter (a_{DD}) has to be lower than the droplet-surface parameter (a_{DS}).
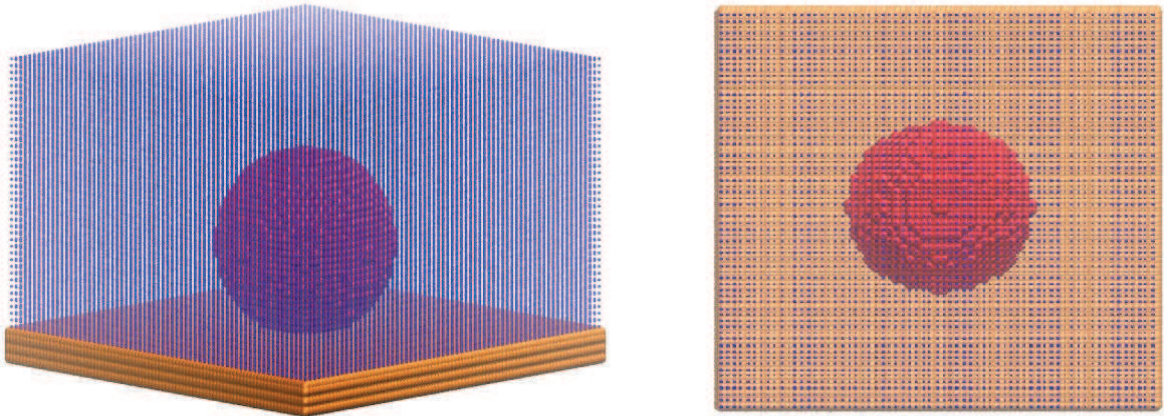

Figure 3.6. Side and top view of CG model for a droplet (red beads), immersed in a medium (blue beads), laid on surface (orange beads).

By properly tuning the droplet-surface and droplet-medium parameters it is possible to regulate the interaction between the droplet and the external environment, modify the surface wettability (see Figure 3.7) and the contact angle. The possibility to tune the different parameters a_{ij} describing the system does not allow, however, to consider and reproduce many properties that a cell can express: a living cell is an object extremely more complicated than a simple droplet!
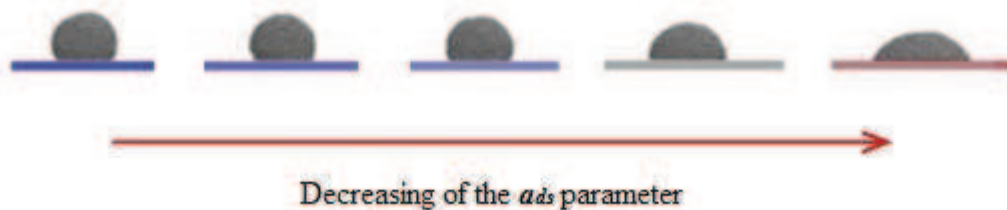

Decreasing of the a_{ds} parameter

Figure 3.7. Decreasing the parameter a_{ds} means increasing the affinity of the droplet for the surface, thus increasing the wettability and decreasing the contact angle and the related interfacial tension. Image adapted from ref. 52

A liquid droplet is an intrinsically passive system. Its shape is governed by the interfacial tension between the medium and the surface. The use of simple equations to govern the model means lowering the computational cost and for this reason the control of the droplet

interfacial tension only with a combination of simple linear repulsive parameter would be a possible solution. Unfortunately, a living cell is an active system that governs its shape by internal forces. The simple repulsive inter-particle interactions were thus not sufficient for the general description of active processes, where interfacial tension in no longer ruled by passive thermodynamic equilibrium but by methabolic processes. As a consequence, an improvement of the model was required, with the introduction of an "active" element and the introduction of a long range attractive force (2.15b).

The use attractive force introduces new possibilities for the control of the inter-particle interactions and allows to solve two important limitations. Firstly, with an attractive force it is possible to overcome the necessity to simulate all the different particles affinities only using repulsive parameters. Secondly, the introduction of a second cutoff radius, r_{c2}, permits to extend the range of interactions. For our purposes, as the cells are able to probe the external environment, the capacity of the cell beads to interact with the particles outside is the key to make our drop "active".

However, the intrinsic long-range nature of equation (2.15b) implicates a computational cost increase. As introduced in the computational method section, the activation of the equation (15b) involves the introduction of a second cutoff radius, r_{c2}, higher than r_{c1} (see also Figure 2.6), provoking an increase of the pair interaction to be solved at each time step, decreasing the efficiency of the Verlet list (see also appendix 1 in computational methods).

In order to balance accuracy and computational costs, proper considerations have to be made in the definition of the level of coarse-graining. Increasing the spatial resolution of the beads is possible but implies an increase of the computational costs. One of the main efforts of my work was the attempt to maintain a certain equilibrium between the implementation of new features in the model and the necessity to speed up calculations by reducing computational costs.

The experimental results of Kilian et al and Bischofs et al. demonstrate how a cell is able to deform in relation to a pattern designed onto the surface (see Figure 3.5).[53] Because of the various and complicated shapes displayed by the cells, this experimental work was taken as a benchmark for the improvement of the cell CG model used in ref. 52. From a biological point of view, the process of shape deformation begins when the cell sensing the chemical and physical properties of the surface. The process continues with the action of the cytoskeleton that guides the cell boundaries, pushing the membrane onto the chemical cues. The cell adhesion finishes with the integrin that binds the protein chosen for the

surface functionalization (e. g. laminin). It is clear that the cell coarse-grained model initially developed and based only on three types of beads (namely, the cell, the medium and the surface) is not suitable to describe the complex biological phenomenon of cell shape deformation. Also the standalone introduction of an attractive term in the DPD conservative is not sufficient to properly describe the process of deformation and obtain satisfactory simulation results.

When a living cell adheres onto a surface, it does not establish a continuum of interactions but concentrates the adhesive force onto confined sites. Focal adhesions (FA) are for instance one of the protein based macromolecular complexes that mediate between the extracellular matrix (ECM) and the actin cytoskeleton. The binding with the ECM, which involves integrin, allows to establish strong anchor sites for the cell and myosin molecules, exert a contractile stress on the actin fibers connected to the matrix, concentrating all the tension to the adhesion points.

The living cell adhesion process can be viewed as one of the main divergence points compared to liquid droplets. The capacity of cells to form chemical bonds on specific areas of the surface, made the adhesion stronger in comparison to the continuum non-covalent interactions that a liquid droplet establishes.

In general terms, the capacity of livings cell to concentrate the adhesion stress in specific points is the key factor to understand their different behavior in comparison to non-living matter. In order to mimic the cell behavior during the adhesion process onto surfaces characterized by the presence of chemical cues, the study of the biological processes involved was the starting point. Changing in the wettability of the surface by regulating the soft-repulsive a_{ij} parameter is no longer sufficient to mimic such complicate phenomenon and for this reason, the introduction of another bead type, here called active beads, acting as a connector between the cell body and the chemical cues, was required. The system developed is composed by five types of beads, one representing the cell "C", one the medium "M", one the surface "S", one the chemical cues "P" and one the active beads "A".

Each bead of fluid in the simulation interacts with the beads of the same type (self-interactions) and with the beads of the other types (cross-interactions). The parameters of interaction between the particles that constitute the surface ("S" and "P") have not to be imposed, because these beads have positions frozen in time. To avoid the unphysical phenomenon of the total overlap between beads, a repulsive force is always present, this also prevents the penetration of the fluid beads into the surface. Two attractive interactions
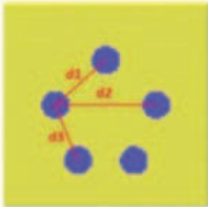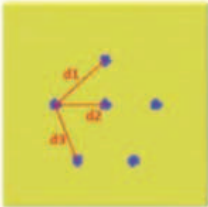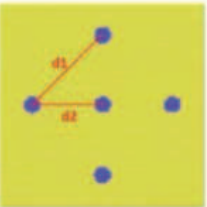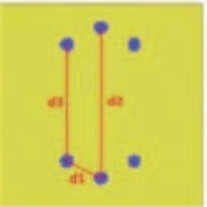
(2.15b) are implemented to simulate the active process of adhesion, the first one involve types "A" and "P", the second one involves types "A" and "C".

The "P" beads are created with a simple substitution of "S" beads, in order to reproduce the chemical patterns used to obtain the geometries in Figure 3.5; four geometries were implemented and investigated (Table 3.1): they are, Flower-like, Pentagon-like, Square-like, and Stretched-hexagon.

The "A" beads are not present at the beginning of the simulation but are dynamically created inside the cell with a transformation process, which involve "C" beads. In terms of number of beads, the entire system is made by about 220000 beads placed inside a simulation box of 36x36x25 r_c. r_c is the length unit, that was set equal to 1.0 for simplicity. The number density of beads (number of beads for unit volume r_c^3) was $\rho_{drop} = \rho_{medium} = 6$ for the fluid part of the simulation box, while for the surface ($\rho_{surface} = \rho_{pattern}$) was set equal to 15, in order to avoid the penetration of "C", "M" and "A" beads in the solid material. The system is initially composed by the three main component of the models, that are "C" beads (about 10300), "M" beads (about 163100) and "S" (about 46500). The chemical pattern "P" is introduced in the model by opportunely modifying the type of surface beads. The number of "P" beads used for each kind of pattern is shown in Table 3.1.

Table 3.1: Top view of the four pattern morphology and their features[a]

Features	Flower-like	Pentagon	Square	Stretched hexagon
Radius of each chemical cue	3.75	1.5	2.25	1.8
d_1	18.0	18.0	26.5	10.05
d_2	27.0	13.5	18.75	42.0
d_3	16.2	16.2		33.0
Total number of pattern beads of the cue spots	582	117	208	160

[a]*S beads, constituent of the surface, are shown in yellow, while P beads, in blue. Distance and radii are in micrometers. Table From ref. 54*

Since the idea of this work was to build up a general model valid for a wide range of morphologies and other cell properties, the main issue was the proper tuning of all the model a_{ij} and b_{ij} parameters in order to find a definitive set of them, valid for each simulation, without the necessity to make adjustment in relation to geometry.

Table 3.2 summarizes the parameters that were set to establish all the interaction between the bead types inside the simulation box. To test the robustness of the approach, for each geometry five statistical independent simulations where performed changing the random seed parameter for the distribution of the initial velocity of the beads. In this way we generated five different trajectories for each geometry maintaining identical the model parameters.

Table 3.2: List of soft repulsive parameters used in for the simulations.

a_{ij}		i =				
		A	**P**	**M**	**S**	**C**
	A	75	200	65	100	12.5
	P		/	100	/	100
j =	**M**			12.5	100	65
	S				/	160
	C					12.5

The cell-cell (a_{CC}) and medium-medium (a_{MM}) interaction parameters were set equal to $12.5 \cdot 10^{-11}$ N. In order to preserve the cell integrity and mimic the presence of the membrane, the cell-medium parameter (a_{CM}) was set equal to $65 \cdot 10^{-11}$ N.

The attractive interactions were defined between adhesion "A" and pattern "P" beads and between adhesion "A" and cell "C" beads. The attractive force "A"-"P" has to simulate the possibility of the cell to sense an external favorable chemical pattern, while "A"-"C" allows the cells to follow the adhesive particles in the direction of the chemical cues mimicking the action of the cytoskeleton that pushes the cell to extent onto a functionalized surface. With this expedient we are able to obtain two important achievements: the first one is to have inside the cell some particles that behave like sensors for the external environment, and they also bind the functionalized surface allowing the cell to adhere to the chemical cues; the second one is to mimic the behavior of cells spreading without an excessive complication of the model properties like adding new types of beads introducing an explicit model for the cytoskeleton.

As it is possible to observe in Table 3.2, the repulsive self-interaction parameters for "C" and "A" are $a_{CC} = a_{AA} = 12.5 \cdot 10^{-11}$ N, meaning that a perfectly homogeneous system is created, like in the presence of only a single type of beads. Setting the self-interaction parameter interaction for the medium beads equal to the one of the cell-cell interaction, that is $a_{MM} = a_{CC} = 12.5 \cdot 10^{-11}$ N, means that we assume the compressibility of the medium comparable with the one of the cell. This assumption is reasonable if one thinks that the main composition (about 80%) of a cell interior is water.

The attractive conservative force (equation 2.15b) is defined only for two pair-wise interactions: the adhesion sites-cell beads and adhesion sites-pattern beads. The corresponding attractive parameters are set $b_{AC} = -2.5 \cdot 10^{-11}$ N and $b_{AC} = -7.5 \cdot 10^{-11}$ N. Figure 3.8b displays the profiles of the total force acting between cell and adhesion sites

beads: the force is repulsive in the distance range between 0 and r_{c1} =1, it becomes attractive in the range between r_{c1} = 1 and r_{c2} = 3.5 r_c and is null for distances greater than r_{c2}.
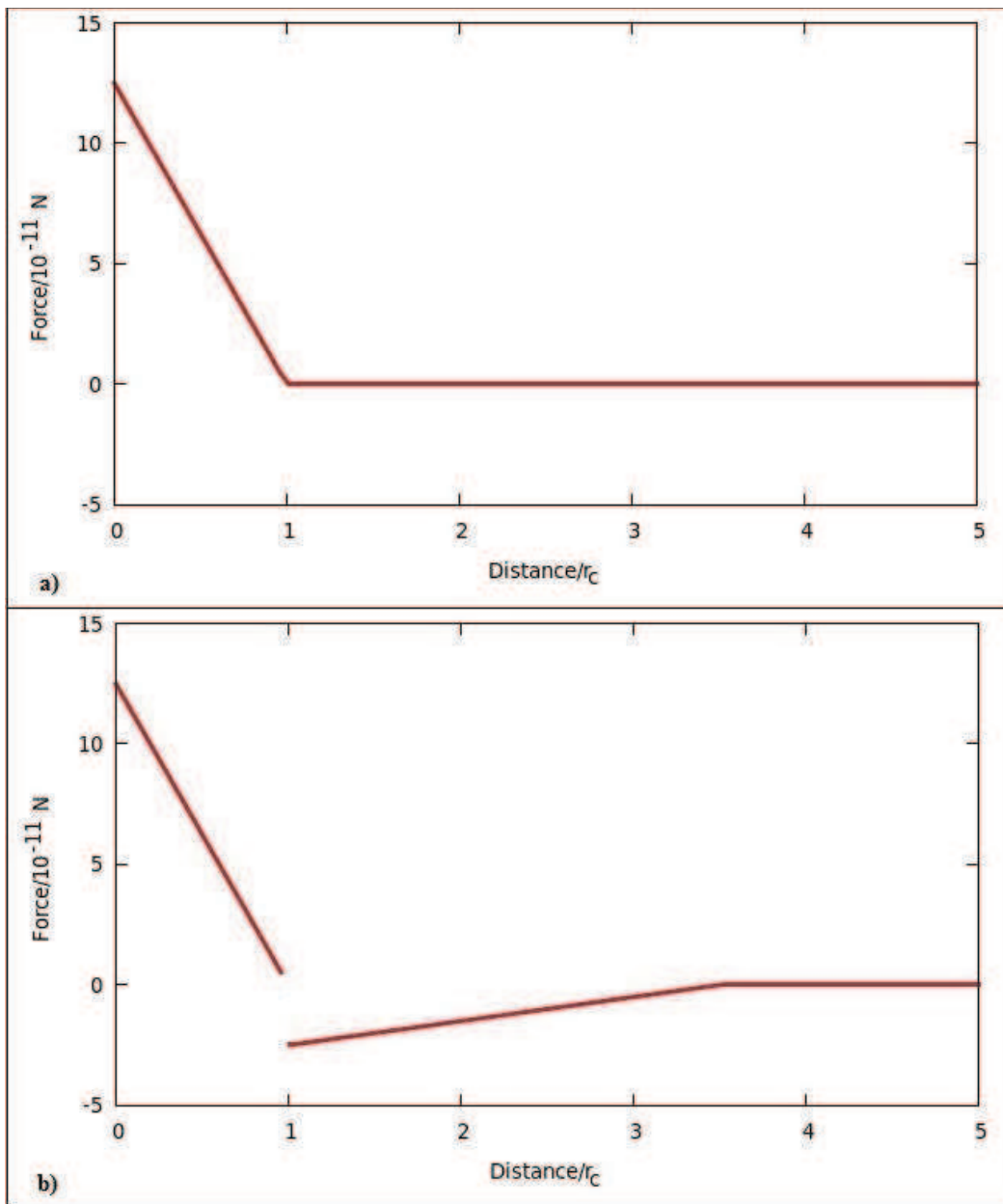

Figure 3.8. Forces of pair interaction profiles between two beads: a) General repulsive force interaction profile with a_{ij}=12.5 and r_c = 1.0, it could represent the self-interaction between C and C or the interaction between beads of type "M" and beads of type "M". Over the cut-off radius the value of the force is 0, meaning that the beads are not touching each other and so they do not interact; b) Force interaction profiles where both repulsive and attractive force are present, in this specific case a_{ij}=12.5, b_{ij}=-2.5, r_{c1}= 1.0 and r_{c2}= 3.5 such as in the interaction between Adhesive beads and Cell beads.

41

The procedure adopted to run the dynamics is the same for each kind of pattern, this is necessary to prove the robustness of the model. In brief, after the initial deposition of the spherical, drop-like aggregate on the surface, 2500 steps of equilibration where performed to thermalize the system. No "A" beads are present in the simulation box from the beginning to the end of this first equilibration run. When the cell is in equilibrium with the medium and the surface, a process of creation and deletion of "A" beads is performed inside the cell. Practically, "C" beads that constitute the cells can be transformed into "Adhesive beads" that trigger the cell deformation. Since the cut-off radius $\mathbf{r}_{c2}$ for the attractive force is set to $3.5r_c$, in order to decrease the computational cost, a list of "C" beads that are at a distance of less than $3.5\ r_c$, is generated and updated every 200 steps. Only the "C" beads inside the list can be transformed into "A" with a probability that reads

$$p = (1 - exp(-k\delta t) \qquad (3.1)$$

where k is empirically set to 0.05 and δt is the timestep.

For each "C" bead inside the list, at every time step, a random number with a value between 0 and 1 is generated and only if the value is smaller than p, particle "C" is transformed into "A". The number of "A" beads created at every time step depends on the size of the "C" list that can increase as far as the cell spreads over the surface.

A reverse mechanism where "A" beads are transformed to "C" beads is also implemented in order to avoid an excess of "A" beads in the cell structure. In particular, the back transformation is performed only for the "A" beads with a distance from the surface higher than $1.0\ r_c$. The dynamic process of creation-deletion is performed for at least 2200 steps and promotes a better distribution of the "A" beads on the "P" particles, allowing the removal of the "A" excess on the crowded spots (their position is high from the surface) and increasing them in the lacking zones (they can be closer to the surface).

At the end of this step, other 2500 steps of equilibration are performed before another single step of back-transformation from "A" to "C" to make sure that all the "A" in excess are removed. The final step of the protocol is composed by few re-equilibration steps where the cell can stabilize its energy and its morphology with a constant number of "A" beads in its inside. A synthetic scheme of the procedure used is given in Figure 3.9.

In order to show how the implementation of the attractive force is important to make the droplet "active", a reference run with only repulsive forces was performed for each kind of pattern. In this case, although "A" beads are created with the same procedure described for

the other dynamics, the cell does not have any driving force to move on P, its shape remain substantially spherical.
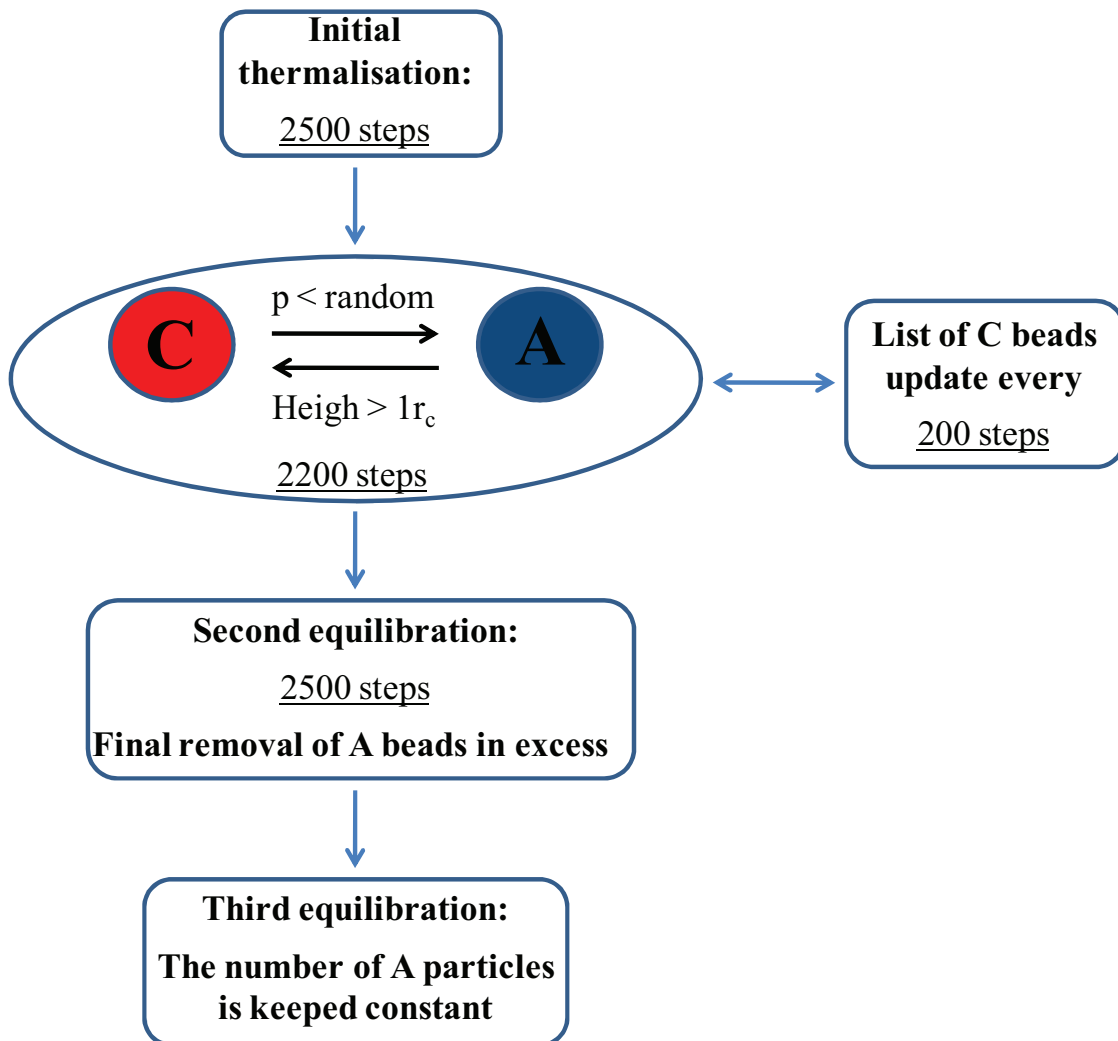

Figure 3.9. Scheme of the protocol of the simulations.

3.4. Simulation parameters and physical units

All the model parameters are expressed in dimensionless units. Mapping into physical units is possible. In order to link our simulations to reality, some assumption with a strong connection to experimental data is necessary. As mentioned above, the first assumption has been done for the force units, that assumes the value of $1x10^{-11}$ N. The second assumption is for the cell bead spatial resolution. Setting the length scale,1 r_c= 1.5 µm means that a cell bead has the dimension similar to that for organelles inside a living cells.[55,56] The bead radius is equal to 0.51 µm and the entire "drop-like cell" has a diameter of 15 r_c = 22.5 µm, consistent with the dimension of various living cells.

The length scale plays a fundamental role in the determination of an important physic quantity, the timescale **τ,** and as a consequence, the link between the simulation time and the spreading time for a living cell.

The timescale is determined using equation (3.2), that relates the experimental and theoretical diffusion coefficients of cell beads:

$$\tau = \frac{D_{calc}}{D_{exp}}[r_c]^2 = \frac{0.016}{5 \cdot 10^{-16}\ m^2/s} \cdot (1.5 \cdot 10^{-6}\ m)^2 \approx 70\ s \qquad (3.2)$$

The self-diffusion coefficient for the "C" beads, calculated from their mean square displacement, is D_{calc} = 0.016 r_c^2/τ. As a cell bead has a size comparable to that of mithocondria, the bead diffusion coefficient was compared to the experimental one of mithocondria in the cytoplasm, D_{exp} = 5x10^{-12} cm^2/s.[57]

It is important to clarify that the derived timescale depends a on the experimental data used, mitochondria, for example, have a dimension of around 2μm, close to the dimension of the beads, but their diffusion coefficients can range between 10^{-11} to 10^{-12} depending on their dimension and shape.

Using the Stokes-Einstein relationship (3.3) for a sphere of diameter 2 μm, the derived value of diffusion coefficient in water is around 3x10^{-9} cm^2/s, higher than the one found for mitochondria, this can be justified since the cytoplasm is not composed only by pure water, but is a complex matrix conditioned also by the presence of the cytoskeleton.

The Stokes-Einstein equation reads:

$$D = \frac{k_b T}{6\pi\eta r} \qquad (3.3)$$

where k_b it's Boltzmann constant, T the absolute temperature, η the liquid viscosity and r the radius of the spherical particle.

Considering the mitochondrial diffusion coefficient, one can estimate that the cytoplasm viscosity is ca. 70 cP, a value that is different from the water viscosity, that is around 0.7 cP at ~ 37 °C. Considering the size of the beads in the simulations and the viscosity of 70 cP, the diffusion coefficient calculated with Stokes-Einstein equation would be 0.65x10^{-14} m^2/s, less than two orders of magnitude compared to the mitochondria, that leads to a timescale of 6 s.

Considering the number of steps to perform the simulations and the input parameter of 0.02 τ for each timestep, the result is that in the first case, with a timescale of 70 s, the deformation process takes place in about 2 h, while in the second case in only 15 min. Taking into account that the timescale must be taken as only indicative, the experimental data of mitochondria diffusion and the relative 70 s timescale was chosen as reference for the model.

The parameter of thermostat friction coefficient γ was set to 5.61, in combination with a reduced temperature T* of 0.53. The reduced temperature can be correlated to the physical absolute temperature T = 310 K through the relation T = 133T* + 240.[58,59] We followed Groot's recommendation[12] of selecting values for time-step integration dt = 0.05 and γ = 5.61. The dimensionless system temperature T* was set to 0.53. Due to this choice of parameters, the cell retains its integrity over time and no bead leaves the aggregate, while we observed that for T* = 0.6 beads may escape from the aggregate. The cell is indivisible for the purpose of our simulation.

3.5. Results and discussion

Figure 3.10 displays the shapes of the model cells attached to solid surfaces, for four different patterns, at the end of the simulations. In addition to the simulations where the attractive forces were switched on (second and third column of Figure 3.10), also a reference simulation with only repulsive forces was performed (first column of Figure 3.10).

The computational results show the importance of the use of an attractive force (see equation 2.15b) for simulating the process of cell spreading and deformation. If an attractive negative force is applied on the pair interaction Adhesive-Pattern and Adhesive-Cell, the cell is able to sense and reach the chemical spot on the surface, reaching good agreement with the experimental images used as reference (fourth column of Figure 3.10). In other words, it is the attractive force that makes the droplet "active", giving to it the energy to overcome its initial spherical equilibrium geometry. On the other side, shape deformation is not achieved for the drop reference simulation.
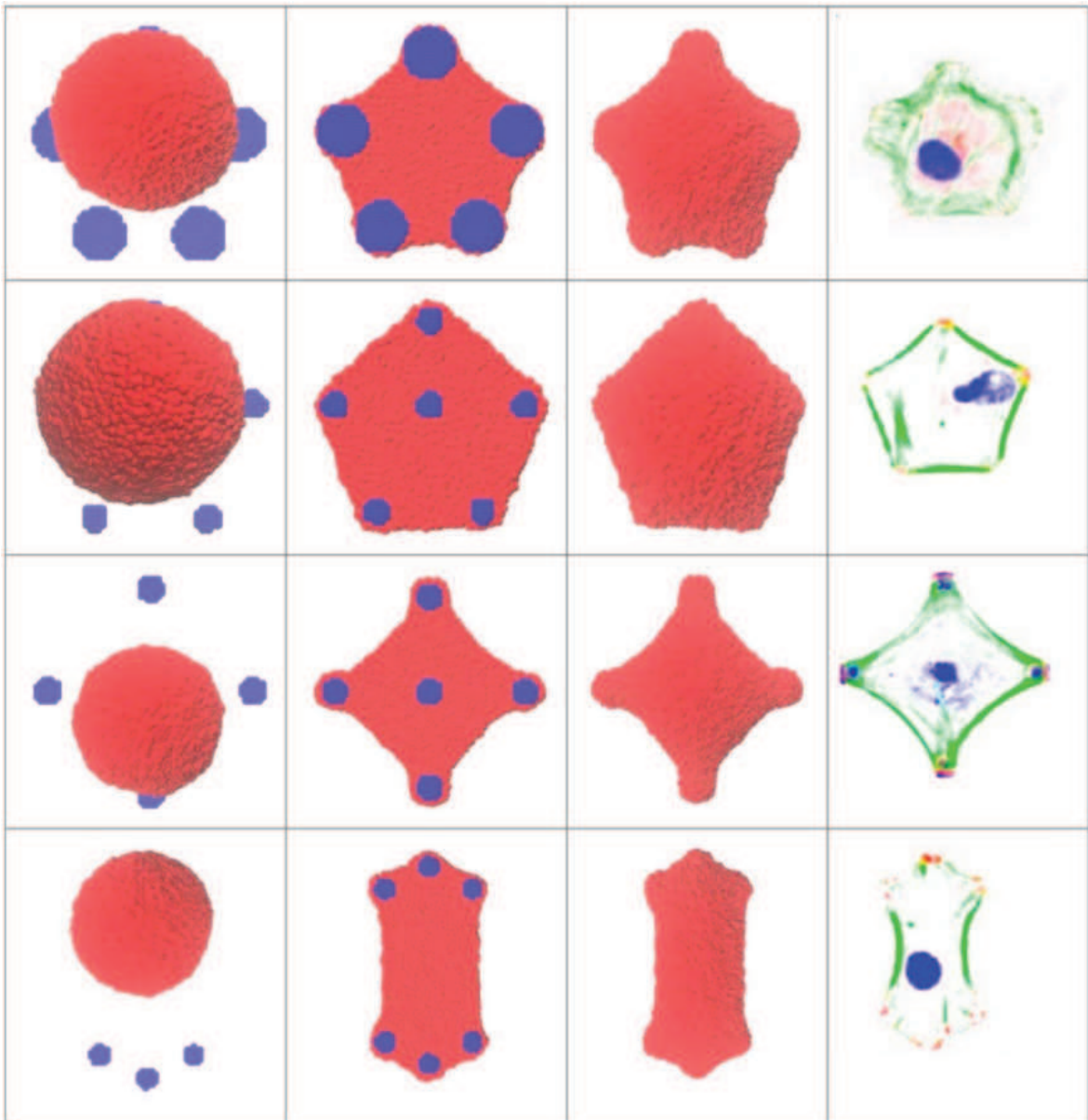
Figure 3.10. Results of the simulations for the four geometric cue pattern investigated: top to bottom flower-like, pentagon-like, square-like and stretched-hexagon. In first column is presented the results for the reference simulations without attractive force implementation, in second and in third columns the reverse and top view of the final geometries with "active" "A" beads, in fourth column the experimental images adapted from Figure 3.5.

It has been observed experimentally that the kinetics of the cell spreading can be described using a logistic equation, as follows[60]

$$\frac{dA}{dt} = rA\left(1 - \frac{A}{A_{max}}\right) \qquad (3.4)$$

where A_{max} is the maximum contact area that a cell expresses and r is the rate constant of spreading. Cell contact area was monitored during the spreading simulation and the data were fitted with the solution of the differential equation, as follows:

$$A(t) = \frac{A_{max}}{1 + exp[-r(t - m)]} \qquad (3.5)$$

where m is the constant of integration and gives the time where the inflection point of the curve ($A_{max}/2$) occurs.

The parameter m, r, and A_{max} were determined for the four simulated geometries and are listed in Table 3.3.

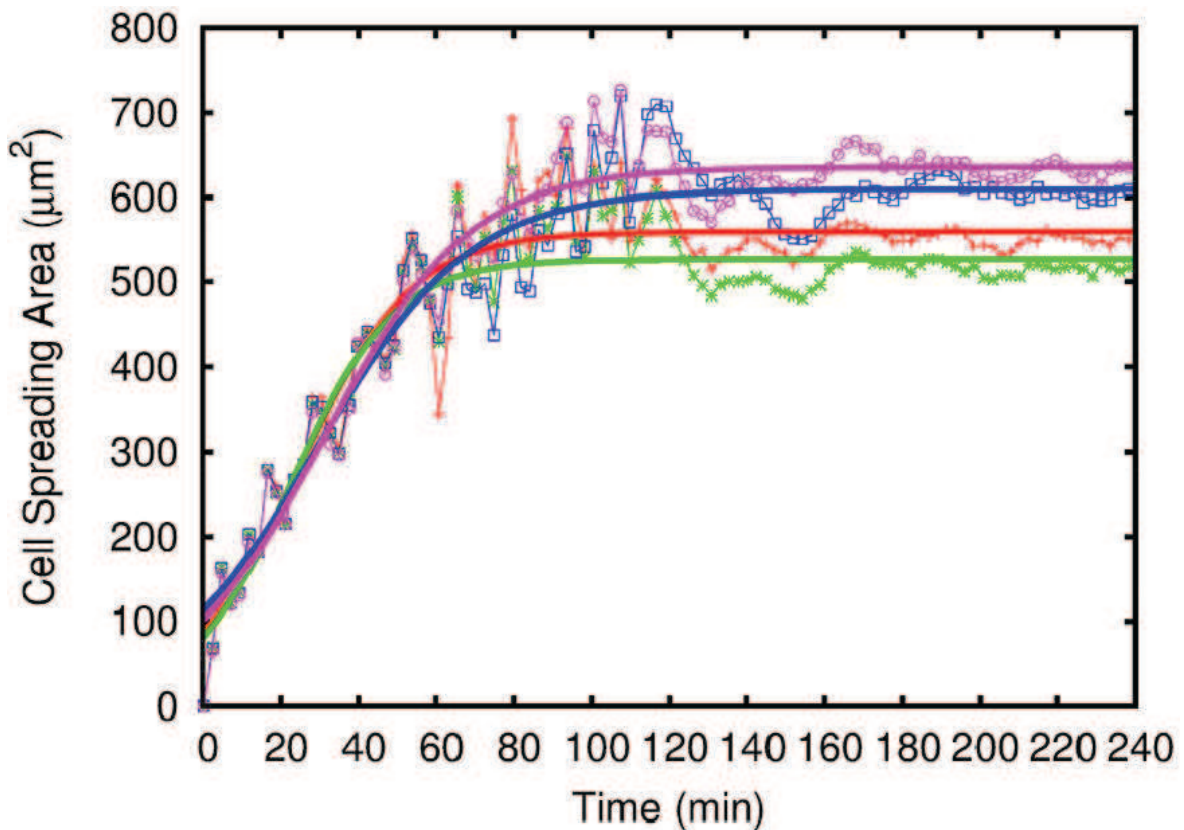Figure 3.11 displays the spreading curves in time on the four different patterns.

Figure 3.11. Simulated cell spreading curves on the four geometries, green for pentagon-like, red for flower-like, blue for square-like and magenta for stretched hexagon. Dotted curves shown the experimental point mediated for the five independent simulations performed for each geometry while lines are the fitted curves obtained from (3.5).

Table 3.3: Fitting parameters obtained using the logistic equation (3.5) to the simulation data reported in Figure 3.11.

Pattern	A_{max}	r (min^{-1})	m (min)
Flower-like	559 ± 4	0.0684 ± 0.005	559 ± 4
Pentagon-like	526 ± 4	0.0752 ± 0.006	559 ± 4
Square-like	609 ± 4	0.0504 ± 0.003	559 ± 4
Stretched-hexagon	635 ± 4	0.0531 ± 0.002	559 ± 4

Time t=0 corresponds to the instant when the spherical cell contacts the surface. A "passive" spreading takes place, the cell increases its contact area because of favorable interactions between cell and surface beads, but the cell shape remains spherical. In the simulations, at t = 60 min, the cell starts expressing adhesion beads. Their number is proportional to the number of pattern beads. Adhesion beads anchor the cell to the substrate through attractive forces and induce the cell to further spread over the pattern, covering all cue spots. Then the cell contact area reaches a plateau. The final covered area A_{max} of the cells depends on the geometry of the pattern and on the size of the adhesive spots.

Data obtained from experiments on stem cells spreading during their process of differentiation are comparable with the parameters found in our simulations.[61] Other important experiments, carried out on different cell lines and different substrates, found that, before the activation of any mechanism involving the force generated by the actin polymerization, the cells behave like passive liquid droplet that spread on a surface.[62]

The adhesive beads introduced in our simulation have an important influence on the final shape and on the final contact area of the cells but do not affect the growth velocity, in agreement with experimental results. The small differences in the growth rate observed also in the early stages of the spreading process can be justified if we consider that the number of "A" beads in the simulations depends, in time, on the size of the cell list. As a consequence, at the early stage of "A" beads creation, a lower number of them is generated inside the droplets when the pattern is characterized by spots with a large distance from the center of mass of the cells and with a small spot size (this is the case of the stretched-hexagon and the pentagon-like pattern). On the contrary a large number of "A" is created for the patterns with the opposite features (square-like and flower-like).

Although at the early stages the "passive spreading" dominates the process of deformation, the adhesive beads exert a force on the cell structure and a difference in their number may induce a different cell behavior in relation to the pattern, such that it is possible to justify the little variation in the growth rate of the cell in the first 50 minutes of dynamics.

A more precise characterization of the final shapes of the cells can be used for the determination of other cell properties that can be compared with experimental data on living cells. Starting from a geometrical point of view, the final shapes are characterized by the presence of inward curves between the adhesion islands that constitute the pattern. The curvature, also presenting living cells on similar patterns, can be described using circular arcs and appears spontaneously in the simulations. As can be observed in Figure 3.12 the radius of the curvatures increases with the increase of the distances between two spots, as is well showed by the stretched-hexagon geometry and in agreement with the work of Bischofs et al. (ref. 53).
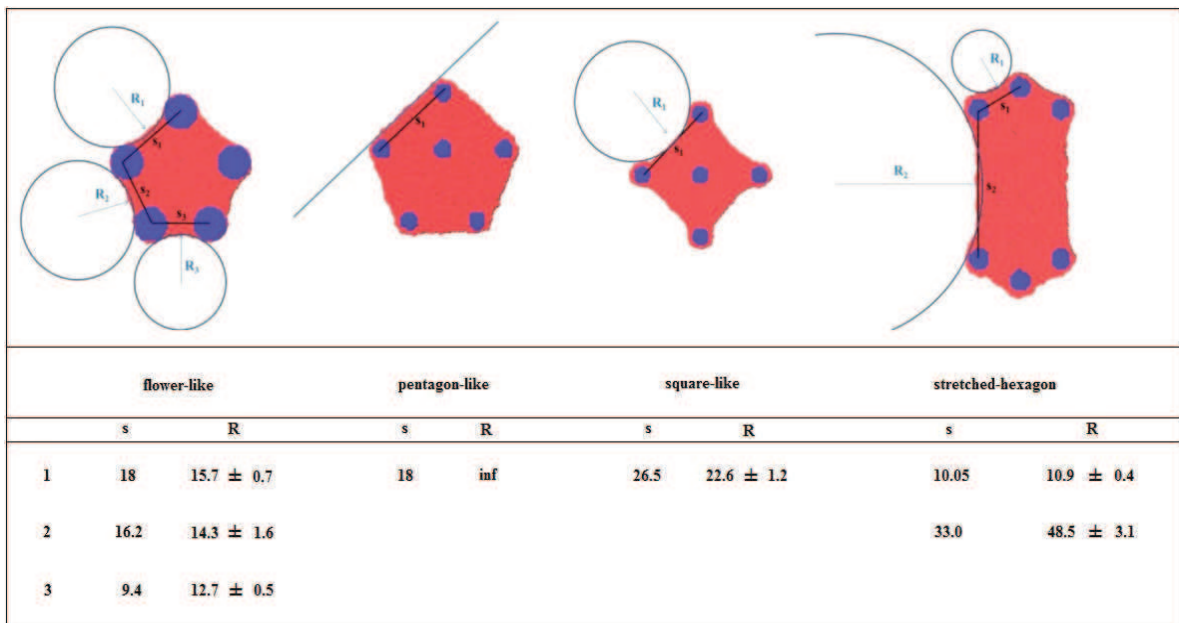

	flower-like		pentagon-like		square-like		stretched-hexagon	
	s	R	s	R	s	R	s	R
1	18	15.7 ± 0.7	18	inf	26.5	22.6 ± 1.2	10.05	10.9 ± 0.4
2	16.2	14.3 ± 1.6					33.0	48.5 ± 3.1
3	9.4	12.7 ± 0.5						
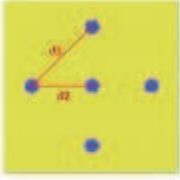
Figure 3.12. Analysis of the curvatures of the cell boundaries of the four different cell geometries. R is the fitted arc radius while s is the distance between the two spots that forms the curvature. Like all other parameters, these are also averaged over the five independent simulations.

Another property that comes from the model is the relation between the radius of curvature and the area described by the pattern bead. An increase in the area of the adhesive spots influences the final number of "A" beads in the simulation and provokes an increase of the

adhesion force. Proof of this is obtained for the pentagon-like geometry, where the small radius of the chemical cues, 1.5 μm, forbids the formation of inward curvatures, despite the fact that the same geometry with cue spot radius of 2.25 μm allows them. In order to characterize the relationship between curvature and pattern geometries we carried out other simulations of cell adhesion on patterned surfaces, by changing the features of the pattern. In particular, we focused on the pentagon-like and square-like geometries see Table 3.4.

Table 3.4: Shape changes under modification of the surface pattern[a]

D1= 18 D2=13.5 D3=16.2	Rspot=1.5	Rspot=2.25	Rspot=3.75
	R1=inf R2=inf R3=inf	R1=20.74 R2=19.25 R3=12.27	R1=15.7 R2=14.3 R3=12.7
Rspot=2.25	D1=26.5 D2=18.75	D1=19.09 D2=13.5	D1= 22.2 D2= 18.75
	R1=22.6	R1=inf	R1= 29.9

[a]*Top: from the left to the right, the effects of the changes of the spot radius for the pentagon-like pattern. Bottom: the effect of the changes in the distance between the spots for the square-like pattern.*

Concerning the adhesive beads, the analysis of their capacity to mimic the adhesion sites that living cells can express is another important aspect to keep in mind when we want to compare the coarse-grained model to the experiments. The process of cell adhesion is a complicated sequence of biological events that starts from the capacity of the living cells to sense the external environment, especially favorable sites on the surface, then continues with the actin polymerization that pushes the cell on the preferred sites and terminates with

the adhesion to the surface via protein-links. The cell-matrix adhesion complexes, formed by integrin and other proteins, mediates the adhesion of the cell to an external substrate. Chemotaxis is the process that drives a living cell towards favorable areas of surface. Also the application of external forces to the cell membrane can stimulate the cell to create or to the guide the growth in size of an adhesion sites, suggesting a mechanosensing behavior.[63] In our simulations beads "A" are created only if the cell is close to the chemical spot, meaning that the deformation and adhesion sites can be created only if the cell is close enough to the pattern to sense them. Adhesive beads have the hard task to summarize all the biological processes that create, form and maintain an adhesion site. To account for all these processes, we evaluated the forces exerted by our adhesion beads and compared them to experimental results on focal adhesions. Our results, for each geometry, are obtained averaging the forces exerted by all adhesive beads in the simulations(see Table 3.5),

Table 3.5: Force exerted by "A" beads on the surface and relative force surface density[a]

Geometry	n° of "A" beads	Force per "A" bead (10^{-11} N)	Surface covered by "A" beads (μm^2)	Force/surface covered by "A" beads (nN/ μm^2)	Force/surface covered by the cell (nN/ μm^2)
Flower-like	649 ± 8	-177.7 ± 0.8	220.9	5.22 ± 0.09	2.1 ± 0.1
Pentagon-like	137 ± 5	-53.1 ± 0.6	42.4	1.71 ± 0.08	0.1 ± 0.1
Square-like	416 ± 8	-66.1 ± 0.3	79.5	3.46 ± 0.08	0.5 ± 0.1
Stretched-hexagon	254 ± 7	-65.2 ± 0.9	61.1	2.71 ± 0.1	0.3 ± 0.1

[a]*For each geometry are reported: the number of "A" beads created, column 2, the force expressed by every single "A" bead, column 3, the total dimension of the spots, column 4, the force normalized by the surface of the chemical pattern and by the entire cell structure, column 5 and column 6, respectively. The value are averaged over the five statistical independent simulations.*

With the aim to measure the local force exerted onto a surface by cells via adhesion sites, in 2001 Balaban et al. set-up a clever approach combining micro-patterning and fluorescence onto an elastomeric matrix used as support.[64] The results on adherent and stationary cells obtained in their work were comparable to previous experimental analysis and were in agreement with the data that come from the simulations made with our

model.[65,66] In particular, observing their final result of 5.5 ± 2 nN/μm^2, is possible to assert that the parameters chosen to modulate and trigger the activity simulated droplet can reproduce also the peculiar experimental data of adherent living cells.

It is well-known that in nature a water droplet assumes a spherical shape to minimize the exposed surface to the external environment. This concept can be, more or less, extended to every "inactive" liquid droplet exposed to a medium.

Since the shape of liquid droplets substantially depends on their surface tension, the analysis of this property becomes crucial to understand how the model is able to reproduce the shape of living cells. One of the easiest way to calculate the interfacial tension between a droplet and a solid surface is to connect this parameter with the contact angle by using the Young equation:[67-69]

$$\gamma_{CS} = \gamma_{MS} - \gamma_{CM} \cdot \cos\theta_C \qquad (3.6)$$

where γ_{CS}, γ_{MS} and γ_{CM} are the cell-surface, medium-surface and cell-medium interfacial tensions, and θ_C is the contact angle between the cell and the surface. The contact angles were measured following the procedure described by Jones et. al. where the average number of beads in a cross section of the drop was fitted as function of the height (z-coordinate).[70] The cross section was taken as showed in Figure 3.13b and the fitting equation to find the number of particle per unit height was:

$$\pi\rho[(R^2 - z_0^2) + 2zz_0 - z^2] \qquad (3.7)$$

where R and z_0 are the two fitting parameters and ρ is the beads density. With the values of R and z_0, the contact angle can be calculated as follow:

$$\theta_C = 90 + \sin^{-1}(\frac{z_0}{R}) \qquad (3.8)$$

If it is quite simple to estimate the contact angles starting from the geometries, less trivial is the procedure necessary to determinate the interfacial tension between two pairs of beads (for our case the two pairs medium-surface and cell-medium). As demonstrated by previous DPD simulations,[67,68] the surface tension depends only on the repulsive parameter a_{ij}, thus γ_{MS} and γ_{CM} are constant during our spreading dynamics. The pair-wise surface

tension terms can be estimated from the calculation of the three diagonal component of the pressure tensor following the application of the Irving – Kirkwood (IK) equation:

$$\gamma_{12} = \int \left[p_{zz} - \frac{1}{2} \left(p_{xx} + p_{xy} \right) \right] dz \qquad (3.9)$$

In practice, two dynamics were performed consisting of a two-phase system: medium-surface and cell-medium beads were placed in a simulation box of size 10 x 10 x 25 r_c and DPD runs of 10000 steps with timestep 0.02 τ were carried out in order to form a phase separation along the x-y plane. The application of the IK integration along the z-axis allows to derivate the value of the interfacial tension for the two types of beads under investigation, namely $\gamma_{MS} = 0.233$ mN/m and $\gamma_{CM} = 0.251$ mN/m.

As described in equation (3.6), the calculation of the Cell-Surface interfacial tension needs the determination of the value of the contact angle. However, because of the asymmetry of the simulated cell shapes, the cell contact angle value is not constant along the contour length of the cell. A liquid droplet in contact with a surface at equilibrium is characterized by a single value of contact angle (see Figure 3.13a). The drop/cell contact angle in fact results equal to 85° corresponding to a surface tension value of $\gamma_{CS} = 0.211$ mN/m.

On the other side, different points along the contour length of the cell boundary behave in different ways in relation to the changes in the affinity with a heterogeneous surface. This is the case of the behavior of a cell where adhesive sites and no adhesive zones are present at the same time. In practice, for a complete description of the cell morphology and tension, a number of different contact angles have to be calculated in relation to the different adhesive points of the cell. (see Figure 3.13 b).
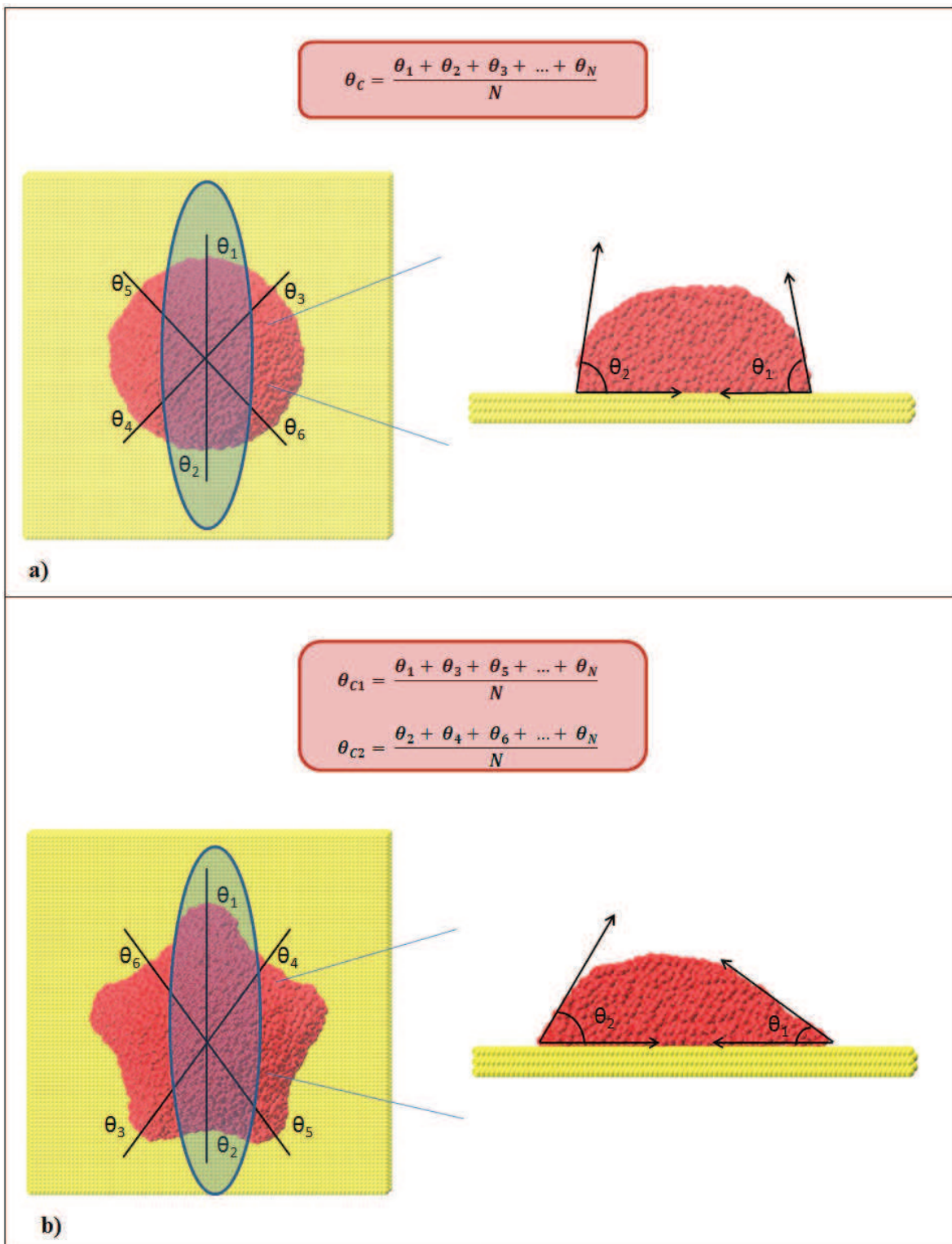
Figure 3.13. Analysis of the cell morphology in terms of contact angles: for a round shape, an infinite number of cross sections can be designed to average the single contact angle and one is sufficient to describe the entire cell morphology, see a). For a more complicated geometry, such as the flower-like, two (or more) contact angles must be provided to describe the different regions that the cell describes: the adhesive one and the "relaxed" one, see b).

The surface area of a cell attached to a micropatterned surface experiences two different physico-chemical zones, that is the adhesive pattern "P" and the non-adhesive surface "S". For this reason, we estimated at least two cell contact angles for each pattern geometry (see values in column 2 of Table 3.6). The first value is calculated as an average of the contact angles at different positions where adhesive sites are present, while the second is calculated as an average of the contact angles in the regions of the cell without adhesive sites, that is in correspondence of the tangential point of the circular arc. The interfacial tensions derived (see data in column3 of Table 3.6) for each shapes are a direct consequence of the differences in contact angle measurements and express also the adhesion and spreading characteristics of a high adherent cell compared to another one with low affinity for the surface.

Table3.6: Contact angles and CS interfacial tension for every surface[a]

Geometry	θ_C(degree)	γ_{CS}(mN/m)
Flower-like	75 ± 1(1)	0.17 ± 0.02
	49 ± 2(2)	0.07 ± 0.02
Pentagon-like	79 ± 1(1)	0.18 ± 0.02
	48 ± 3(2)	0.06 ± 0.04
Square-like	84 ± 1(1)	0.21 ± 0.02
	42 ± 2(2)	0.05 ± 0.02
Stretched hexagon	81 ± 2(1)	0.19 ± 0.02
	42 ± 1(2)	0.05 ± 0.02

[a]*In column 2 are reported the contact angles of each geometry, in column 3 the associate interface tensions. (1)The contact angles are calculated at the cell boundary regions where no adhesive spots are present (typically between two adhesive spots). (2)The contact angles are calculated at the cell boundary regions where adhesive spots are present. The contact angles are averaged for the five statistically independent simulations.*

Examining the contact angles calculated with our model is possible to observe how the cell-surface interfacial tension differs in relation to the zones where adhesive beads are present and where they are not. Substantially, the areas far from the chemical cue show an interfacial tension similar to the one observed for the reference simulation, where the cell morphology appears to be spherical-like in the absence of any chemical functionalization. The role of the cell-surface interfacial tension is crucial to understand how it is possible trigger the cell deformation from a spherical shape to a more complicated one.

In general terms, inducing changes in the shape of a droplet can be only possible giving to it an energetically favorable pathway. It is possible for example acting on the surface where the cell is laying, or providing external forces or, in the case of living matter, using the energy that comes from the metabolism. In any case, the shape of matter, living or not, is governed by thermodynamic equilibrium that require energy to be broken. In our model, the use of attractive Adhesive beads has the objective to introduce inside the droplet the energy that is needed to trigger its change in shape, acting substantially with a perturbation of the forces that govern the droplet equilibrium stability.

A spherical shape is the results of the droplet that attempts to minimize its surface tension reducing the surface exposed to the medium. Since the surface tension can be considered as the work required to increase the area of a fluid exposed to another fluid, the introduction of Adhesive beads has the crucial role, in the simulation, to provide the energy required to beat the surface tension and break the thermodynamic equilibrium that forces the liquid matter to have a spherical shape.

In our model, beads act indirectly on the surface tension, influencing instead the interfacial tension between the cell and the surface where chemical cues are present. Like in the chemotaxis process of living cell, particles "A" have the possibility to establish a special favorable interaction, pushing the cell to expand the exposed area to the surface (decreasing the interfacial tension cell-surface) and, as a consequence, its exposed area to the medium (overcoming the surface tension cell-medium). In brief, the CG dropletmodel has the possibility to become "active", overcoming its surface tension and spontaneously deforming, through a process that comes from the inside of its body, just like in the classic chemotactic behavior of living cells.

3.6. Conclusions

The coarse grained model developed hasthe capacity to describe the process of cell adhesion onto chemical patterned surface. Starting from the model developed in our research group.[52] important improvements were made to introduce "active" features and close the gap between a passive droplet and a living cell.

Using a simple mechanical model based only on the use of forces, we built up a system where all the metabolic processes required to induce living cell deformation are included in only one type of bead and in one type of attractive force.

As demonstrated above, the morphology of the simulated "active-drop" is in good agreement with the ones displayed by living cells on several geometrical chemical patterns.

The cell curvatures along its contour length between adhesive spots appear spontaneously and can be described with circular arcs, whose radius depends on the characteristics of the functionalized surface. The process of self-production of Adhesive beads inside the cell/droplet drives the cell to an adhesion process whose kinetics well reproduces experimental data. In particular the spreading kinetics can be modeled via a logistic equation whose parameters are in agreement with experimental results.[61] The mean force exerted by the adhesive sites on the surface is also comparable with the experimental one found for focal adhesion in living cells.[64-66]

In conclusion, the coarse-grained nature of the model allows to simulate a system with a size comparable to that of living cells, reducing the degrees of freedom to solve and the computational cost. The main limitation of the model comes from the low spatial resolution of the beads, where each one represents a portion of volume of the order of micrometers. With the increase of computer performances it will be possible to decrease the so-called "coarse-grained degree", thus increasing the number of particles per volume unit and introducing a higher level of details inside the droplets such as an explicit model of the cytoskeleton, the cell membrane, vesicles, organelles, the nucleus etc.. Because of the generality of our approach and its capacity to reproduce a wide range of cellular properties in terms of morphology, spreading kinetics and active motion, future improvements of the model can be helpful to assist the experiments, providing a theoretical counterpart for the prediction of cell response in different environment or the design of new biomimetic materials.

4. Chemically Induced Neuritis Growth In Neurons

4.1. Introduction

On the basis of the results obtained in the study of living cells spreading and morphology, other cells properties were investigated by using the coarse grained model developed here. In particular, I focused on the study of the process of neuritis growth in neurons.

Neurons are the fundamental cell entities that compose the nervous tissue and the central nervous system. They are able to receive, transmit and elaborate chemical and electrical signals (ions cascade) and are present in many living species on Earth.

From an anatomical point of view, the central part of a neuron is composed by the "soma" that contains all the organelles responsible for the cellular function, and the by the nucleus, which contains the genetic heritage.

A neuron is characterized by the possibility to express prolongations from the soma, generally called neuritis. The term "neurite" is used to indicate both dendrites and axons, the two kinds of prolongations that a neuron can produce. A neuron never originates more than one axon but can induce the growth of many dendrites. Because of the dimension, especially in terms of length, an axon can be considered the major neuritis present and is a single prolongation with length that in some case can reach more than 1 meter. Dendrites are thinner and extremely branched prolongations compared with axons, with dendritic tree morphology. The contact between two neurons is called synapses and can be an axon-axon, dendrite-dendrite and axon-dendrite contact.

Like the other kinds of living cells, neurons express many features and have an intricate biochemistry, for this reason they can be divided according to the function of their morphology, their biological function, their cytochemistry and other features. The present model object of this thesis is not suited to simulate molecular details and the metabolic complexity, as already showed in the section dedicated to the description of cellular adhesion. Following the same path of the previous section, only a general and simple modeling of neuron will be presented, without the description of cellular details. This is functional for the general purpose or this work that has the aim to show some peculiar activities of neurons without focusing on metabolic processes and molecular properties.

A peculiar and interesting property of neurons is the influence that a chemical cue can have for the growth of neuritis. The presence of particular proteins of the Extra Cellular Matrix(ECM) can trigger the axon growth or induce a bias in the growth direction.

The study of the cell capacity to follow chemical gradients or react in peculiar ways under mechanical stress or geometrical constraints originates at the beginning of XX century. In 1911 Harrison discovered that cells incubated on fibers of spiders tended to grow along the fiber direction.[71]

The progress in neuroscience and biology gave to the scientific community the keys to understand the processes that govern the Central Nervous System (CNS) development and the roles of Extracellular Signaling Proteins (ESP) as guides for synaptogenesis and axon growth.[72]

ESP are soluble proteins expressed by the cell to form gradients both in solution and bounded to substrates. Their role is to help the axon growth direction in the formation of neuronal networks.[73,74]

Before the use of microcontact printing as a mature technology applied to microelectronics and surface functionalization, the majority of experiments on axon guidance in the presence of a chemical gradient were made in solution using three-dimensional gel matrices such as collagen gels.[75-78] The great advantage of microcontact printing is the possibility to design with extreme accuracy a wide range of specific pattern geometries in a fully reproducible way, along with an enormous range of compatible active molecules that can be used as chemical cues. Many papers have demonstrated that, the types of ECM or ESP proteins used as active molecules to coat a surface, are not the only factors able to guide neuronal response; also the pattern design can have a substantial influence and affect in many ways axon growth.[79-81]

Yeung et al. were able to obtain neuritis of 2 mm of length after 3 weeks of brain stem neurons incubation on a substrate of polystyrene covered by laminin. They also set-up a laminin mesh-like pattern (see Figure 4.1) and observed that the track width and the node size were crucial to the success of neuronal slice patterning. They also showed that there is a preference for the surface covered by laminin with respect to the non-laminin one, and finally concluded that a specific pattern geometry can enhance or reduce the laminin effect.
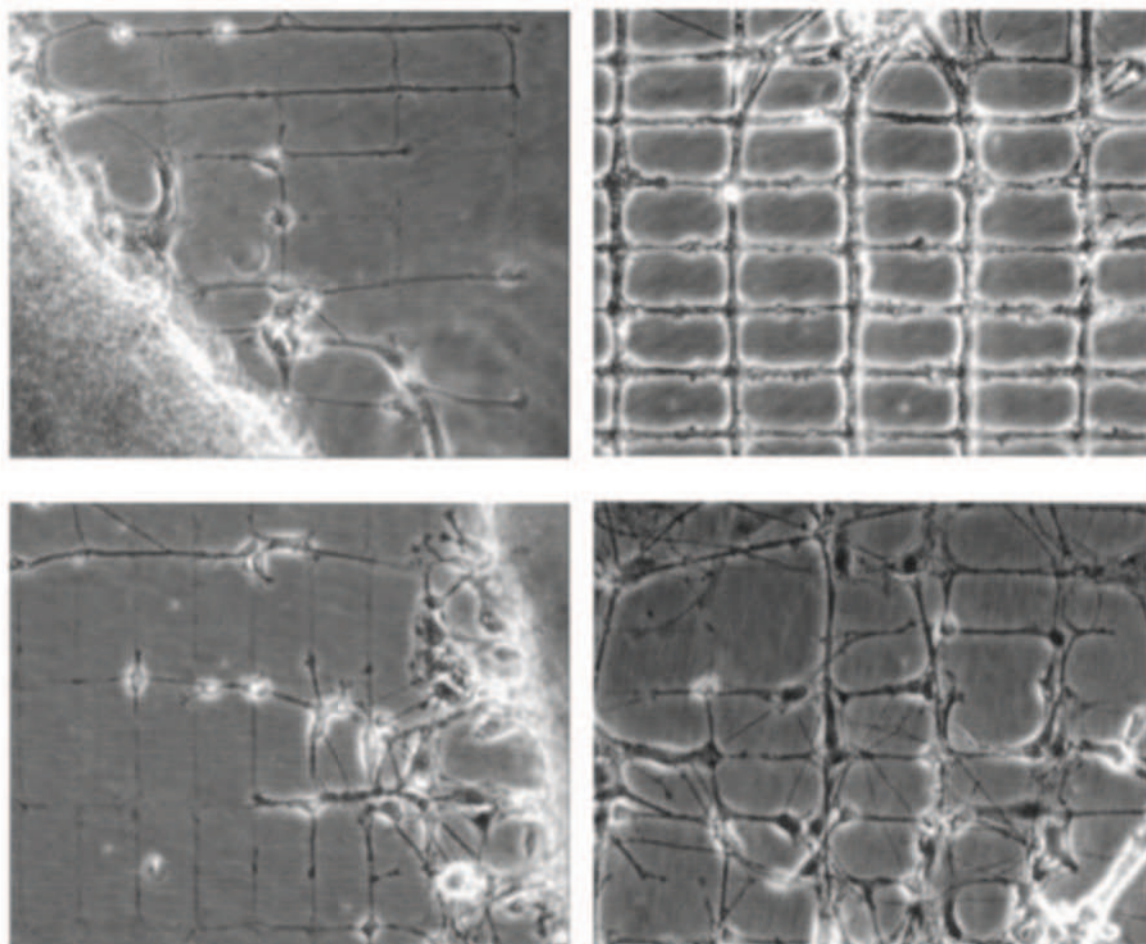
Figure 4.1. Neurons grown on ECM mesh like pattern presented by Yeung and coworkers in reference 79. Top: pattern with node size of 10 μm and track length of 2 μm. Bottom: pattern with node size of 12 μm and track length of 4 μm. Images of neurons after 3 days of cell incubation (left) and 10 days of incubation (right). The neurons show a clear preference for the ECM protein and reproduce the pattern.

The type of active molecule and its geometrical deposition are two important factors in guiding and controlling the neuritis growth. Also the substrate used as a support can play a primary role. An interesting paper by Jang et al. demonstrated that using carbon natotubes (CNTs) as a substrate for poly-L-lysine (PLL) can enhance the capacity of neurons to stimulate neuritis growth.[82] Using photolithography, the authors deposed strips of CNTs alternated with strips of Octadecyltrichlorosilane (OTS) and covered all the surface with PLL. Since CNTs form an intricate mesh with an intrinsically high level of corrugation, the poly-L-lysine used for the coating as an active stimulator for neuronal growth can penetrate inside the network in a favorable way and stimulate a "major neuritis" (an Axon) growth along the CNTs strip. Although the PLL covers both CNTs and OTS, the Axons

growth along the CNTs strips seems to be on average about three times greater (~1 mm) than on OTS strips.

The substrate can also be of importance for other measurements associated with the process of neuritis growth such as the capture of electric signals emitted by the cells during the growth process or during the formation of the neuronal networks. In this case, the use of supports like conductive CNTs can be helpful.

Fricke et al. used different micro-patterns of Laminin and PLL/Laminin to induce asymmetrical axon growth. In their work, they proved the capacity to guide the growth of a rat cortical neuron axon with the use of a functionalized surface.[83] This study aimed to improve the knowledge about axon guidance with a direction focused on the development of new techniques able to control better the processes of neuritis growth in the constitution of neuronal networks. Their method is based on the construction of several gradients of proteins via the production of substrate-bound discontinuous patterns of PLL/Laminin or PLL alone. Fricke and co-workers designed a variety of micropatterns able to generate gradients of proteins deposed onto the surface (see Figure 4.2).
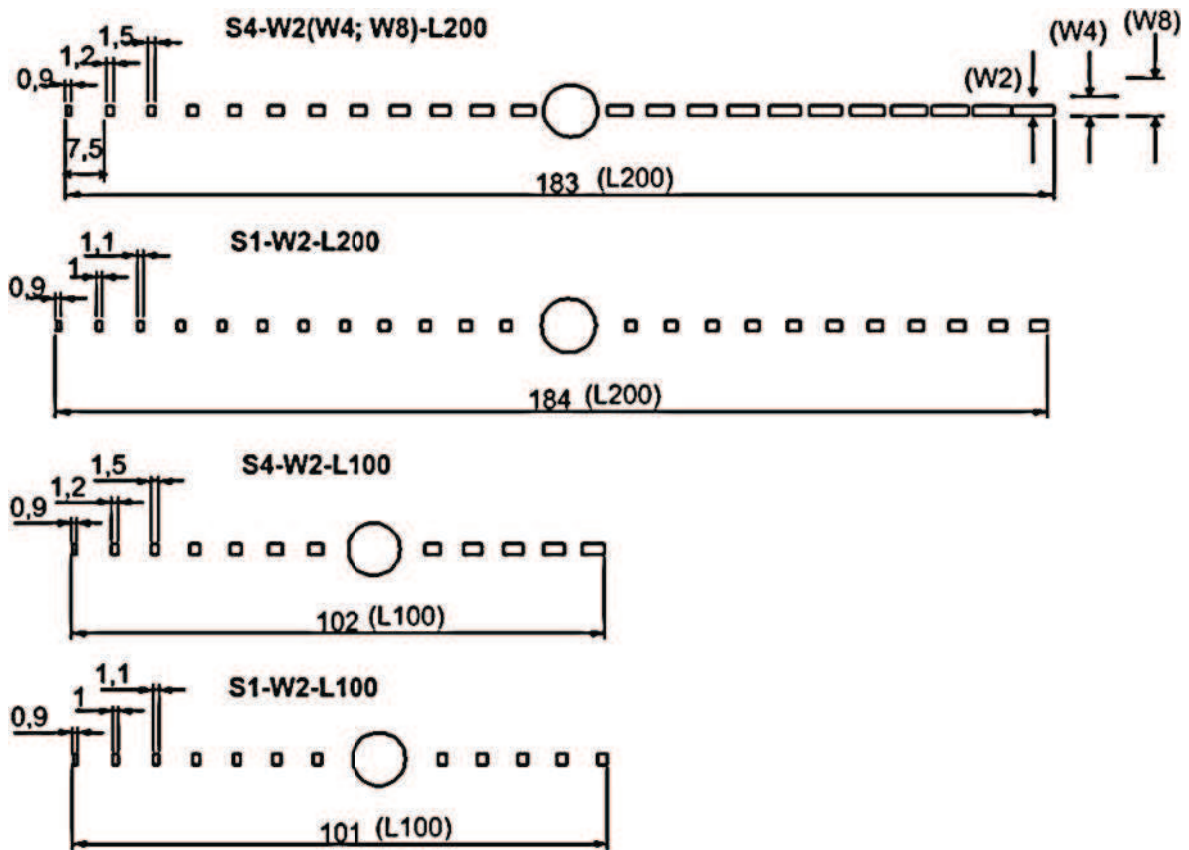
Figure 4.2. Schematic images of the patterns produced by Fricke and co-workers in their study. The letter S represents the slope (e.g. S4 means slope 0.04 = 0.3 μm/7.5 μm), the letter W the width in micrometers and the letter L the overall length of the pattern in micrometers. The numbers 184 and 101 are codes related to the reagent used to create the microstamps (e.g. Sylgard 184). The figure is adapted from Figure 1 of reference 83.

The gradient structure consists of a series of discontinuous rectangles with increasing length, decreasing gap and constant width. The overall length of the pattern is about 100 μm or 200 μm and, in the middle of the gradient, a Laminin circle of 5 μm in radius is integrated to anchor the soma. The central spot forbids the spontaneous movement of the neuron body and provides a strong adhesion site (e. g. focal adhesion), able to restrict the starting point of the neurite outgrowth. The process of adhesion follows the same procedure described in the previous chapter but in this case, because of the position and the circular geometry, the morphology of the cell is not influenced. The results obtained by Fricke et al. are interesting in terms of neuritis growth and guidance. Using the central spot as reference point in the definition of the system coordinates, it is possible to define a positive growth direction when the neuritis follows the increase in the protein concentration and a negative growth when the neuritis grows in the opposite side. After

three days of incubation, they analyzed the neuritis-growth promoting-index (NGPI) that can be defined as the ratio of neurite length in the positive direction to neurite length in negative one, in all the different patterns designed. They observed that both the protein functionalization and the pattern design can influence the neuritis growth. In particular, the PLL gradient has less effect in the absolute neuritis growth value than in the PLL/Laminin gradient, underlying the Laminin promoting effect. In both PPL and PLL/Laminin, the NGPI is positive, providing a clear effect on axon guidance in the positive direction. The effect of the pattern design is also visible and has a strong influence both on the neuritis absolute growth and on growth direction.

The cell coarse-grained model implemented during my PhD work was improved in order to simulate the active behavior of neuritis growth. As the process of a neuritis growth implies a process of mass creation, the model presented in the previous section of this thesis needed to be extended and improved.

4.2. Description of the model

The neuron cell was modeled as a droplet of fluid made by beads of type "C", surrounded by a fluid medium ("M" beads) and deposited onto a solid surface, made by five layers of particles with a fixed position in time and space (surface beads, "S"). The five layers had a face-centered cubic geometry. The whole system, enclosed in a box of size 135 x 30 x 25 r_c, consisting in about 676000 beads in total, where 14000 beads describe the spherical cell (neuron) with a radius of 10 r_c, 517000 beads represented the medium and 145000 beads described the entire surface. The number density of beads (number of beads per unit of volume r_c^3) was set to $\rho_{drop} = \rho_{medium} = 6$ for the fluid, while the surface density was set to $\rho_{surface} = 15$. The friction coefficient γ was set to 5.61, the reduced temperature T* to 0.53. The length unit is set equal to 1 r_c and the integration timestep was set equal to 0.02 τ. In order to describe the patterns geometries presented by Fricke and co-workers (Figure 4.2), two more types of beads were introduced: beads "P1" (Pattern 1) represent the rectangular gradient on the surface and beads "P2" (Pattern 2) represent the central spot. The pattern beads were created by converting the "S" beads placed on the top of the five solid layers into "P" beads. In addition to the five types of beads presented above, two more beads types were introduced in the model, one for the simulation of the neuritis growth (neuritis beads "N") and one to represent the adhesion of the cell to the central spot (adhesive beads "A"). Since the active process of growth implicates an increment of the neuron cell mass,

the creation of the neuritis beads is made with a transformation that involves the medium beads "M" that are closer to the soma. The "N" beads are created gradually during the simulation in a continuous dynamical procedure that will be further described below.

As discussed by Fricke, all the patterns are made by rectangles and by a central spot that hasthe unique aim to fix the soma in the correct position to sense the gradient. Following this experimental condition, all the adhesive beads "A" were created in a single step inside the soma before the beginning of the simulation. As in the cell adhesion model presented in the previous chapter, "A" beads anchor the cell to the central chemical cue, preventing the net movement of the cell center of mass during the simulation. About 300 "A" beads are created inside the soma.

In summary, 7 types of beads were implemented in the model:

- Cell beads ("C") represent the soma.
- Medium beads ("M") represent the fluid surrounding the neuron.
- Adhesive beads ("A") represent the adhesive sites of the cell onto the surface.
- Neuritis beads ("N") describe the neuritis.
- Surface beads ("S") describe the solid surface above which the neuron is placed.
- Pattern 1 beads ("P1") describe the beads of the patterned surface.
- Pattern 2 beads ("P2") describe the beads of the central circle of the patterned surface.

For the computational study we chose to study the neuritis growth only on three of the eight relevant geometries proposed by Fricke and co-workers in their work (see Figure 4.3). The first geometry (Geometry 1) is made by rectangles having a width of 1.33 r_c and a slope of 0.3 r_c. The second one (Geometry 2) has a different slope (0.1 r_c) compared to Geometry 1 while Geometry 3 has the same geometrical characteristics as Geometry 1 but rectangles with double width (2.66 r_c). In all the three geometries the overall length of the pattern is 135 r_c.
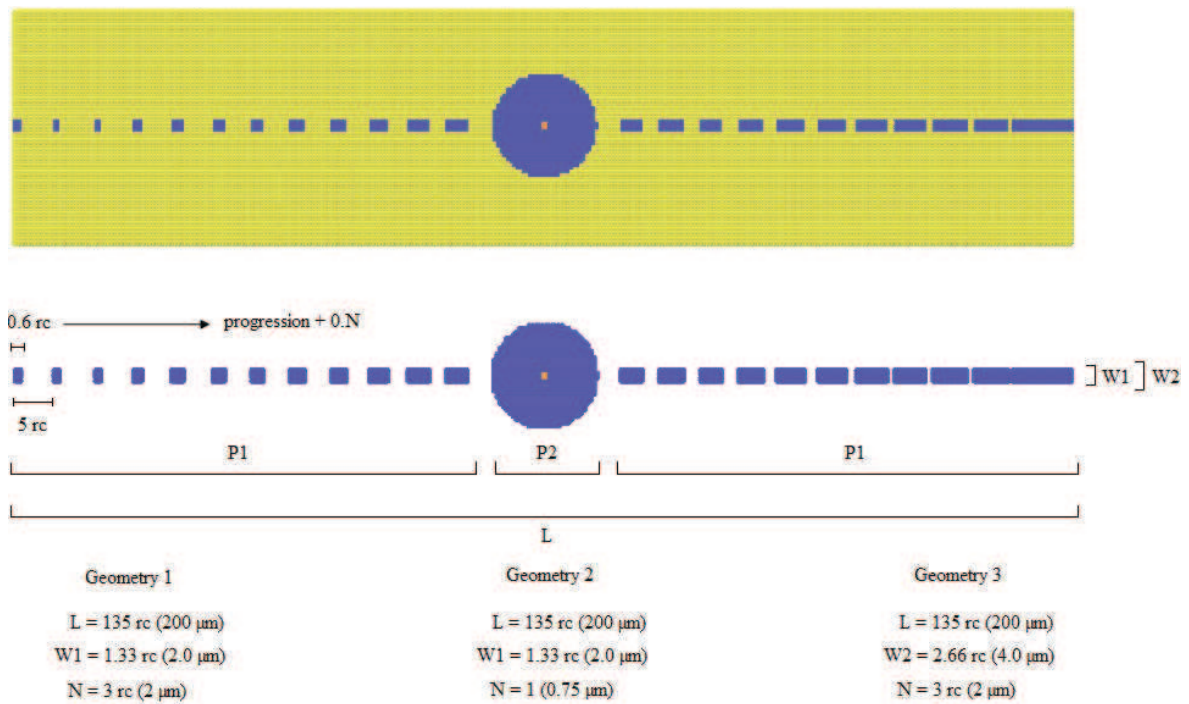
Figure 4.3. Coarse-grained reproduction of the patterned surface created by Fricke et al. for axon guidance. The image at the top displays the rectangles and the central spot (blue beads) that represent the chemical functionalization of the surface (yellow beads). The central image represents the same pattern of the top image, with details of the parameters that can be used to modify its geometrical characteristics. Geometries 1, 2 and 3 are the three patterns implemented in the model for the simulations.

No interacting force is necessary between the solid particles as they are fixed in time. For all the other beads in the model, different types of forces (attractive and repulsive) are implemented. In order to avoid the unphysical phenomenon of the total interpenetration between beads, the soft repulsive force described by equation (2.15a) is defined between all the particles of the system. In addition to the repulsive force, a linear attractive force (see equation 2.15b) is activated for some pairs of bead types in order to express active phenomena. In particular, a linear attractive force describes the interaction between beads "A" and "P2" in order to attract and stick "A" onto the central spot. Furthermore, the same type of force acts between beads "A" and "C" in order to anchor the cell onto the central spot. This allows the formation of strong interactions between the soma and the surface, using the adhesive beads as mediators. To perform the process of neuritis growth the linear attractive force was implemented also between the "N" - "P1" pairs and the "N" - "C" pairs. In this way the neuritis beads can sense the surface gradient and at the same time maintain the integrity of the cell.

In order to avoid an uncontrolled neuritis growth and possible breakdown of its structure during the growth process, a further force was implemented between beads "N" and "P1". This interaction (equation 4.1) can be defined as a recall force acting to brake the "N" beads that are growing from the soma. The more "N" beads move away from the soma, the greater the recall force is.

The equation that describes the recall force has the form:

$$F_{CP\text{-}N} = \left[q * e^{(-0.05*d)} - a\right] \begin{cases} F_{CP\text{-}N}(x) = \left[q * e^{(-0.05*d)} - q\right] * cos\theta \\ F_{CP\text{-}N}(y) = \left[q * e^{(-0.05*d)} - q\right] * sen\theta \end{cases} \quad (4.1)$$

where q is the force intensity parameter, d is the distance between an "N" bead and the center of the P2 pattern (CP) (orange beads in Figure 4.3), θ is the angle formed with the straight line of the pattern. The recall force acts in x and y directions, where x-y plane defines the plane of the solid surface. As the rectangles gradient is designed along the x-axis, it follows that the "x" component of the recall force is dominant. From the equation, it appears that the greater is the distance between "N" beads and CP, the stronger is the restoring force pulling back "N" to the center. In Figure 4.4 the recall force as a function of the distance is displayed. It is possible to observe that the closer an "N" bead is to the soma, the lower is the attractive/negative (recall) force applied.
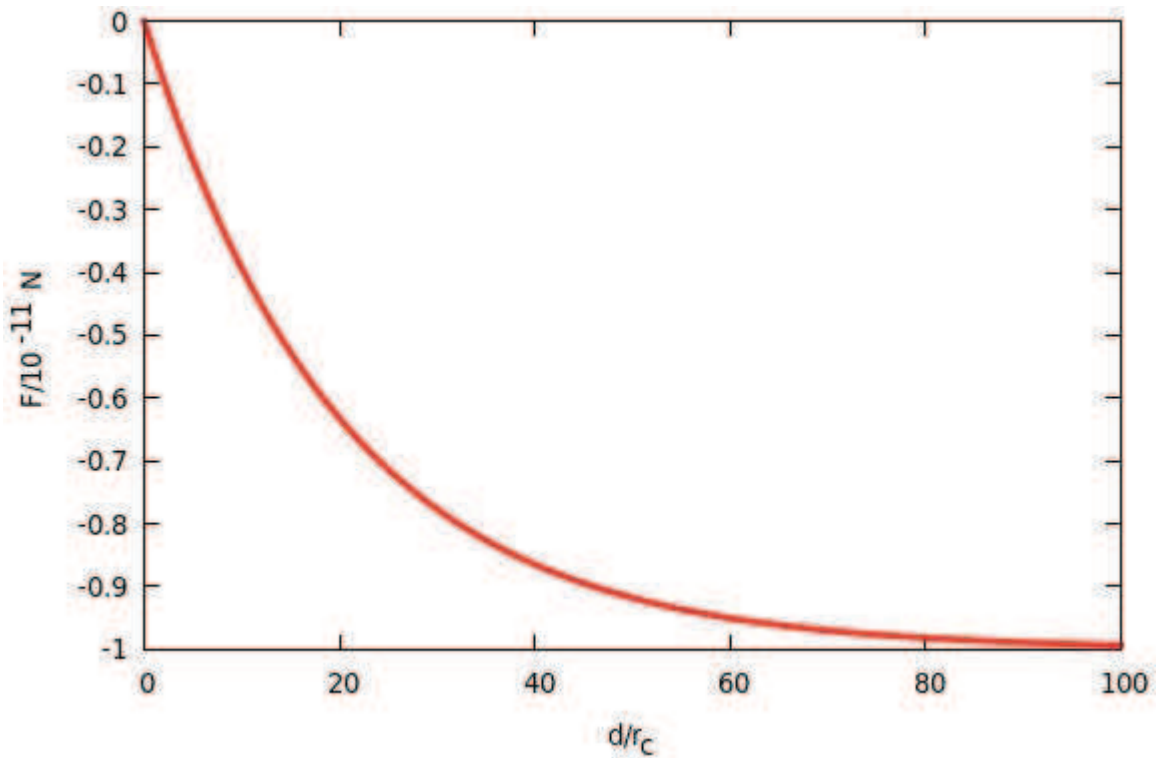
Figure 4.4. Long-range interaction, between "N" and CP, with q parameter set to 1.0. As the distance increases also the attractive (negative) recall force increases.

The parameter q for the long range recall force was set to 1.0×10^{-11} N in the model simulation set-up. The same set of parameters were used in the simulations of neuritis growth on the three different geometries. The a_{ij} parameters of the soft-repulsive forces are listed in Table 4.1. The parameters used in this work are similar to the ones used for the cell shape model presented in Chapter 3.

Table 4.1: Parameters a_{ij} (in 10^{-11} N) of the soft repulsive forces

a_{ij}		i =						
		A	P1	P2	M	S	C	N
	A	100	12.5	100	65	100	12.5	12.5
	P1		/	/	100	/	65	100
	P2			/	100	/	65	65
j =	M				12.5	100	65	65
	S					/	65	100
	C						12.5	12.5
	N							75

The simulation procedure and the characteristics of the attractive force and the relative b_{ij} parameters will be now discussed. At the beginning of the simulation, the system was built up with the proper pattern geometry (see Figure 4.3). A single spherical neuron cell with a radius of 10 r_c and containing ca. 14000 "C" beads was placed onto the top of the central spot of the surface (bead P2). The cell is surrounded by medium "M" beads. 2500 simulation steps (timestep 0.02 τ) were performed to equilibrate the system at the reference temperature of 0.53 T*. The presence of ca. 300 anchoring beads "A" in the cell ensures the cell immobilization onto the surface forming a strong adhesion site, as shown in Figure 4.5.
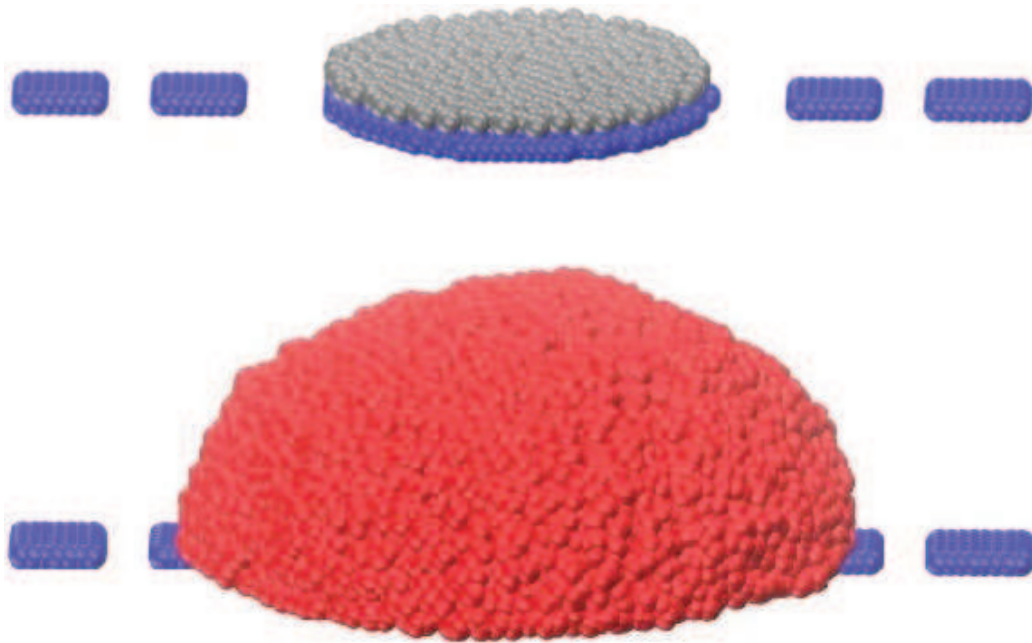
Figure 4.5. Top: the grey beads represent the cell adhesion sites placed on the central spot of the pattern (blue beads). Bottom: red beads represent the entire neuron cell after equilibration run.

At this point, the process of neuritis growth is simulated with a dynamical transformation of "Medium" beads into "Neuritis", according to the following procedure: a bead "M" close to the cell (i.e., with a distance "M" - "C" smaller than 0.6 r_c) is converted in to bead "N" with a probability P_r, given by:

$$P_r = exp(-\alpha \cdot t) \qquad (4.2)$$

where α is the conversion rate constant and t the timestep. Every time step, a random number R between 0 and 1 is generated and compared with P_r. The conversion of "M" into "N" is done only if $P_r > R$.

During the production run, that is performed without an upper limit of the number of steps, the "N" beads that are dynamically created, diffuse inside the cell and may be attracted to "P1" beads. Because of the presence of an attractive force between "N" and "C" beads, the neuritis growth and adhesion to the patterned surface does not cause fragmentation of the cell. In terms of interactions, "A" beads establish an attractive force with "P2" beads (b_{AP2}= -6.0 ; r_{c2} = 2.0 r_c), the same for "N" and "P1" (b_{NP1}= -1.5 ; r_{c2} = 4.0 r_c), while both "A" and "N" express an attractive force with the cell (b_{CA}= -0.5 ; r_{c2} = 2.0 r_c and b_{CN}= -1.0 ; r_{c2} = 2.0 r_c). See Table 4.1.bis.

Table 4.1.bis: Parameters a_{ij} and b_{ij} (in 10^{-11} N) of the soft repulsive and attractive forces[a]

a_{ij}/b_{ij}		i =						
		A	P1	P2	M	S	C	N
j =	A	100	12.5	100/-6.0	65	100	12.5/-0.5	12.5
	P1		/	/	100	/	65	100/-1.5
	P2			/	100	/	65	65
	M				12.5	100	65	65
	S					/	65	100
	C						12.5	12.5/-1.0
	N							75

[a]*The repulsive b_{ij} parameters are reported in red.*

Although in the Fricke experiments the same protein type was used to functionalize both the central spot and the rectangular gradient, in the model the two different geometries were represented with two different bead types, namely "P1" for the central spot and "P2" for the rectangles. This is necessary in order to model with different interactions the two different biological processes that take place, that is the anchoring adhesion of the cell on the central spot and the neuritis growth along the pattern gradient. In computational terms, this expedient allows to treat the two different interactions independently, with two different attractive force strengths. In particular, by using two bead types representing the same pattern functionalization, it is possible to avoid the attraction of the neuritis to the

central spot, that would not originate axon growth, and the attraction of the adhesive sites on the lateral patterned rectangles, that would spread the cell all over the surface.

One of the biggest problem faced during the force field set-up was the use of an attractive interaction between "C" and "N" beads. This force was introduced with the aim to induce Cell beads to follow the Neuritis beads during the growth process and maintain cell integrity. The drawback of the use of this interaction is to push some of "N" beads into the center of the neuron cell, thus preventing their movement towards the rectangles positioned outside the cell center of mass. In fact, when a "N" bead is created at the interface soma-medium, its distance with the "C" beads is obviously smaller than the distance "N"-"P1". In order to avoid this, the parameters of the attractive force of equation (2.15b) were set as:

- "N"-"P1" interaction, b_{NP1} = -1.5 ; r_{c2} = 4.0 r_c
- "N"-"C" interaction, b_{CN} = -1.0 ; r_{c2} = 2.0 r_c

Figure 4.6 displays the plot of the attractive force for the interaction N-C (green line) and N-P1 (red line).
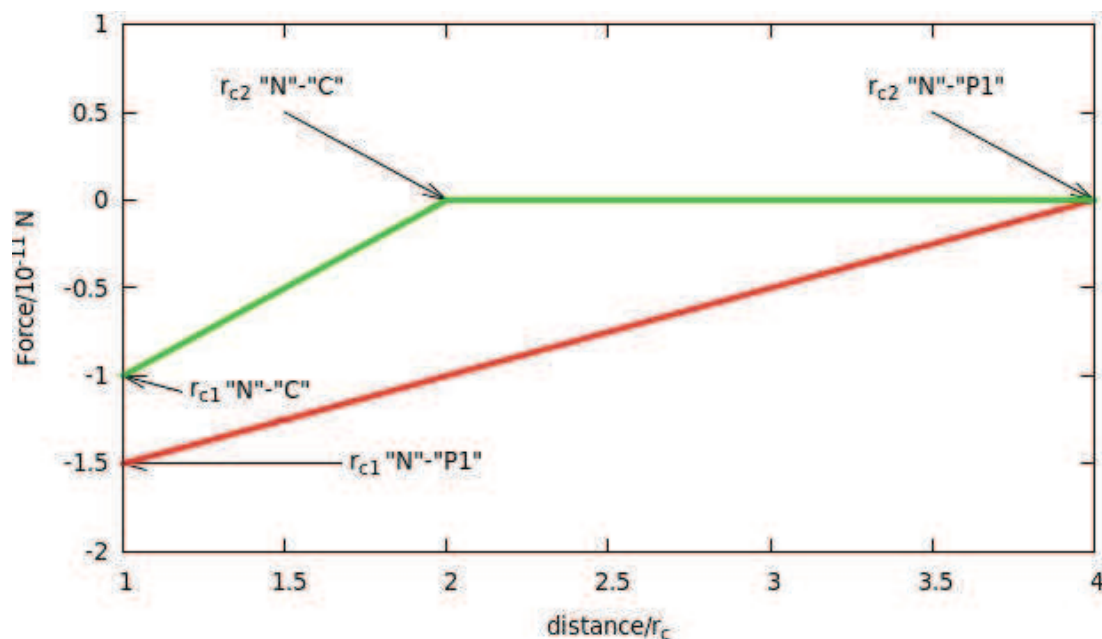

Figure 4.6. Plots of the two attractive forces used to simulate the "N"-"C" interaction (green) and the "N"-"P1" interaction. If an "N" particle has a distance with a "C" particle close to r_{c1} and the same "N" has a distance with a "P1" bead close to r_{c2} , the "N"-"C" interaction can be more negative than the "N"-"P1", pushing "N" into the cell center.

In order to avoid an excessive creation of "N" beads inside the cell, during the process of neuritis growth a process of conversion from "N" to "C" was performed every 50 steps for all the "N" with a distance smaller than 8 r_c to CP, the center of the pattern. The back transformation has also the advantage to simulate the metabolic cell mass growth that takes place during the axon growth.

A schematic diagram of the simulation procedure is presented in Figure 4.7.
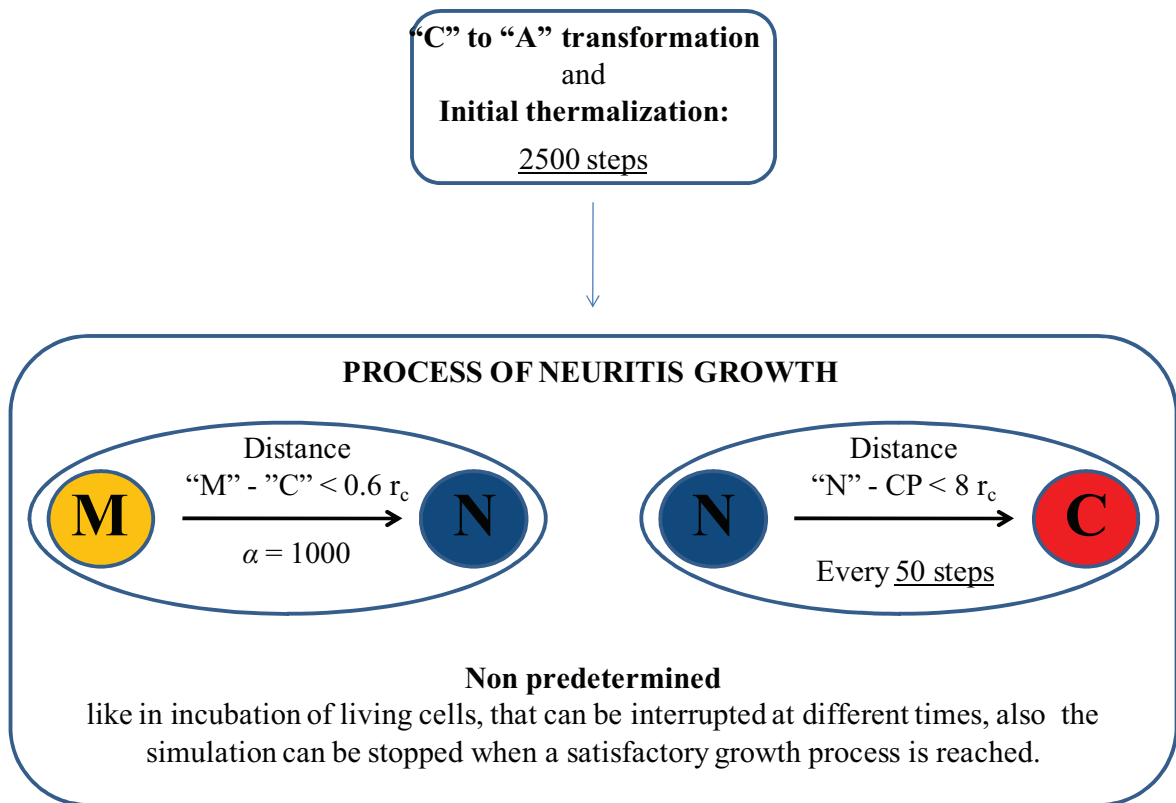
Figure 4.7. Scheme of the simulation process, after the equilibration, an indefinite number of steps can be performed in the process of neuritis growth.

It is clear that the model for the simulation of axon growth is more complicated than the one for cell adhesion described in Chapter 3. In this case in fact the biological process involves also the metabolic process of mass creation, that is not trivial to deal with since the model works with a constant number of system particle (NVT ensemble). Furthermore, as it will be explained later in the dissertation, one of the greatest problems related to this model was due to the extensive computational cost.

## 4.3. Results and discussion

In this section the main results obtained for the axon growth simulations on the three pattern geometries are presented. The analysis of the simulation results starts from the observation of the neuron behavior in time and its capacity to follow the rectangles patterns. Quantitative analysis of the time required for the neuron to expand and the ratio between the different growth directions has also been made.

4.3.1. Pattern S4-W4-L200

The first pattern that was investigated is the Geometry 3 displayed in Figure 4.3, that corresponds to the experimental pattern S4-W4-L200 described in reference 83. Compared to the other geometries, this one has the largest active surface ("P1" beads) due to the greater width of the rectangles ($w = 2.66$ r_c corresponding to about 4 μm, W4). The total pattern length, including the central spot, is about 135 r_c (corresponding to 200 μm, L200). The estimated force exerted by the Adhesive beads "A" on the pattern "P2" after the equilibration process was 9.6 nN/μm^2, the same order of magnitude of the previous simulation and of experimental results obtained for focal adhesion sites.

The simulation, after the first 2500 steps (50 τ), was performed for about 36000 steps (720 τ) corresponding to 14 hours of real time (36000*0.02*70/3600). At the beginning of the simulation, the neuron "senses", in reality explores thermally, the rectangular pattern both along the positive and the negative direction. In fact, around the central spot, the spacing between two subsequent rectangles is not very different in positive direction compared to the negative one. Small neuritis start to grow in the two directions with comparable probability. The pattern gradient is relevant only in the region far from the central circle. After about 400 τ (about 7.8 hours), the cell starts "to sense" the differences in the patterns provoking a preferential growth direction to the right (see Figure 4.8), as also experimentally observed by Fricke and colleagues.

In fact, after about 360 τ, the neuritis stops its growth to the left direction while continues its process along the positive direction, due to an increase of favorable interactions with "P1" beads. The recall force between "N" beads and CP (see equation 4.1) acts as a brake for the "N" beads growth, avoiding their excessive run towards the "P1" beads. At the same time, the attractive force between the Cell beads "C" and the Neuritis beads "N" prevents "N" beads escaping outside the cell.
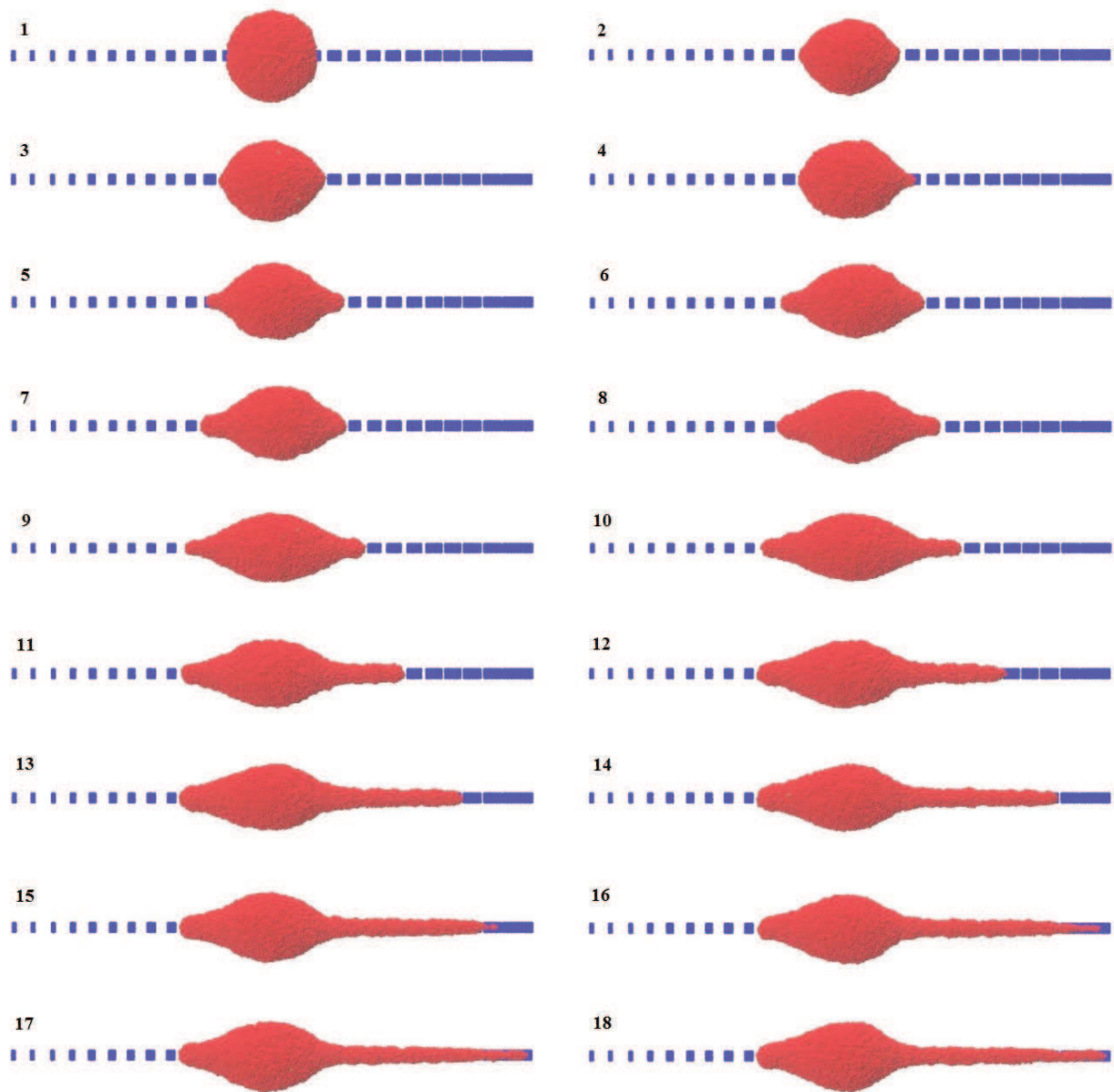
Figure 4.8. Simulated neuritis growth evolution for Geometry 3. Each successive number corresponds to 40 τ, meaning that in the figure the process starts from the top left image, at 40 τ, and finishes to bottom right, at step 720 τ.

Because the rat cortical neurons used as reference were analyzed after three days of incubation, the growth velocity of the simulations appears to be about five time faster than in the experiments. This fact can be explained considering the high computational costs necessary to run these simulations, a really heavy problem for the development of the process in the right timescale. The long time required to solve a single timestep considerably reduce the speed of the tests necessary in the model development and forbids the possibility to perform an higher number of simulation steps. In order to perform a

simulation in a reasonable amount of time, the production of "N" was accelerated, with a strong effect on the parameter α of (4.2), forcing the process to become faster.

In order to quantitatively characterize the axon growth, the neuron beads ("C" + "N") distribution in time were counted along the x axis (the axis along the gradient direction). The normalized bead number is defined as the number of cell beads ("C" + "N") at a position x divided the total number of beads of the cell. The normalized distribution profiles in time are displayed in Figure 4.9.
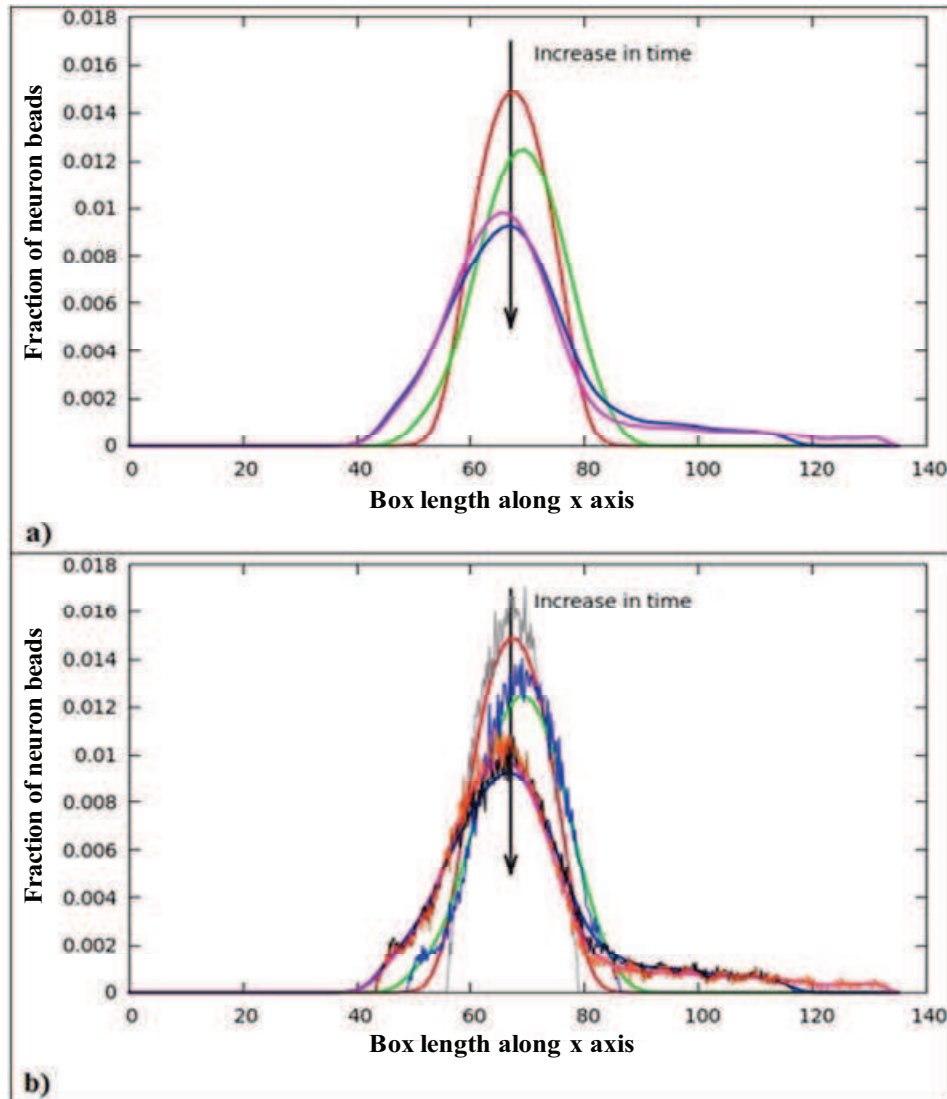

Figure 4.9. Fraction of neuron cell beads along the growth direction. a) Smoothed curves obtained by data interpolation. The red curve shows the distribution at time 0, the green one at time 240 τ, the blue one at 480 τ and the magenta at 720 τ. b) The smoothed curves compared with the real data (beads count) used for the interpolation. The asymmetric growth in time is evident.

In order to compare the simulation results with the experimental, the neuritis growth promoting index (NGPI) was evaluated (see Figure 4.10). NGPI is a quantity defined as the ratio between the growth in the right direction (positive) and the growth in the left one (negative):

$$NGPI = \frac{Positive\ growth}{Negative\ growth} \qquad (4.3)$$

The NGPI parameter gives a quantitative idea of how the pattern design can influence the growth direction.
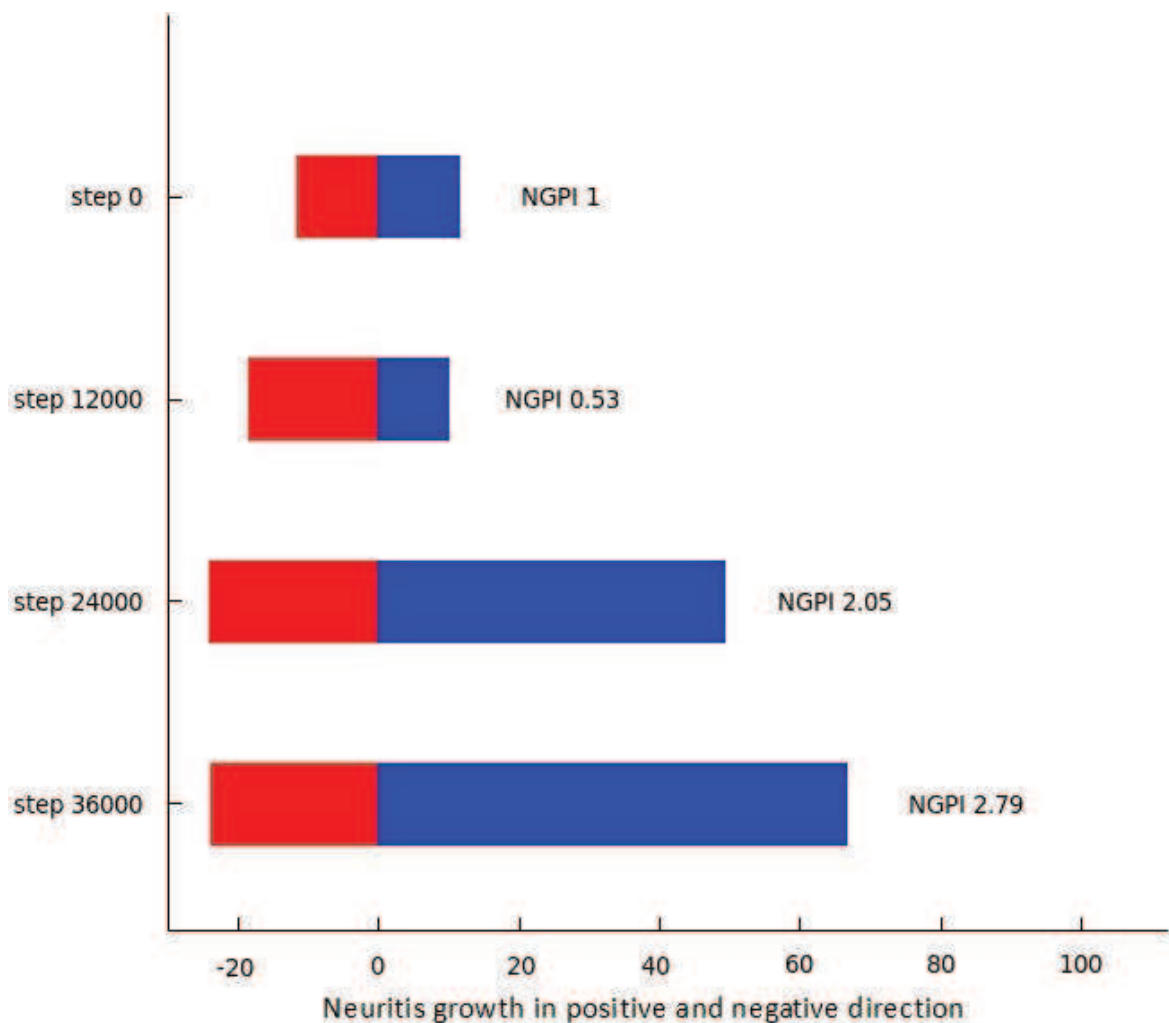

Figure 4.10. Neuritis growth in negative direction (left direction, red) and positive one (right direction, blue), at four different simulation steps (0, 12000, 24000, 36000).

Observing the results obtained by Fricke et al. on PLL/Laminin pattern S4-W4-L200, the experimental NGPI of 2.09 appears to be comparable with the one obtained bythe simulations (NGPI=2.05 at τ 480). Based on this single parameter is possible assert, with some caution, that the acceleration factor imposed to the simulation in the "N" creation process, it is about 7.7 time higher than the natural neuritis growth.

4.3.2. Pattern S4-W2-L200 and S1-W2-L200

The effect of pattern Geometry 1 (S4-W2-L200) and Geometry 2 (S1-W2-L200) on the axon growth was also investigated. The analysis of these two patterns offers the possibility to understand how the differences in the active substrate geometries can influence the results of the simulations.

The general characteristics of the gradients in Geometry 1, Geometry 2 and also Geometry 3 are similar; all the three patterns are made by a central spot and lateral rectangles. The differences between the three geometries are both in the rectangle slope and width. The first geometry (Geometry 1) is made by rectangles having a width of 1.33 r_c, (the half of Geometry 3) and a slope of 0.3 r_c. The second one (Geometry 2) has a slope of 0.1 r_c (one third of Geometry 1). The whole geometrical characteristics are summarized in Figure 4.3. In Geometry 1 the pattern beads "P1" covers 50% less than in Geometry 3, while in Geometry 2 about they are 85% less.

The presence of less "active" areas on the surface leads to a major difficulty to induce neuritis growth and extremely complicate the attempt to reach a general and effective parameter combination valid for a wide range of different "P1" beads geometries. The results of the simulations of patterns S4-W2-L200 and S1-W2-L200 actually reflect what has just been asserted:

- On pattern S4-W2-L200, where the "P1" beads covered area is 50% less than in Geometry 3, the growth appears less effective and also symmetric for left and right sides with NGPI of 1 (see Figure 4.11).

- On pattern S1-W2-L200 the growth is not induced and the simulated neurons maintain a complete spherical shape (Figure 4.12).
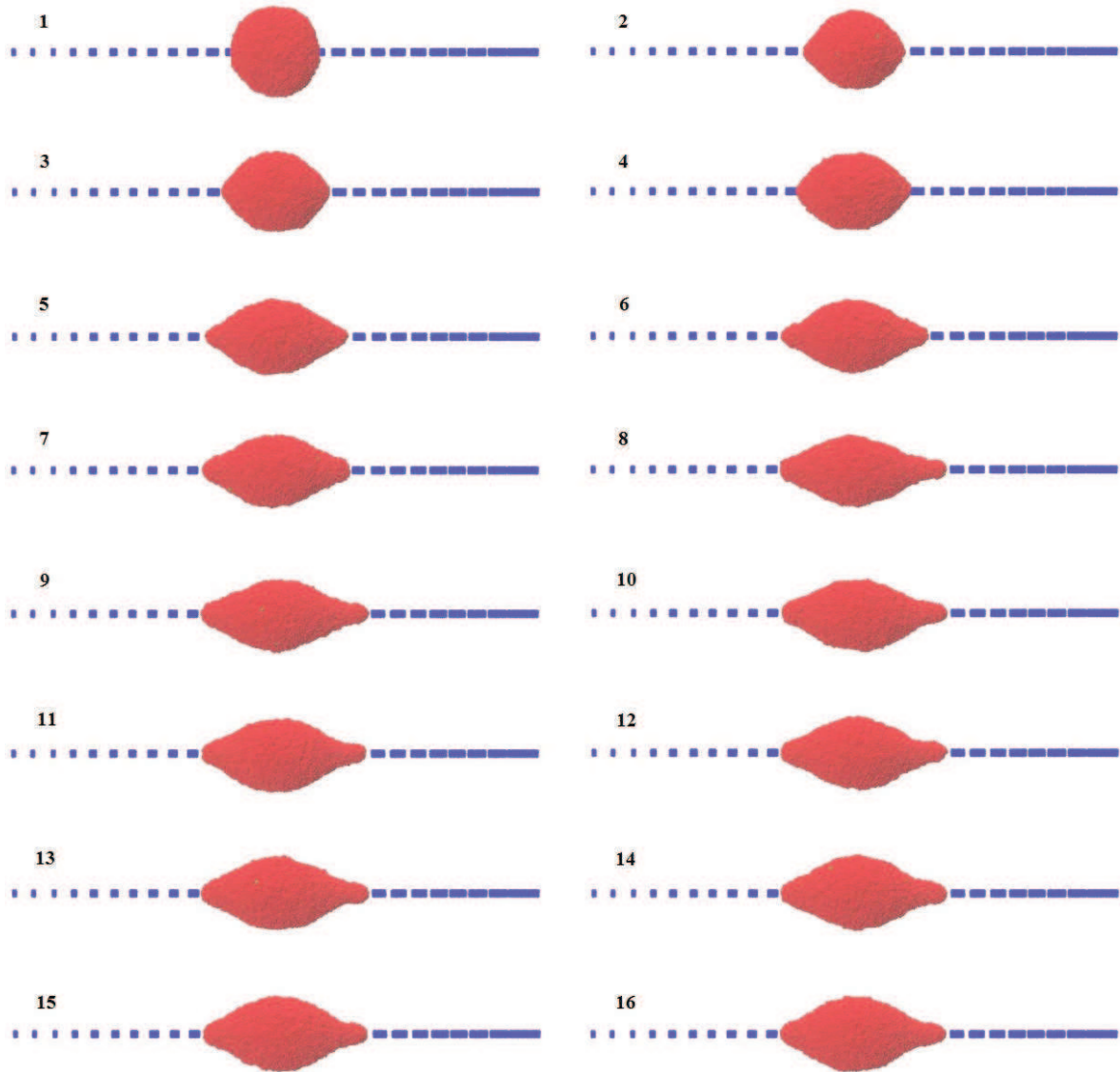
Figure 4.11. Simulated Neuritis growth evolution for Geometry 1. Each number correspond to 40 τ, meaning that in the figure the process starts from the top left image, at time 40 τ, and finishes to bottom right, at 640 τ. At 320 τ the neuron reach a stationary state and the neuritis growth process it is no longer performed.

Figure 4.12. Simulated Neuritis growth evolution for Geometry 2. The neuritis growth is not induced and the shape remains spherical during the simulation.

Similarly to the previous pattern geometry (S4-W4-L200), the experimental results obtained by Fricke et al. for the two Laminin/PLL geometries under investigation show the presence of a preferential axon growth direction (NGPI=1.75 for S4-W2 pattern and NGPI=1.19 for S1-W2 pattern) and an induced growth of about 60 μm or more in both directions.

Although the experimental data demonstrate a decrease in the preferential axon guidance in correspondence to a decrease of the Laminin/PLL active surface area, the simulation results are still far from the experimental ones. What emerges from an accurate analysis of the simulations is that the main limitation for a regular and appropriate neuritis growth is not preferentially due to the absolute value of the force, but mainly to the "N"-"P1" r_{c2} cut-off value, that is set equal to 4.0 r_c. The r_{c2} parameter, which defines the cut-off of the attractive force, is in fact the principal factor responsible for the incapacity of the "N" beads to have a sufficient force to move from one rectangle to the next one on the surface. The greatest effort during the parameterization process was in the creation of the correct balance between the long and the short range forces. Increasing the negative "N"-"P1" parameter without a modification of the r_{c2} means primarily increasing the short range force. The main consequence of such behavior is the accumulation of the "N" beads on the center of each rectangle (where a single "N" bead can "sense" the higher number of "P1" beads) with the formation of an irregular neuritis constituted by wide and narrow zones.

Another effect is the increasing difficulty to slow down the "N" beads movements when they reach the zone of the pattern characterized by short distances between the rectangles (positive direction) and, the difficulty to "jump" thermally from a rectangle to the next one when their distance appears to be high (negative direction). On the contrary, reducing the "N" - "P1" b_{ij} parameter would cause a competition of interactions with the "N" - "C" attractive force, thus causing "N" accumulation inside the soma. The increase of the cut-off radius of the same interaction would cause an increase of computational costs.

Considering all these issues, the increase of the cut-off radius for the long range interactions appears to be, however, the theoretical smartest solution, firstly because it reduces the differences between the short range region of the force and the long range one (lower slope of the linear force), and secondly because it increases the long range capacity of the force (see Figure 4.13).
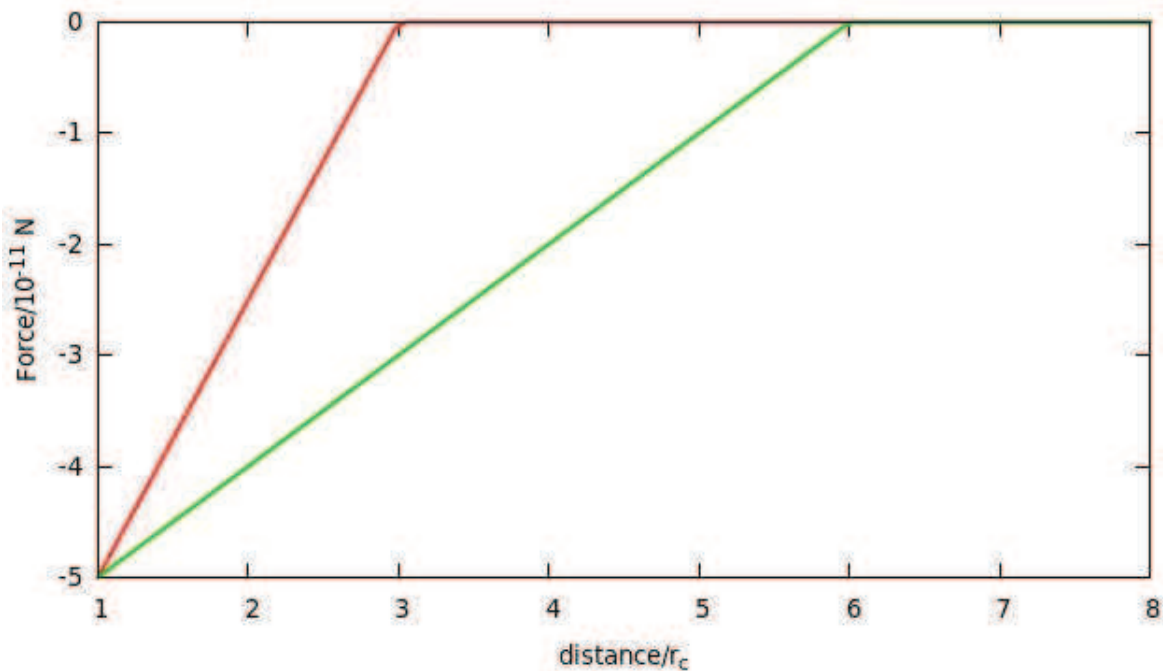
*Figure 4.13. Attractive force profile vsinterparticle distance in the case of the same negative **b** parameter (-5.0) and different long range r_{c2} cut-off radius (3 r_c red curve, 6 r_c green curve). The cutoff radius acts both in the long and short range.*

An increase of the cut-off radius would probably improve the simulation, but it would cause an enormous increase of the computational cost. An alternative solution could be the decrease of the coarse-grained level, with a consequent decrease of the simulation details, or a deep action on the equations that rules the inter-particle forces interaction.

In the case of this PhD project, however, I tried to maintain to maintain as much as possible the same conditions both for the neuron and for cell adhesion process. The results can be considered as a proof of concept of the development of a coarse-grained model valid for biological phenomena representation.

4.4. Conclusions

The CG model developed for the simulation of neuronal cell, with particular attention to the neuritis growth process on "active" substrates, represents an improvement of the cell adhesion model described in Chapter 3. In this case the adhesion process is only used to anchor the neuron to the central spot, while another and more complex biological process is investigated.

The model presents a higher level of complexity due to an increase of the number of beads types which leads to an increase of the number of parameters to set up. Because of this, the

parameterization of the inter-particle forces is non trivial and requires a high level of accuracy, in order to make the model general and valid for a wide range of patterns.

The validation of the model was performed trying to reproduce experiments carried out by Fricke and colleagues, where rat cortical neurons were deposed on "active" substrates with peculiar geometries. With the CG model,it was possible to reproduce the experimental functional surface gradients and compare their results with the ones obtained with our simulations.

Despite some good results related to the pattern S4-W4-L200 (Geometry 3), where the neuritis absolute growth and the NGPI index appears in good agreement with experiments, the model still presents some issues related to the capacity of reproducing a wide range of experimental data. In particular, in pattern S4-W2-L200 (Geometry 1) and S1-W2-L20 (Geometry 2), where the number of "P1" beads it is less than in Geometry 1 (and consequently also the active portion of surface), the neuritis growth appears to be modest (Geometry 1) or absent (Geometry 2) and no preferential growth in a particular direction was observed.

One possible solution to overcome the limitations could be the modification of the attractive force between "N" and "P1" beads (eventually with small adjustment to other parameters), both in terms of its value and the long range cut-off radius, with a preferential action on the second parameter. Unfortunately, this action appears not to be so straightforward, due to the high computational costs derived from the high coarse-grained level and, more importantly, due to the high long range cut-off radius that makes compulsory the calculation of an extremely high number of pair-interactions.

5. Guided droplet motion under the effect of an external transient perturbation

5.1. Introduction

In the two previous systems presented here, the drop-like CG model developed during my PhD thesis was used to investigate active processes that take place in biological phenomena. In fact, living cells belong to the class of "active soft matter" as they can produce forces, via complex metabolic processes, as a response to external chemical or mechanical stimuli. The cell adhesion onto a surface and the neuritis growth are active processes that can be controlled by the proper use of specific chemical cues on the surface. An inanimate droplet needs an external energy supply to perform non-equilibrium activities. Droplet can be used to collect energy or to transport substances inside them. These two important processes explain why the capacity to control their movement appears to be a primary challenge to deal with. The question arises of how it is possible induce and control droplets movement. In chapter 3 I have already presented an exhaustive introduction of how, with a clever use of physics and chemistry, it is possible induce droplets to became "active" and in some particular cases to behave like living cells. José Bernà and collaborators found a very interesting method to convert the energy of photons into a mechanical one. Using properly photo-excitable 'molecular shuttle' (rotaxanes), they were able to induce biased Brownian motion of a droplet of diiodomethane up to a twelve degrees incline.[84] Other experiments on droplets guide the motion by the use of photochemistry, electrochemistry, and the creation of surface tension or other chemical or thermal gradients.

The cis-trans light-promoted isomerization of azo-benzene monolayer substrates, were for example exploited to induce the guided motion of many different kind of droplets. The isomerisation process that occurs in the restricted surface area under illumination strongly acts on the local surface wettability creating a driving force for the movement.[85] Gallardo and co-workers were able to induce a biased organic fluid droplet motion by the proper control of the surface-tension gradient in an aqueous fluidic network.[86]

Also the creation of wettability gradients on a surface can be a good approach to stimulate self-propelled droplets movements. The clever use of non-covalent interactions that govern the wettability of a surface can be a good way to induce a mechanical transportation of small aggregates. Recently, it has been showed that the motion of liquid droplets on

electrically active substrates can be used to design devices able to harvest electrical energy. As demonstrated by Yin and co-workers, using a single layer of graphene as a conductive substrate for a small salty water droplets (volume smaller than 100 µL), it is possible to capture a small voltage, proportional to the droplet induced drag velocity (about 0.15 mV for induced velocities of 2.25 cm/s). The droplet movement process is purely mechanical: in this case in fact the superior part of the water is in contact with a SiO_2/Si wafer, able to produce favorable chemical interactions with the polar nature of water molecules (hydrogen bonds). The movement of the wafer at a constant velocity drags the droplets with the formation of a contact angle hysteresis of about 30 degrees andproduces a dynamic double layer with the graphene surface due both to the salt ions circulation and images charges produced by the metallic nature of single layer of grapheme.[88]

Other recent works demonstrated the possibility to harvest electrical energy from water movement on hydrophobic polymers deposed on a metallic electrode and to employ it to switch on LEDs or to power other small electronic devices.[89-92]

Many investigations were focused on droplets properties under the effect of statics or dynamics electric fields, with special attention to water droplets, that were studied as pure or as electrolytic salts solutions.

Research activities in this field were performed with different goals that ranged (a) from the desire of manipulating fluids at the micro length scale, which relates to the design of microfluidic systems or to the control of the biological matter like single biological cells, to (b) the study of droplet movements stimulator devices for electrical energy harvesting.

The self-propulsion of water droplets under the stimuli of electric fields (EF) is nowadays object of many studies in order to understand the principles that govern droplet motion or shape perturbations. These phenomena are observed in relation to the experimental procedure or the device geometry. The dielectrophoretic technique, that is the use of a non-uniform electric field to move particles made by dielectric materials (in many case fluids), is widely used to induce mass transport or shape deformation of systems that do not present net charges inside them but have only polarization capacity. Applications in the mass transport, such as the design of devices able to control the movement of carriers from a starting to a final point, or the capacity to set-up micro-reactors with the ability to induce a controlled collision between droplets containing different reagents, are an intriguing and interesting perspective.

The work of Mhatre and Thaokar shows for example how it is possible to induce pure water droplets motion in castor oil using an asymmetric design of electrodes. Droplets of

about 250 µm in radius were put under an extremely high potential difference (up to 900 V) between two electrodes separated only by 2.6 mm and, for this reason, highly stimulated to be polarized (high shape deformation proportional to the potential applied), forcing their movement from an electrode to the other one.[93] Ahn and colleagues used the same dielectrophoretic principle to obtain a controlled water-droplet separation in a microfluidic channel. They were able to make a system capable of guiding the particles in different microfluidic channels simply regulating the potential applied to the electrodes incorporated in the system.[94] The dielectrophoresis technique can be applied also to move bulk fluids (not only spherical droplets) from an inner reservoir to an outer one with the creation of a thin "finger" of flowing film of fluid between two strip electrodes at high potential.[95] This technique could also be used as a separation technique for living cells. In fact, bacteria, or other types of cells, can behave like dielectric droplets under non-uniform electric fields and can be attracted to particular areas of a device designed for cell separation and captured with the use of appropriate antibody or receptors. An example of this hybrid dielectophoretic system was presented by Allahrabbi and co-workers to show a possible alternative to cell separation techniques or, more challenging, for water purification against dangerous bacteria.[96]

Many further references could be presented to emphasize how dielectrophoresis can be a wide and promising technique to move liquid droplets.[97-99]

In addition to experimental work, also computational studies were made to understand the principles that govern droplets behavior during their movement and their interaction with surfaces.

The Molecular Dynamics technique was frequently used to simulate droplets at the nanoscale, with the aim to appreciate the molecular level of the phenomena that occur during translational or wetting processes.

Hong and colleagues made comparisons between static and dynamic contact angles for a water droplet deposited onto a surface. They analyzed the effect of the changes in the surface wettability and studied the advancing contact angle after provoking droplet movement. In their computational experiments, they supplied a constant acceleration to the hydrogen and oxygen atoms that compose the water molecules creating an artificial body force.[100]

Other MD and DPD studies were made on droplet spreading and wetting with the aim to understand the phenomena that occur at the boundaries of the droplet in contact with the surface. Using the many-body Dissipative Particle Dynamics, Zhao et al. were for example

able to show how the surface properties can influence both droplet morphology and contact angle, also considering impingement phenomena.[101] Computational studies on the effects that electric fields have on droplets were also taken into account. Droplet oscillations experimentally observed using dielectrophoresis were studied numerically for water droplets on insulating surfaces.[102] Molecular dynamics was also used to investigate the coalescence process between charged particle under constant and pulsating EF.[103]

An important topic concerning the possibility to control the droplet movement using electric fields is a process calling electrowetting. Electrowetting is based on the application of EF to change the wetting properties of a surface. As asserted by Mugele and Baret in an important review on this subject "Electrowetting has become one of the most widely used tools for manipulating tiny amounts of liquids on surfaces."[104] The applications of elettrowetting range from the microscale to the macroscale. A practical example is the set-up of lab on a chip devices for the control of the movement of fluid droplets in order to perform chemical reactions in the microscale dimension range. Another example that concerns everyday life is the invention of electronic displays based on electrowetting technology with the use of proper transistors and a combination between water and colored oil that constitute the pixels. The use of computational chemistry in this field helps in the understanding of the properties governing the electrowetting phenomenon. The continuum theories were the first to be applied with the aim to study the general behavior of the fluids on surfaces. Later studies performed using MD provided instead the possibility to discover new properties that become evident only at the molecular level, such as the possibility to build-up water micropumps via electric-driven flows through carbon nanotubes.[105]

Despite the fact that many different ways for the control and the manipulation of droplets are reported, a study of the effect of transient forces on fluids has not been considered.

In particular, a systematic scheme of the influence that a transient force can have on fluid droplet movement and possible morphological consequences has not been directly addressed in any scientific study. For this reason an application of the coarse-grained model can be its use for the analysis of droplets behavior in the presence of non-static forces, or in other words, under the effect of non-static substrates. In this way, the last part of my PhD work was focused on the observation of another and different aspects of active droplet behavior; no longer in relation to a static geometrical pattern acting as chemical cue, but instead under a transient and dynamic perturbation. A practical possible example of a transient force, can be the one generated by the charge flux passing through a Thin Film Transistor (TFT). Thin Film Transistors (TFTs) are devices where a flux of charges

can be forced to pass through a semiconductor channel, generating an electric field able to be sensed from the outside. TFTs are widely used as electronic devices where an electric field is used to control the current flow by acting on the semiconductor (Figure 5.1).
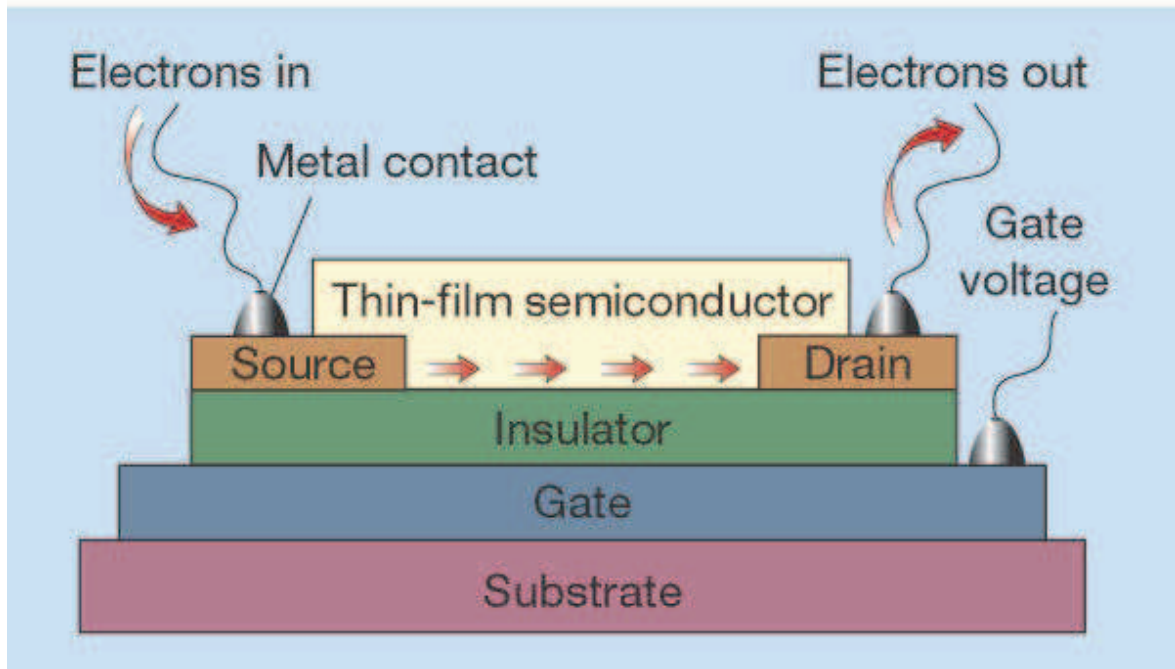
Figure 5.1. Cross section of a thin film transistor (TFT). The voltage applied at the gate activates the semiconductor and the application of a potential difference between source and drain allows the charge flow. Image from reference 106.

The current can pass through two terminals, the Source (S) and the Drain (D), under the control of the third terminal, the Gate (G) that influences the conductivity of the semiconductor inserted between S and D. The "activation" of the semiconductor depends on the voltage applied by G and thus on the intensity of the related electric field (they are in fact named "Field Effect Transistors", FETs).

I implemented a coarse-grained model based on the DPD method in order to theoretically investigate the motion of a liquid droplet driven by transient forces, applied on a solid substrate. In particular, I studied the motion of a small liquid droplet placed on a solid surface. The motion is induced by modifying in time the interaction forces between the droplet and a portion of solid substrate. The driving force can be controlled by tuning the strength and the velocity of translation. The effect of the surface wettability was also considered.

The surface wettability represents the capacity of the droplet to form interactions with the surface. Normally, the higher the surface wettability, the higher the capacity of the surface to form strong non-bonded interactions with the droplet and reduce its movement.

I carried out 150 independent simulations, by changing one parameter at time. This systematic study offers the possibility to understand the effect of each parameter on the droplet movement. Our model would like to be nonspecific and to assume a broad valence showing the general behavior of soft matter droplet movements in a systematic way. This can be crucial in the process of development of new techniques, providing guidelines for creating new experimental set-ups.

5.2. Description of the model

Brief consideration:

Since the DPD technique is based on the use of reduced quantities, all the data in this chapter will be presented in dimensionless units. This allows to show the correct proportions and trends without the necessity to refer to a specific real system. The mapping to real physical values can always be done by considering a real precise system, that at this point of the work was not considered.

The system consists of a box of dimensions 36x36x25 r_c, in which a spherical coarse-grained droplet of diameter 10 r_c is surrounded by a fluid medium and is placed on a solid surface, at the center of the simulation box. The surface is made by two fixed layers of beads, one on the top of the other, with a face centered cubic (fcc) arrangement. The system is composed by 205500 beads, 3030 for the droplet ("D" beads), 182870 for the medium ("M" beads), 9800 for each surface layer ("S1" beads, to the top and "S2" beads to the bottom). The beads density for the fluid part of the simulation box is set to $\rho_{drop} = \rho_{medium} = 6$ beads/r_c^3, while a higher density of $\rho_{surface} = 21$ beads/r_c^3 was chosen for the solid layers to avoid, in combination with the fcc geometry, the penetration of "D" and "M" inside the surface. Figure 5.2 displays the initial arrangement of particles, without fluid medium.
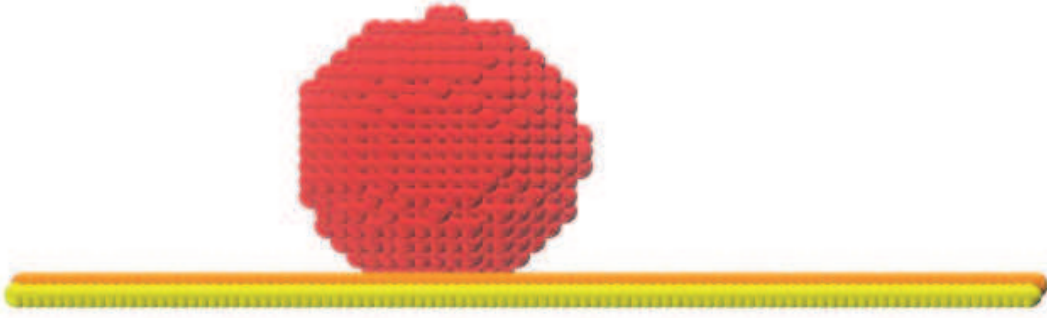
Figure 5.2. Side view of the droplet (red beads) placed on the top of the two layers of fixed particles ("S1", top orange beads and "S2",bottom yellow beads). The medium that surrounds the droplet is not showed.

In addition to the four types of bead already mentioned, a fifth type of bead was introduced for the implementation of the force. This force acts between the droplet and a single bead that is modified at the bottom of the surface during the simulation. This "active" bead "A" is dynamically created bya conversion of a bead "S2" into "A". The position of an "A" bead is always inside the plane, called x-y, of the bottom layer. The solid surface has a square area of 36x36 r_c^2 and, considering the solid density of 21 beads/r_c^3, this means that each layer is formed by about 9800 beads. These particles are perfectly arranged in a square lattice, with an inter-particle distance of 0.364 r_c.

The effective movement of the "A" bead takes place along the x-axis in the positive direction. In reality, the bead does not move, it is its identity that moves from "S2" to "S2" bead. The x-coordinates of the "S2" beads can be defined as x(i)=0.364*i, with the index i ranging from 1 to 99. The first "A" bead is created by converting randomly a "S2" bead with x(i=1) and y between 16 and 20 r_c. The subsequent transformations are a consequence of the position of the "A" bead as follows:

1. A list of the three "S2" vicinal particles of "A", with $x_{S2} > x_A$ is created.
2. The new "A" bead is created with a random transformation of one of the vicinal S2.
3. A back transformation process of the previous "A" bead into "S2" is performed. Only one "A" beads is present, at any time, in the simulation.

The creation of the "A" bead takes place every ΔT_A time steps. By tuning this parameter, one can control the velocity of translation of the perturbation force, v_{PF}, as:

$$v_{PF} = \frac{0.364}{\Delta T_A} \qquad (5.1)$$

The higher is v_{PF}, the higher the "A" translation velocity is.

Figure 5.3 displays schematically the procedure just explained.
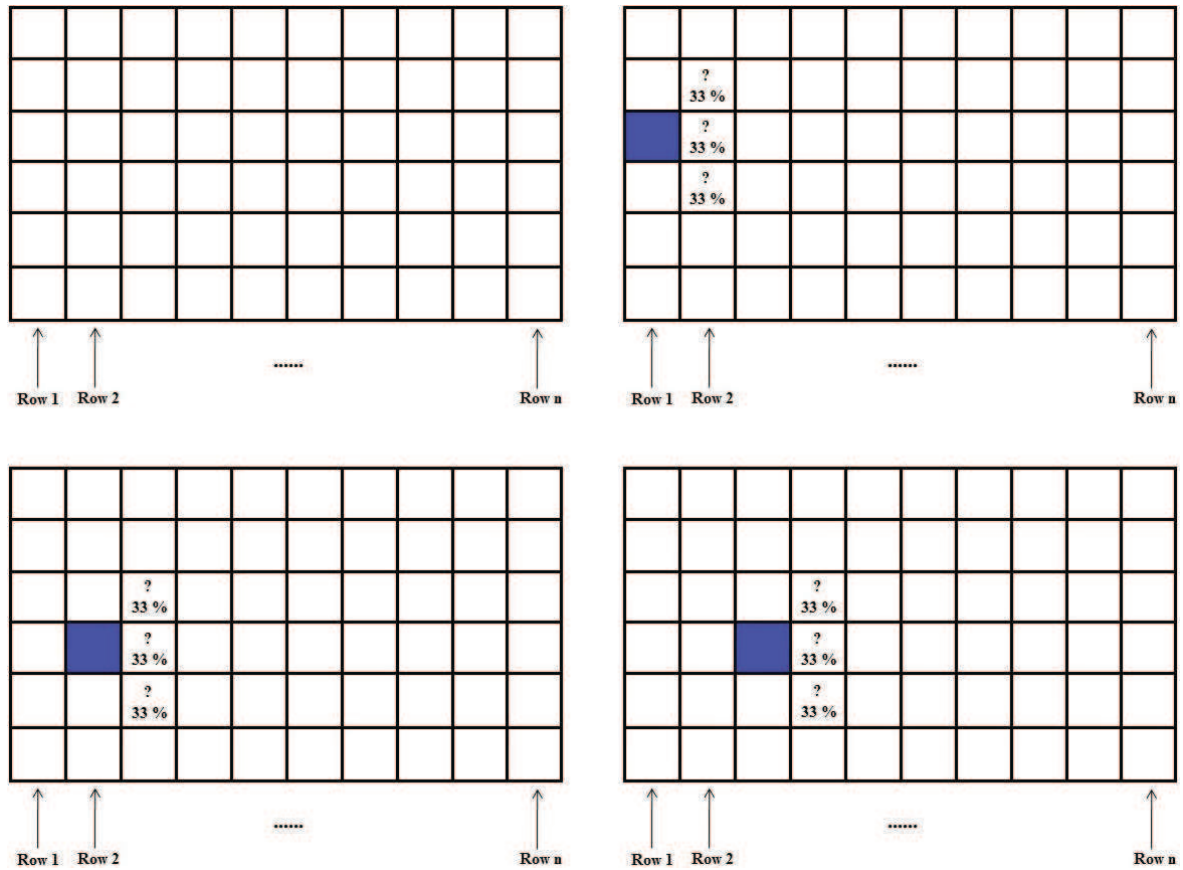
Figure 5.3. Procedure of creation of "A" beads during the simulation. The grid represents a simplification of the surface geometrical disposition of "S2" beads. In blue the "A" bead position is schematized. The "S2" neighbors of "A" have a probability of 33% to be converted into "A".

The temperature of the system is controlled by the DPD thermostat. The γ friction parameter of the Dissipative Force was set to 5.61, the reduced temperature $T = 0.53$ and the timestep $\delta t = 0.02\ \tau$, where τ is the dimensionless time unit.

The conservative forces implemented in the model will be now presented.

The interaction between the fixed particles ("S1", "S2" and "A") is not defined, as it is not necessary.

All the other interactions are soft repulsive, able to avoid the unphysical phenomenon of the interpenetration between particles and penetration into the surface. The repulsive interaction is described by the soft linear force of equation (2.15a) of the Computational Method chapter.

Only one attractive interaction as described by equation (2.15b) is implemented in the model and acts between beads "A" and "D". The parameter b_{ij} that represents the maximum strength of this interaction can be tuned. The effect of the value of b_{ij} on the droplet motion was also investigated.

A complete list of the soft-repulsive parameters a_{ij} used in all the simulations is presented in Table 5.1. The cut off radius r_{c1} for all these interactions was set to 1.0 r_c. The "D"-"S1" interaction parameter (a_{DS1}) can control the wettability of the surface. Different wettability degrees were considered, thus the corresponding parameter in the Table is a "variable".

Table 5.1: List of soft repulsive parameters used for the simulations[a]

a_{ij} (k_bT/r_c)	i =					
		D	S1	S2	M	A
j =	D	12.5	Variable	100	65	100
	S1		/	/	100	/
	S2			/	100	/
	M				12.5	100
	A					/

[a]*The repulsive parameter "D"-"S1" was used as variable to test different wettability conditions.*

Several systems were considered:

1. The surface wettability is controlled by the "D"-"S1" repulsive parameter a_{DS1}. The higher the parameter, the lower the wettability of the surface. In particular, we considered three surfaces, corresponding to a_{DS1}= 25, 50 and 100 k_BT/r_c.
2. The velocity of translation of bead "A" is controlled by the parameter v_{PF}. Five values were considered, v_{PF}= 0.364, 0.182, 0.121, 0.091, 0.073 r_c/τ.

3. The strength of the interaction between the droplet and the transient particle in the surface, namely the b_{DA} parameter. It determines the favorable interaction between the "A" bead and the droplet. Ten different values of b_{DA} were considered: -0.5, -1.0, -1.5, -2.0, -2.5, -3.0, -3.5, -4.0. -4.5, -5.0 $k_B T/r_c$. The cut-off radius for the attractive force $r_{c2\text{-}DA}$ was set equal to 3.0 r_c for all the simulations.

The scheme presented in Figure 5.4 shows that a total of 150 systems were investigated.
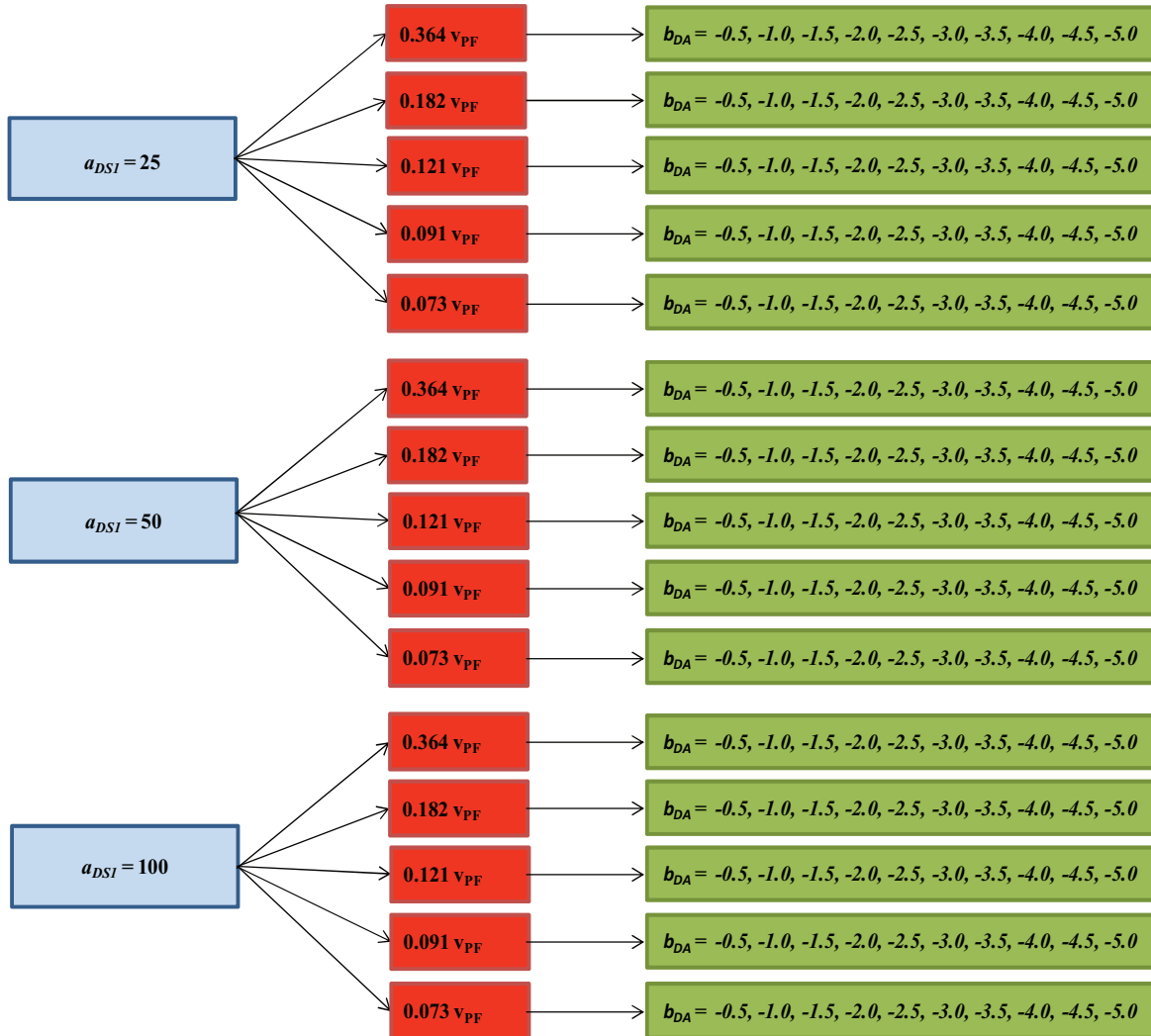
Figure 5.4. Scheme of the 150 systems investigated. For each "D"-"S1" interaction (blue rectangles) 5 different v_{PF} were considered (red rectangles). Ten "D"-"A" different attractive forces were implemented for each combination (green rectangles).

At the very beginning of the simulation, the spherical droplet is placed on the top of the surface with its center of mass at coordinates $x_{CM} = 15 r_c$ and $y_{CM} = 18$ r_c.

Each simulation consists of about 99 "A" bead movements, meaning 99 transformation of an "S2" bead to an "A" and the contemporary back transformation of the previous "A" to "S2". Since 99 movements are required to walk along the entire surface in the positive x-direction, 1 complete cycle was performed for each simulation. The initial set-up of the droplet along with the first "A" bead creation procedure (y coordinates between 16 and 20 r_c) increases the possibility that the active beads passes under the droplet during its random path.

For all the systems, the same protocol was applied: 2500 equilibration steps were performed to thermalize the system, before the introduction of the "A" bead in the surface. After this procedure, the process of "A" creation starts and continues for 99 steps. The total simulation run time depends on the translation velocity of the transient force.

5.3. Results and discussion

In this section an overview of the droplet behavior in relation to the different parameters combination will be presented.

During the simulation, the "A" bead exerts a force on the droplet whose intensity is related to the b_{DA} value and to the average distance between the "D" beads and "A". The value of the cut-off radius for the attractive force ($r_{c2\text{-}DA}$) was set equal to 3.0 r_c: this means that all the "D" beads with a distance from "A" higher than 3.0 r_c are not involved in the attractive interaction. However, since the droplet can be considered as a unique entity of soft matter, even the influence on a small portion of it can affect the entire system and guide the movement of the full entity, with important morphological implications that will be further described.

All the simulations were characterized in terms of motion of the droplet center of mass (CM), contact angle hysteresis (θ_{hyst}), transient force analysis, and work exerted by the "A" bead to the droplet center of mass. However, in order to rationalize the results, only some representative analysis and explicative parameters combinations will be presented.

We considered the same droplet on three different surfaces, characterized by three droplet equilibrium contact angles (see Table 5.2) As in all the three surfaces the equilibrium contact angle is lower than 90 degrees, we can consider the three surfaces as hydrophilic.

Table 5.2: Droplet equilibrium contact angle (θ₀) as a function of the droplet-surface soft repulsive parameter (a_DS1).

Surface	a_{DS1} ($k_B T/r_c$)	θ_0 (degree)
SURF-A	25	55
SURF-B	50	65
SURF-C	100	75

First, we analyzed the effect of the velocity of translation of the perturbation force applied on the droplet as a function of three different interaction strengths. Figure 5.5 displays the x-coordinate of the droplet center of mass (x_{CM}) as a function of the "A" bead position on the surface "SURF-A" (first row) for the systems with b_{DA}=-5.0 (first column),-3.0 (second column) and -1.0 (third column) $k_B T/r_c$. The same analysis was performed also for the surface "SURF-B" and "SURF-C" (see Figure 5.5 second and third row, respectively).
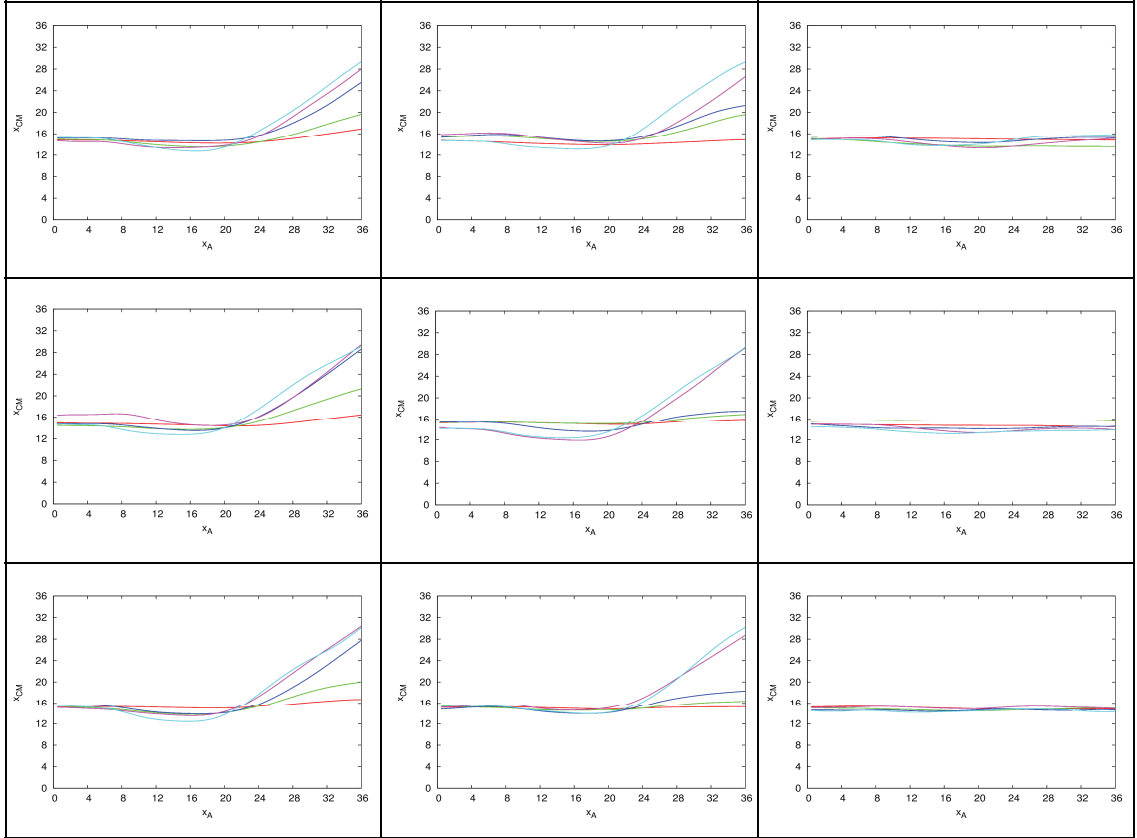
Figure 5.5. x-coordinate of the droplet center of mass (x_{CM}, expressed in r_c) as a function of the x position of "A" bead (x_A, expressed in r_c) for three different values of the b_{DA} parameter (b_{DA}=-5 first column, b_{DA}=-3 second column, b_{DA}=-1 third column) and for the three surfaces ("SURF-A" first row, "SURF-B" second row and "SURF-C" third row). Each plot displays the curves for the five different attractive force translational velocities: v_{PF} = 0.364 (red), 0.182 (green), 0.121 (blue), 0.091 (magenta) and 0.073 (cyan) r_c/τ.

Except for the simulations with a mild attractive force (b_{DA} = -1 k_BT/r_c),it is possible to observe that effectively a single attractive force is able to move the entire droplet. In fact, in all three surfaces and for higher strength of the attractive force (b_{DA} = -5 and b_{DA} = -3 k_BT/r_c), the droplet starts to move toward the positive x-direction as soon as the "A" bead is below the droplet-surface contact area. When the droplet beads start to "sense" the "A" bead, i.e. when $x_A \approx$ 10 r_c, there is an effect of back-bounce: the droplet center of mass moves slightly toward smaller values of x.

This fact can be explained considering the trajectory that "A" has during the simulation: it starts from the left side of the surface (x_A=0 r_c and finishes at the right of the simulation box (x_A=36 r_c). The droplet center of mass is initially positioned at about 15 r_c along the x-coordinate. Because the "A" bead starts its walking path from the left side, it primarily provokes a transient left-side push of the droplet.

If the velocity of x-translation is not too large (for v_{PF} < 0.073 r_c/τ), the droplet starts to follow the "A" bead. The slower the velocity, the higher the possibility for the droplet to "sense" the attractive force.

It is not surprising that the higher is the negative force, the higher is the effect on the droplet.

Since the analysis of the center of mass of the droplet beads does not provide any information of the droplet shape during its movement, further inspection of the trajectories was carried out in order to detect anomalies. Figure 5.6 displays few snapshots of two simulations:
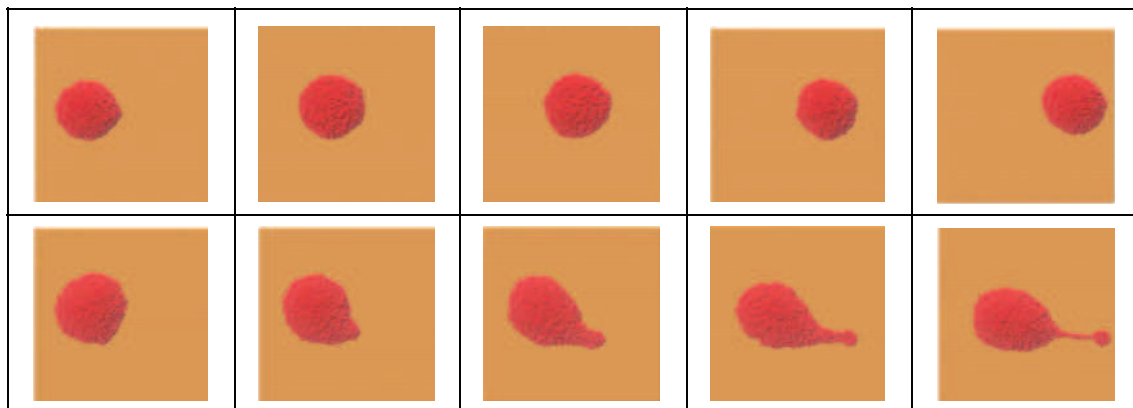

Figure 5.6. Snapshots of the droplet response (red beads) on surface (orange beads) in different droplet simulations under the effect of a transient attractive force. Top row: droplet motion onto "SURF-C" with b_{DA}=-5.0 k_BT/r_c and v_{PF}= 0.073 r_c/τ; bottom row: droplet motion onto "SURF-A" with b_{DA}= -5.0 k_BT/r_c and v_{PF} = 0.364 r_c/τ.

The effects of the surface wettability and of the "A" speed appear evident for the control of the droplet movement and deformations. At the same negative b_{DA} values and high v_{PF} do not allow the "D" beads to rearrange and follow the perturbation. The high wettability encourages spreading of the droplet and the formation of a front tail. This combination leads to high deformation and possible droplet break-up. Low wettability and low "A" speed cause the entire droplet structure to follow the perturbation and maintain a quasi-spherical shape.

In addition to the analysis of the beads trajectories, also the study of the contact angles can be helpful to understand the morphological characteristics of the droplet under the perturbation.

During droplet motion along a solid surface, the contact angle is not at equilibrium, but undergoes an asymmetric deformation, with a difference between the "advancing contact angle" (θ_a) and the "receding contact angle" (θ_r). The difference in advancing and receding contact angles has been denoted as contact angle hysteresis (θ_{hyst}) (i.e., $\theta_{hyst} = \theta_a - \theta_r$).[107] The analysis on the advancing and receding contact angles and relative contact angle hysteresis (θ_a - θ_r) were made with the aim to deeper study the deformations that can occur to the droplet during the motion.

Table 5.3 reports the average hysteresis contact angles calculated for the droplet motion on the three surfaces, for three representative control parameters v_{PF} and b_{DA}. The contact angles were estimated with the software ImageJ (*https://imagej.nih.gov/ij/*) when the "A" bead is under the droplet-surface contact area, that is when the droplet starts to "sense" the attractive force and thus eventually moves.

Table 5.3: Advancing, receding and contact angle hysteresis[a]

SURF-A	v_{PF} = 0.364	b_{DA} = -1.0	θ_a = 55°	θ_r = 55° *	θ_{hyst} = 0° *
		b_{DA} = -3.0	θ_a = 55°	θ_r = 55°	θ_{hyst} = 0°
		b_{DA} = -5.0	θ_a = 25°	θ_r = 55°	θ_{hyst} = -25°
	v_{PF} = 0.121	b_{DA} = -1.0	θ_a = 55°	θ_r = 55°	θ_{hyst} = 0° *
		b_{DA} = -3.0	θ_a = 40°	θ_r = 55°	θ_{hyst} = -15°
		b_{DA} = -5.0	θ_a = 35°	θ_r = 60°	θ_{hyst} = -25°
	v_{PF} = 0.073	b_{DA} = -1.0	θ_a = 55°	θ_r = 55°	θ_{hyst} = 0° *
		b_{DA} = -3.0	θ_a = 35°	θ_r = 55°	θ_{hyst} = -20°
		b_{DA} = -5.0	θ_a = 35°	θ_r = 55°	θ_{hyst} = -25°
SURF-B	v_{PF} = 0.364	b_{DA} = -1.0	θ_a = 65°	θ_r = 65° *	θ_{hyst} = 0° *
		b_{DA} = -3.0	θ_a = 55°	θ_r = 65°	θ_{hyst} = -10°
		b_{DA} = -5.0	θ_a = 35°	θ_r = 65°	θ_{hyst} = -30° *
	v_{PF} = 0.121	b_{DA} = -1.0	θ_a = 65°	θ_r = 65°	θ_{hyst} = 0° *
		b_{DA} = -3.0	θ_a = 60°	θ_r = 65°	θ_{hyst} = - 5° *
		b_{DA} = -5.0	θ_a = 50°	θ_r = 70°	θ_{hyst} = -20° *
	v_{PF} = 0.073	b_{DA} = -1.0	θ_a = 65°	θ_r = 65°	θ_{hyst} = 0° *
		b_{DA} = -3.0	θ_a = 55°	θ_r = 65°	θ_{hyst} = -10° *
		b_{DA} = -5.0	θ_a = 60°	θ_r = 60°	θ_{hyst} = 0° * *
SURF-C	v_{PF} = 0.364	b_{DA} = -1.0	θ_a = 75°	θ_r = 75° *	θ_{hyst} = 0° *
		b_{DA} = -3.0	θ_a = 60°	θ_r = 75°	θ_{hyst} = -15°
		b_{DA} = -5.0	θ_a = 50°	θ_r = 70°	θ_{hyst} = -20° *
	v_{PF} = 0.121	b_{DA} = -1.0	θ_a = 75°	θ_r = 80°	θ_{hyst} = -5° *
		b_{DA} = -3.0	θ_a = 55°	θ_r = 80°	θ_{hyst} = -25° *
		b_{DA} = -5.0	θ_a = 45°	θ_r = 80°	θ_{hyst} = -35° *
	v_{PF} = 0.073	b_{DA} = -1.0	θ_a = 80°	θ_r = 80°	θ_{hyst} = 0° *
		b_{DA} = -3.0	θ_a = 55°	θ_r = 75°	θ_{hyst} = -20° *
		b_{DA} = -5.0	θ_a = 70°	θ_r = 80°	θ_{hyst} = -10° * *

[a]*The contact angles were obtained when the position of "A" was at 75% of its walking path (27 r_c) so that the droplet was under its influence. The first column defines the wettability, the second one the "A" velocity, the third one the "A" attraction capacity, the fourth one both the advancing and receding contact angles and the fifth column the contact angle hysteresis. The colored asterisks remark important data relationship.*

In the most common cases of droplet motion on a surface, the contact angle hysteresis assumes a positive value. This is normally due to the differences between the molecules that are close to the surface (and interact with it) and the molecules on the top of them, which are freer to move and have a higher number of degrees of freedom. An example of this situation can be the case of a droplet sliding on an inclined surface (Figure 5.7), where the external force acting on the body is the gravity force.
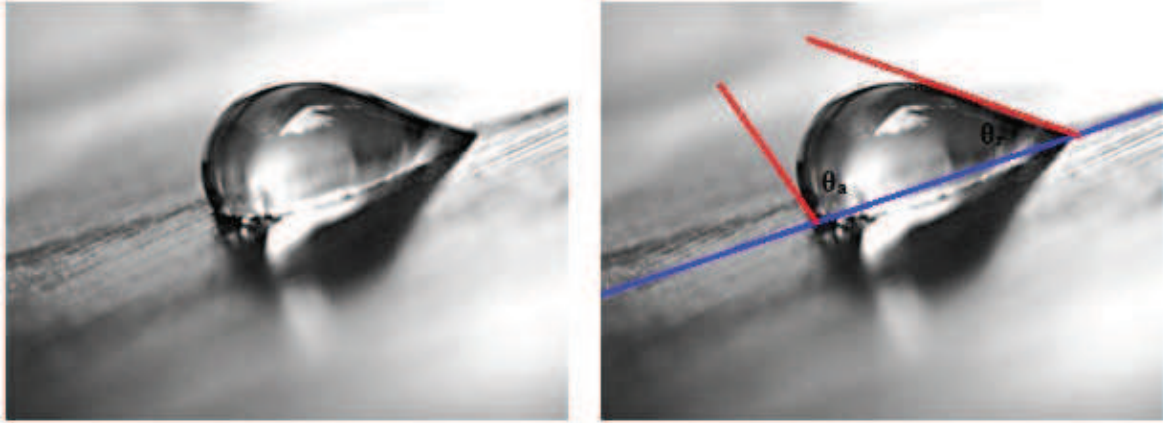
Figure 5.7. Water droplet moving on inclined plane. The movement provokes a positive hysteresis, $\theta_{hyst} = (\theta_a - \theta_r) > 0$.

In this simple situation, the interactions of the molecules with the surface plane, make them stick on the surface and reduce their freedom while the molecules on the top, less constrained, have a higher capacity to move under the action of the external force.

On the contrary, the data presented in Table 5.3 show negative values of the hysteresis. This difference can be fully understood by analyzing the characteristics of the force implemented inside the CG model. First, it has to be considered that the "A" bead is forced to pass at a certain distance (0.72 r_c) under the droplet, in the plane of the lower layer of the surface. This means that the attractive force acts always at the bottom of the droplet body. The second aspect to be considered is related to the $r_{c2\text{-}DA}$ value (3.0 r_c) that defines the cut-off of the attractive force between beads "D" and "A". Since the "A" movement follows a precise direction, also the "D" beads attracted by "A" will follow the same direction. Therefore, the front part of the droplet will be more influenced by "A" compared to the other side.

The condition just described avoids the formation of a back tail but instead promotes the formation of a front tail. The other parameters involved in the process, such as for example the surface wettability, can help or hinder both the formation of a front tail and the droplet movement.

A negative hysteresis can for instance appear in the presence of a hydrophilic surface gradient, where the front part of a water droplet "senses" a more favorable interaction than the rear part. An explicative computational study of a water nanodroplet on a wetting gradient surface made by Wang et al. showed the same front tail behavior, with the front water molecules attracted by the more favorable surface.[108]

The relationship between our mechanical model and the case reported by Wang is in the interaction; in both cases the force acts from the bottom and the rear part of the droplet "senses" a lower interaction than the front one. In any case, it is known that the degree of hysteresis can give a measure of the force that drives the droplet motion.

To better understand the droplet behavior in relation to the parameter combination applied, a deeper analysis of Table 5.3 is required and a schematic list of observations is reported:

1. The attractive interaction b_{DA}= -1.0 is not sufficient to cause droplet deformation. For any parameter combinations the hysteresis it is always 0. Red asterisks (*).

2. The contact angle increases as the parameter a_{DS1} increases and the surface decreases its wettability. Black asterisks (*).

3. The hysteresis absolute value decreases in relation to ΔT_A. Higher velocities implicate higher deformations. High negative b_{DA} values in combination with high ΔT_A allow droplet motion without any geometrical perturbation (θ_{hyst} = 0°). Green asterisks (*).

4. In relation to v_{PF}, an increase of the b_{DA} negative force can produce higher or lower contact angle hysteresis. Purple asterisks (*).

It has already been explained that when b_{DA} it is sufficiently high to induce the "D" beads to follow "A", the deformation of the droplet (formation of a front tail) depends both on the "A" velocity (v_{PF}) and surface wettability. Faster "A" movement, decreases the ability of "D" beads to re-organize their position under the perturbation, in particular for those beads which are far and "sense" little or no attraction (higher distance than r_{c2} = 3.0). The consequences of this is that only few beds have the ability to follow "A" and the formation of a thin front tail it is produced. If the surface is poorly wettable, the thin tail can be reabsorbed into the droplet body. In the presence of the opposite conditions (e.g. high wettable surface), the tail can instead detach from the droplet body such as in the bottom row of Figure 5.6.

An increase of the negative force not always provokes a higher hysteresis, as asserted at point 4 (purple asterisks in Table 5.3). Due to the time required to the "D" beads to rearrange, if the "A" bead is sufficiently slow, the contact angle hysteresis decreases. On the opposite, if "A" is fast, the contact angle hysteresis increases because the entire droplet structure has no time to rearrange and the formation of a strong front tail is promoted.

The total interaction force between the droplet and the transient "A" bead was calculated as a function of the "A" bead x-position (see Figure 5.8).

This information allows to have an idea of the perturbation exerted on the whole droplet by the "A" bead. The calculation of the average force that acts on "D" beads in time is in fact a valid method to understand how much force is required to influence the droplet, also in relation to the other parameters that play a role in the simulation.

As showed in Figure 5.8, an extended presence of the force along the x-coordinate is a clear indicator of the droplet capacity to follow "A".
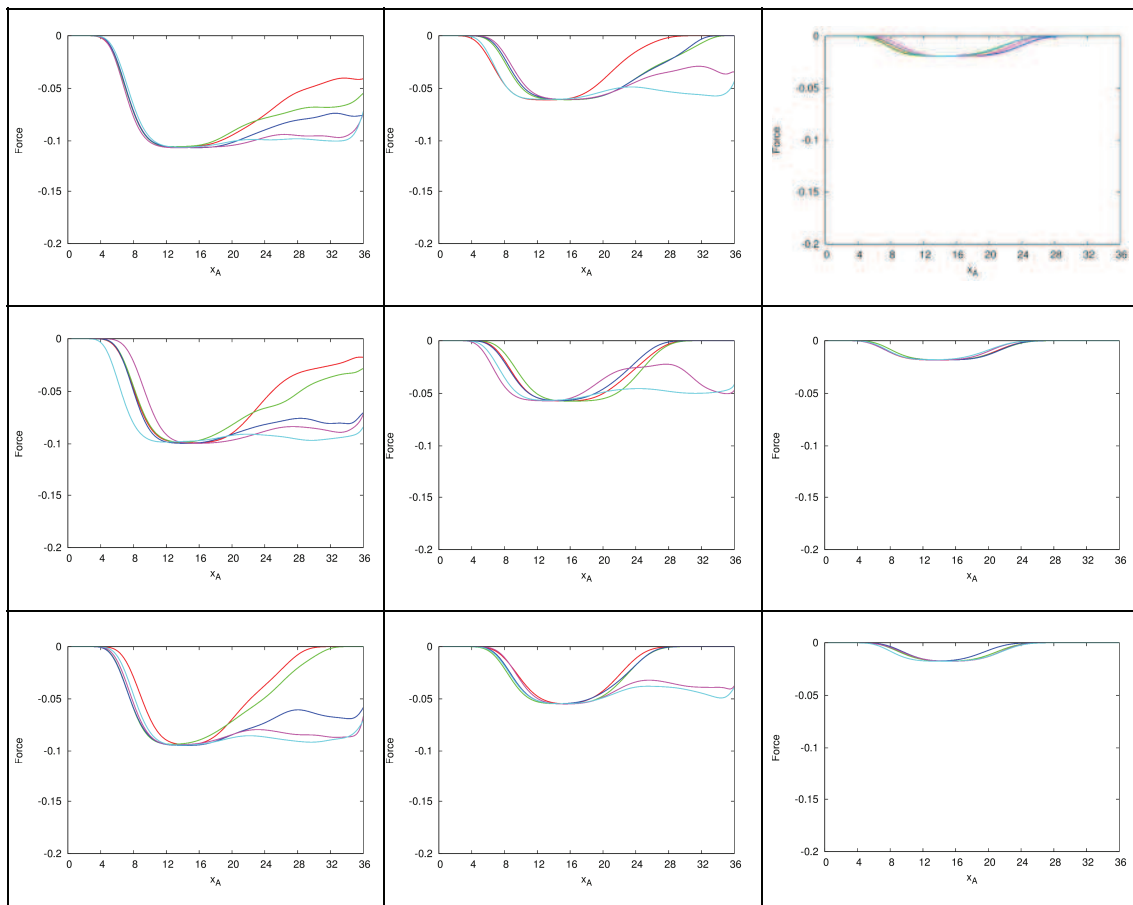
Figure 5.8. Mean force exerted on the "D" beads (expressed in k_BT/r_c) as a function of the x position of "A" bead (x_A, expressed in r_c) for three different values of the b_{DA} parameter (b_{DA}=-5 first column, b_{DA}=-3 second column, b_{DA}=-1 third column) and for the three surfaces ("SURF-A" first row, "SURF-B" second row and "SURF-C" third row). Each plot displays the curves for the five different attractive force translational velocities: v_{PF} = 0.364 (red), 0.182 (green), 0.121 (blue), 0.091 (magenta) and 0.073 (cyan) r_c/τ.

A mean attractive force of about -0.02 $k_B T/r_c$ is not sufficient to cause droplet motion. This is the case of the simulations with $\boldsymbol{b_{DA}}$ parameter set to -1.0 $k_B T/r_c$.

By increasing the $\boldsymbol{b_{DA}}$ parameter, it is possible to induce a stronger attractive force between the droplet and the "A" bead. But also a proper tuning of the velocity of the transient force is necessary: if the velocity is too high, the droplet can eventually undergo a break-up.

In order to understand in which cases it is possible to effectively move the droplet, the work (L) done by the droplet under the action of the attractive force was calculated as follows:

$$L = F_{CM} \cdot \Delta x_{CM} \qquad (5.2)$$

where F_{CM} is the force acting on the center of mass and Δx_{CM} is the center of mass displacement along the x-coordinate.

Figure 5.9 displays the plots of the droplet work as a function of the "A" beads position.
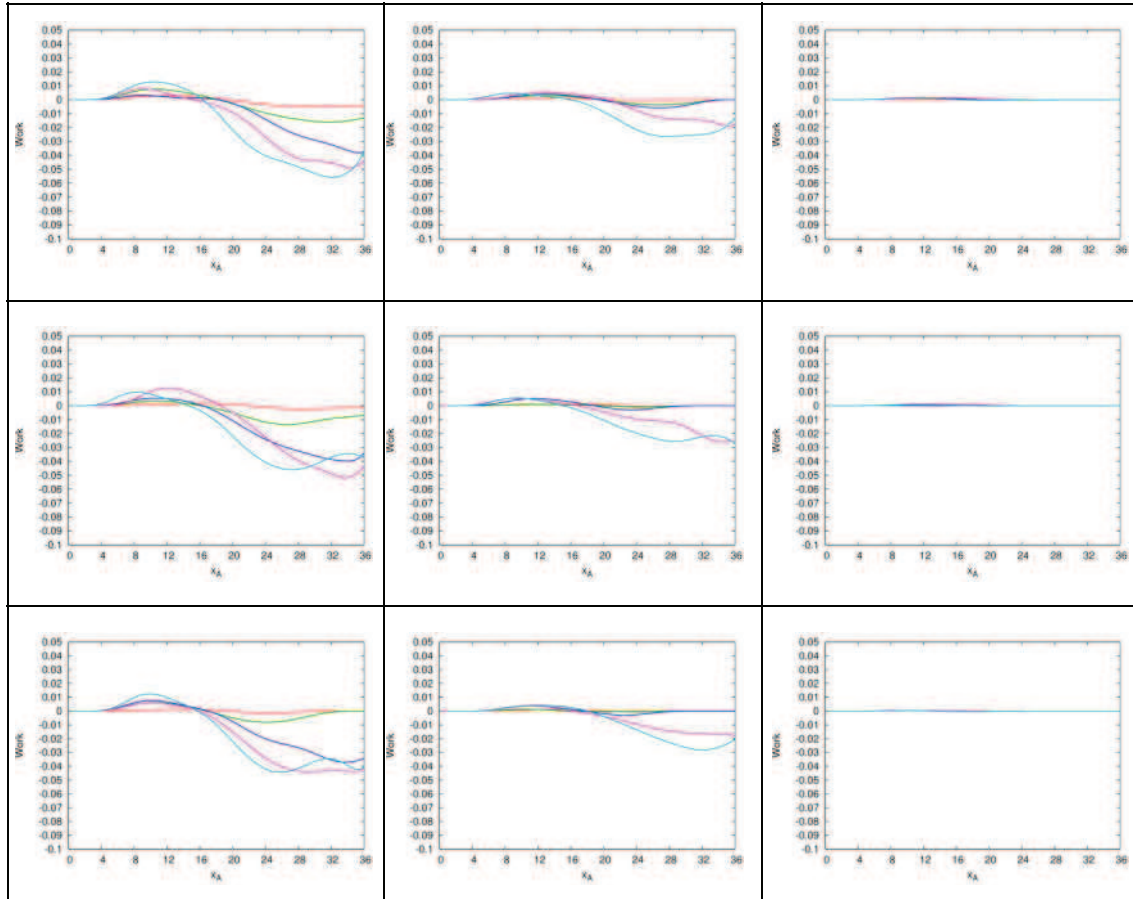

Figure 5.9. Work done by the droplet center of mass (expressed in k_BT) as a function of the x position of "A" bead (x_A, expressed in r_c) for three different values of the $\boldsymbol{b_{DA}}$ parameter ($\boldsymbol{b_{DA}}$=-5 first column, $\boldsymbol{b_{DA}}$=-3 second column, $\boldsymbol{b_{DA}}$=-1 third column) and for the three surfaces ("SURF-A" first row, "SURF-B" second row and "SURF-C" third row). Each plot displays the curves for the five different attractive force translational velocities: v_{PF} = 0.364 (red), 0.182 (green), 0.121 (blue), 0.091 (magenta) and 0.073 (cyan) r_c/τ.

The sign of the work depends both on the sign of the force (always negative) and the center of mass displacement. As asserted before during the observation of the center of mass displacement (Figure 5.5), since the "A" trajectory starts from the left side of the surface, the work presents an initial positive trend, due to the back-bounce effect.

The "A" velocity and the surface wettability cannot be considered as secondary parameters in comparison to the attractive $\boldsymbol{b_{DA}}$ force. They not only influence the morphology of the droplet during the movement, as suggested by the contact angles analysis, but can also hinder or promote the motion.

The data showed in this section provide a wide range of cases on the most important parameters to control in order to perform real experiments with the aim to control the motion of fluid droplets.

This could be for example the case of a water droplet on the top of a field effect transistor (FET), where the charge/carrier flux in the channel could ideally represent the "active" part of the system. In this case the charge mobility, or in other words the speed of the charges, could represent the parameter to decrease, in order to intensify the effects of the transient electric field. Also the chemistry of the surface and the electronic properties of the semiconductor are important parameters to control. The thickness of the semiconductor regulates the distance between the droplet on the top of the device and the channel, increasing or reducing the effects of the mobile charges.

From the results provided by the simulations the use of organic thin film transistors would be a better choice compared to inorganic one. Organic materials establish normally lower interactions with water molecules, for this reason the use of lipophilic organic molecules is preferred than using polar species or chemical compounds able to form hydrogen bonds (such as silica, SiO_2). Organic semiconductors express, in most cases, also a lower charge mobility.

In another real situation, such as in the use of a mobile ultramicroelectrode positioned at close distance to a micrometer size water droplet, the possibility to control the voltage applied and to regulate its position means to control two of the three parameters described in the model.

Also the surface chemistry can be controlled through a smart material selection, in combination with the use of surrounding media able to reduce the friction or other perturbations to the motion of the droplet (e.g. the use of a water droplet in an oil matrix instead that a droplet exposed to the air).

5.4. Conclusions

As suggested in the introduction, the capacity to guide the motion of small portion of fluid can have a variety of chemical and biological applications such as nano/microfluidic device, microreactors or microelectronics engines.

In this section, the study of droplet motion on a surface under the influence of a mobile external force was performed. A CG model of a fluid droplet immersed in a medium and

deposed on a solid surface was set up and used to analyze the general effects that a transient force provokes on the droplet movement and morphology.

A systematic scheme of variation of three different parameters involving the droplet interaction with the surface and the characteristics of the transient force was investigated. The parameters were the repulsive a_{DS1} force (surface wettability), the attractive b_{DA} force (strength of the perturbation), and the velocity of the transient interaction.

A number of 150 independent simulations were made with different combinations of the parameters. The aim of the study was to collect the highest possible number of data in relation to the widest possible range of simulations parameter combinations, in order to perform a complete analysis of the droplet motion able to be used for the set-up of real experiments.

The model is able to provide much information about the motion characteristics in terms of morphological changes and transient response in a large variety of cases.

Each one of the parameters under control provides to the droplet with a peculiarity; furthermore their combination extends the range of situations that can occur.

The possibility to extend the number of cases here presented to specific focus or to other geometrical set-ups could represent a significant improvement of the model, providing to experimentalists the capacity to predict droplet behavior in classical engineering problems.

6. Concluding remarks

In this dissertation I presented my three years of PhD work.

My main activity was the development of a coarse-grained model with the aim to deep study the mechanical behavior of active droplets. The terms "active" means the possibility to induce perturbations in the thermodynamic equilibrium of a droplet, acting on external factors or internal ones. The major part of my work was focused on this second possibility, closing the gap between inanimate matter and living ones.

The capacity of living cells to use their metabolism to overcome energy barriers without the necessity of a direct supply of energy/force represents in fact the biggest difference with respect to non-living materials and systems.

The thesis was articulated in six chapters, where three of them showed the core of my three years research activity. Chapter 3 and 4 were concerned with the development of a CG model for the study of certain living-cell phenomena, while chapter 5 had the aim to show the active behavior of a CG fluid droplet in different conditions.

During the development of the model for the study of cells adhesion and morphology(chapter 3) the focus was to implement a system where the CG droplet was able to perform spontaneous activities from inside its body. The combination of beads types and inter-particle forces provided to the droplet the capacity to have the proper amount of energy required to beat the interfacial tension and modify its shape. Starting from a model able to represent only hydrophobic/hydrophilic interactions, the implementation of attractive forces was the solution to introduce the sought activity inside a totally passive system. This was possible only after reaching an understanding of the principles that govern living cell adhesion. The agreement with experimental work carried out on living cells in terms of interfacial tension and force exerted by the adhesive beads were surprisingly good if compared to the simplicity of the CG model, where no cellular details were implemented. This simplicity was however the key for the modeling of systems that, for computational chemistry, have truly large size.

The problem of the computational cost was evident in the simulations on neuritis growth (chapter 4), where a higher number of particles, if compared to the simulations of the system presented in chapter 3, became necessary to represent and simulate a complicate metabolic phenomenon. In this case the difficulties encountered in the regulation of the parameters, especially in the cut-off radius r_{c2} for the attractive force, made the set-up of the model slow and in some aspects uncomplete in terms of its general validity.

The results obtained were however satisfactory in terms of axon guidance and the increment of the model complexity was an important test bench for its future exploitation.

The work done on active droplets under the effect of a transient force has been a little different approach from the other two (chapter 5). The active behavior of an inanimate droplet fluid onto a surface was studied in relation to an external transient perturbation.

The wettability of the surface, the velocity of the perturbation force and the perturbation strength were the three variables used to study the morphological aspects of the droplet motion and the possible deformations from its normal round shape. The collected data can be used as a guideline for the development of new devices with specific characteristics able to control the motion of fluid.

The model presented in this dissertation can be implemented in other ways. In relation to living cells, the possibility to increase the level of details of the cell body such as including the cellular membrane, the nucleus or an explicit representation of the cytoskeleton could help to perform more sophisticate and accurate simulations.

Also the increment in computer performance will allow to solve the problems in a faster way, with the possibility to increase the system size and simulate bigger and more complicated systems.

7. References

[1] F. Segatta, L. Cupellini , S. Jurinovich, S. Mukamel, M. Dapor, S. Taioli, M. Garavelli, and B. Mennucci, *J. Am. Chem. Soc.*, 2017, **139 (22)**, 7558–7567.

[2] M. Garavelli, P. Celani,F. Bernardi, M. A. Robb, and M. Olivucci, *J. Am. Chem. Soc.*, 1997, **119 (29)**, 6891–6901.

[3] M. M. T. El-Tahawy, A. Nenov, M. Garavelli, *J. Chem. Theory Comput.*, 2016, **12 (9)**, 4460–4475.

[4] D. S. Ruiz, A. Cembran, M. Garavelli, M. Olivucci, W. Fuss, *Photochem. Photobiol.*, 2002, **76(6)**, 622-633.

[5] D. Polli, P. Altoè, O. Weingart, K. M. Spillane, C. Manzoni, D. Brida, G. Tomasello, G. Orlandi, P. Kukura, R. A. Mathies, M. Garavelli, G. Cerullo, *Nature, 2010,***467**, 440–443.

[6] J. Wang, R. M. Wolf, J. W. Caldwell, P. A. Kollman, D. A. Case, *Journal of Computational Chemistry,* 2004, **25**, 1157-1174.

[7] L. Verlet, *Phys. Rev*, 1967, **159**, 98-103.

[8] M. B. Liu, G. R. Liu, L. W. Zhou, J. Z. Chang, *Arch. Computat. Methods Eng*, 2015, **22**, 529-556.

[9] E. Moeendarbary, TY. Ng, M. Zangeneh, 2009, **1(04)**, 737-763.

[10] P. J. Hogerbrugge, J. M. V. A. Koleman, *Europhys Letters*, 1992, **19**, 155-160.

[11] P. J. Hogerbrugge, J. M. V. A. Koleman, *Europhys Letters*, 1993, **21**, 363-368.

[12] R. D. Groot and P. B.Warren,*J. Chem. Phys.*, 1997, **107**, 4423-4435.

[13] P. Español, P. B.Warren, *Europhysics Letters*, 1995, **30**, 191-196.

[14] R. D. Groot, *J. Chem. Phsys*, 2003, **118**, 11265-11267.

[15] P. J. Flory, *Principles of polymer chemistry, George Fisher Baker non-resident lectureship in chemistry at Cornell University, Cornell University Press, Ithaca*, 1953.

[16] P. B. Warren Physical Review, 2003, **68**, 066702(8).

[17] I. Pagonabarraga, D. Frenkel*, J. Chem, Phys*, 2001, **115**, 5015.

[18] S. Y. Trominov, E. L. F. Nies, M. A. J. Michels, *J. Chem, Phys.*, 2002, **117**, 9383.

[19] L. Verlet, *Phys. Rev.*, 1967, **159**, 98.

[20] M. P. Allen, D. J. Tildesley, *Oxford University Press*, New York, 1990.

[21] D. Fincham, B. J. Ralston, *Comput. Phys. Commun.*, 1981, **23**, 127.

[22] F. Toschi, F. Lugli, F. Biscarini and F. Zerbetto, *J. Phys. Chem.,* 2009, **113**, 369-376.

[23] F. Lugli, F. Toschi, F. Biscarini and F. Zerbetto, *J. Chem. Theo. and Comput.*, 2010, **6**, 3516-3526.

[24] S. A. Andujar, F. Lugli, S. Höfinger, R. D. Enriz and F. Zerbetto, *Phys. Chem. Chem.Phys.*, 2012, **14**, 8599-8607.

[25] I. V. Pivkin, G. M. Karniadakis, *Phys Rev. Lett.*, 2008, **101**, 118105.

[26] C. Pozrikidis, *Analysisi of Biomedical Engineering,* 2005, **33**, 165-178.

[27] D. A.Fedosov, B. Caswell and G. E. Karniadakis, *Biophys Journal*, 2010, **98**, 2215-2225.

[28] W. Pan, B. Caswell and G. E. Karniadakis, *Soft Matter*, 2010, **6**, 1-35.

[29] D. A. Fedosov, G. Gompper, *Soft Matter*, 2014, **10**, 2961.

[30] K.A. Kilian, B. Bugarija, B. T. Lahn, M. Mrksich, *Proc. Natl. Acad. Sci. USA,* **2010**, 107, 4872-4877.

[31] R. McBeath, D. M. Pirone, C. M. Nelson, K. Bhadriraju, C. S. Chen, *Dev. Cell.*, 2004, **6**, 483-495.

[32] C. S. Chen, M. Mrksich, S. Huang, G. W. Whitesides, D. E. Ingber, *Science*, 1997, **276**, 1425-1428.

[33] C. T. Lim, E. H. Zhou, S. T. Quek, *J. Biomechanics*, 2006, **39**, 195-216.

[34] A. Yeung, E. Evans, *Biophys. J.*, 1989, **56**, 139-149.

[35] H. C. Can, H. S. Udaykumar, W. Shyy, R. Tran-Son-Tay, *Phys. Fluids*, 1998, **10**, 770-774.

[36] C. Vera, R. Skelton, F. Bossens, L. A. Sung*, Annals of Biomedical Engineering,* 2005, **33***, 1387-1404.

[37] N. O. Deakin, C. E. Turner*, J. Cell. Sci.,* 2008, **121**, 2435-2444.

[38] C. M. Fife, J. A. McCarroll, M. Kavallaris, *British Journal of Pharmacology*, 2014, DOI: 10.1111/bph.12704.

[39] M. F. Coughlin, D. A. Stamenovic, *Biophys J.*, 2003, **84**, 1328-1336.

[40] T. Kim, W. Hwang, H. Lee, R. D. Kamm, *PLoSComput. Biol.* 2009, **5**, e10000439.

[41] F. Lugli, G. Fioravanti, D. Pattini, L. Pasquali, M. Montecchi, D. Gentili, M. Murgia, Z. Hemmatian, M. Cavallini, F. Zerbetto, *Advanced Functional Material*, 2013, **23**, 5543-5549.

[42] S. Lach, S. M. Yoon and B. A. Grzybowski, *Chem. Soc. Rev.*, 2016, **45**, 4766.

[43] I. Lagzi, S. Soh, P. J. Wesson, K. P. Browne and B. A. Grzybowski, *J. Am. Chem. Soc.,* 2010, **132**, 1198-1199.

[44] M. M. Hanczyc, T. Toyota, T. Ikegami, N. Packard and T. Sugawara, , *J. Am. Chem. Soc.,* 2007, **129**, 9386-9391.

[45] K. Ichimura, S. K. oh and M. Nakagawa, *Science*, 2000, **288**, 1624-1626.

[46] P. J. M. Van Haastert and P. N. Devreotes, *Nat. Rev. Mol. Cell Biol.,* 2004, **5**, 626-634.

[47] T. W. Grebe, and J. Stock, *Curr. Biol.*, 1998, **8**, R154-R157.

[48] G. L. Hazelbauer, J. J. Falke and J. S. Parkinson, *Trends Biochem. Sci.*, 2008, **33**, 9-19.

[49] V. Noireaux and A. Libchaber, *Proc. Natl. Acad. Sci. U.S.A.*, 2004, **101**, 17669-17674.

[50] S. Matosevic and B. M. Paegel, *J. Am. Chem. Soc.*, 2011, **133**, 2798-2800.

[51] T. P. de Souza, A. Fahr, P. Luisi and P. Stano,*J. Mol. Evol.*, 2014, **79**, 179-192.

[52] M. Dallavalle, F. Lugli, S. Rapino and F. Zerbetto, *Soft Matter*, 2016, **12**, 3538.

[53] I. B. Bischofs, F. Klein, D. Lehnert, M. Bastmeyer, U. S. Schwarz, *Biophys. J.*, 2008, **95**, 3488-3496.

[54] M. Macis, F. Lugli, F. Zerbetto*, ACS Appl. Mat. Interfaces*, 2017, **9**, 19552-19561.

[55] W. Kuehnel, *Color Atlas of Cytology, Histology & Microscopic Anatomy*, 4[th]ed, Thieme, Stuttgard, 2003.

[56] L. Wiemerslage, D. Lee, *J. Neurosci. Methods,* 2016, **262**, 56-65.

[57] I. Salmeen, P. Zacmanidis, G. Jesion, L. A. Feldkamp, *Biophys. J. *, 1985, **48**, 681-686

[58] M. Venturoli, B. Smit, M. M. Sperotto, *Biophys J.* 2005, **88**, 1778-1798.

[59] X. Li, I. V. Pivkin, H. Liang, G. E. Karniadakis, *Macromolecules*, 2009, **42**, 3195-3200.

[60] W. G. Bardsley, J. D. Aplin, *J. Cell Sci.*, 1983, **61**, 365.

[61] A. Aref, R. Horvath, J. J. Ramsden, *J. Biol. Phys. Chem.*, 2010, **10**, 145-151.

[62] D. Cuvelier, M. Théry, Y. S. Chu, S. Dufour, J. P. Théry, M. Bornens, P. Nassoy, L. Mahadevan, *Curr. Biol.*, 2007, **17**, 694-699.

[63] D. Riveline, E. Zamir, N. Q. Balaban, U. S. Schwarz, T. Ishizaki, S. Narumiya, Z. Kam, B. Geiger, A. D. Bershadesky, *J. Cell. Biol*, 2001, **153**, 1175-1186.

[64] N. Q. Balaban, U. S. Schwarz, D. Riveline, P. Goichberg, G. Tzur, I. Sabanay, D. Mahalu, S. Safran, A. Bershadsky, L. Addadi, B. Geiger, *Nat. Cell. Biol.*, 2001, **3**, 466-472.

[65] C. G. Galbraith, M. P. Sheetz, *Proc. Natl. Acad. Sci. U. S. A.,* 1997, **94**, 9114-9118.

[66] M. Dembo, Y. Wang, *Byophys. J.,* 1999,**76**, 2307-2316.

[67] L. J. Jones, M. Lal, J. N. Ruddock, N. A. Spenley, *Faraday Discuss.*, 1999, **112**, 129-142.

[68] B. Kong, X. Yang, *Langmuir*, 2006, **22**, 2065-2073.

[69] T. Young, *Philos. Trans. R. Soc. London*, 1805, **95**, 65-87.

[70] Janette L. Jones, M. Lal, J. Noel Ruddock, N. A. Spenley, *Faraday Discuss.*, 1999, **112**, 129-142.

[71] R. G. Harrison, *Science*, 1911, **34**, 279.

[72] N. Arimura, K. Kaibuchi,*Nat. Rev. Neurosci.*, 2007, **8**, 195-205.

[73] M. Tessier-Lavigne, CS. Goldman, *Science*, 1996, **274**, 1123-1133.

[74] B. J. Dickson, *Science*, 2002, **298**, 1959-1964.

[75] W. J. Rosoff, J. S. Urbach, M. A. Esrick, R. G. McAllister, L. J. Richards and G. J. Goodhill, Nat. Neurosci, 2004, **7**, 678-682.

[76] M. Tessier-Lavigne, M. Placzek, A. G. S. Lumsden, J. Dodd, T. M. Jessel, *Nature*, 1988, **336**, 775-77.

[77] H. J. Song, G. L. Ming, M .M Poo, *Nature*, 1997, **388**, 275-279.

[78] T. M. Keenan, A. Folch, *Lab. Chip*, 2008, **8**, 34-57.

[79]C. K. Yeung, L. Lauer, A. Offenhäuser, W. Knoll, *Neurosci. Lett*, 2001, **301**, 147-150.

[80] C. D. W. Wilkinson, M. Riehle, M. Wood, J. Gallagher, A. S. G. Curtis, *Mater. Sci. Eng.*, 2002, **19**, 263-269.

[81] R. Fricke, P. D. Zentis, L. T. Rajappa, B. Hofmann, M. Banzet, A. Offenhäuser, S. M. Meffert, *J. Biomat.*, 2011, **32**, 2070-2076.

[82] M. J. Jang, S. Namgung, S. Hong, Y. Nam, *Nanotechnology*, 2010, **21**, 235102.

[83] R. Fricke, P. D. Zentis, L. T. Rajappa, B. Hofmann, M. Banzet, A. Offenhäuser, S. M. Meffert, *J. Biomat.*, 2011, **32**, 2070-2076.

[84] J. Bernà, D. A. Leigh, M. Lubomska, S. M. Mendoza, E. M. Pérez, P. Rudolf, G. Teobaldi, F. Zerbetto, *Nature materials*, 2005, **4**, 704-710.

[85] S. Oh, M. Nakagawa, K. Ichimura, *J. Mater. Chem*, 2002, **12**, 2262-2269.

[86] BS. Gallardo, VK. Gupta, FD. Eagerton, L.I. Jong, VS. Craig, RR. Shah, NL. Abbott, *Science*, 1999, **283**, 57-60.

[87] K. Zhang, F. Wang, X. Zhao, *Computational Material Science*, 2016, **124**, 190-194.

[88] J. Yin, X. Li, J. Yu, Z. Zhang, J. Zhou, W. Gou, *Nature Nanotechnology*, 2014, **9**, 378-383.

[89] L. E. Helseth, *Journal of Electrostatic*, 2016, **81**, 64-70.

[90] S. Kwon, W. K. Kim, J. Park, Y. Yang, B. Yoo, C. J. Han, Y. S. Kim, *ACS Appl. Mater. Interfaces,* 2016, **8**, 24579-24584.

[91] S. Kwon,J. Park, W. K. Kim, Y. Yang, E. Lee, C. J. Han, Y. S. Kim, *Enargy, Environ. Sci.,* 2014, **7**, 3279-3283.

[92] J. K. Moon, J. Jeong, D. Lee, H. K. Pak, *Nat. Commun,* 2013, **4**, 1487.

[93] S. Mhatre, R. M. Thaokar, *Phys. Fluids*, 2013, **25**, 07215-1 - 07215-17.

[94] K. Ahn, C. Kerbage, T. P. Hunt, R. M. Westervelt, D. R. Link, D. A. Weitz, Applied Physics Letters, 2006, **88**, 024104-1 - 024104-3.

[95] T. B. Jones, M. Gunji, M. Washizu, J. Feldman, *Journal of Applied Physics,* 2001, **89**, 1441-1448.

[96] N. Allahrabbi, Y. S. M. Chia, M. S. M. Saifullah, K. Lim, L. Y. L. Yung, *Biomicrofluidics*, 2015, **9**, 034110-1 - 034110-18.

[97] M. Hase, S. N. Watanabe, K. Yoshikawa, *Phys. Review*, 2006, **74**, 046301-1 - 046301-4.

[98] H. Li-min, Y. Dong-hai, G. Rong-na, Y. Tuan-jie, L. Yu-ling, L. X. ming, *Pet. Sci,* 2013, **10**, 548-561.

[99] M. Gunji, M. Washizu, *J. of Phys. D: Appl. Phys*, 2005, **38**, 2417-2423.

[100] S. D. Hong, M. Y. Ha, S. Balachandar, *Journal of colloid and interface science,* 2009, **339**, 187-195.

[101] J. Zhao, S. Chen, Y. Liu, *Applied Surface Science*, 2017, **400**, 515-523.

[102] O. Ghazian, K. Adamiak, G. S. P. Castle, *Journal Of Electrostatics,* 2013, **71**, 489-495.

[103] B.-B. Wang, X.-D. Wang, T.-H. Wang, G. Lu, W.-M. Yan, *International Journal of Heat and Mass Transfer*, 2016, **98**, 10-16.

[104] F. Mugele, J.-C. Baret, *Journal of Physics*: *Condensed Matter*, 2005, **17**, R705-R774.

[105] X. J. Gong, J. Y. Li, H. J. Lu, R. Z. Wan, J. C. Li, J. Hu and H. P. Fang, *Nature Nanotechnol.*, 2007, **2**, 709–712.

[106] M. G. Kanatzidis, *Nature,* 2004*,* **428**, 269–271.

[107] L. Gao, T. J. McCarthy, *Langmuir,* 2006, **22**, 6234-6237.

[108] T. Wang, W. Li, L. Liu, H. Chen, Y. Wang, J. Zhang, Y. Tan, *Comput. Mat. Sci.*, 2015, **105**, 39-46.